NTNU – Trondheim
Norwegian University of
Science and Technology

Testing of Insulation Liquids for Subsea Power Converters

Partial Discharge and Breakdown Testing

Malin Drevdal Borge

Master of Energy and Environmental Engineering
Submission date: July 2015
Supervisor: Arne Nysveen, ELKRAFT
Co-supervisor: Abdelghaffar A. Abdelmalik, ELKRAFT

Norwegian University of Science and Technology
Department of Electric Power Engineering

ABSTRACT

To realise the future subsea power systems, pressure compensated, liquid insulated power converters are subject to development. The liquid insulation provides a higher breakdown strength than air-insulated systems and works like a natural cooling agent. However, liquid contaminations can cause high local electric fields that could deteriorate the insulation. In order to avoid the influence of contaminations, electrode surface covering like Parylene can be applied.

Sharp edges in electrode trenches at the electrodes in power electronic equipment give rise to high local electric fields. Electrical field values in the range of 10^8 V/m may initiate partial discharges (PD) or ultimately breakdown. PD activity and breakdown behaviour in high electric fields in such electrode trenches have been investigated by progressive breakdown testing of Printed Circuit Boards (PCBs). Measurements with both sinusoidal and fast turn-on switching voltage (100 ns rise time) have been performed with three different dielectric liquids. A mineral oil (Nytro 10XN), a synthetic oil (Midel 7131) and one fluorinated liquid (Galden HT230) have been tested to get a variety of liquid properties. The PCBs submerged in liquid are tested both with and without Parylene surface cover.

The PD activity has been recorded in an attempt to determine the PD inception voltage (PDIV). PDs are detected by the use of electrical, optical and acoustic methods in a low-noise test setup. The setup had a peak-to-peak noise less than 2 pC. Test results show that PDs were detectable for sinusoidal voltage testing.

Optical and acoustic PD detection methods should be immune to switching noise, however, results indicate that the transients at fast switching will influence them. When performing tests with positive polarity switching voltage, the PDs were not measurable in most cases because of the noise. In the commonly used transformer oil, Nytro 10XN, some optical and acoustic PD activity was recorded at approximately 20 kV during the fast switching testing before breakdown occurred. At negative switching polarity, PDs were more frequently observed, due to the effect of space charges.

Comparison of sinusoidal and fast turn-on switching at low power-frequency of 38.5 Hz, was performed with Weibull statistical analysis. The fast switching showed at slightly higher breakdown voltage (BDV) for Nytro and Midel, with an increase from 21.8 to 23.1 kV (5 %) and 20.6 to 23.7 kV (15 %) respectively. Fast turn-on resulted in significantly higher BDV for Galden at 34.2 kV, which corresponds to an increase of 58 %. The reason for this increase can be that only homo charges can be generated at unipolar switching.

Parylene cover increased the breakdown strength by 65 % compared to at same conditions without cover. The test voltage across the object was limited to 40 kV peak voltage that was not sufficient to break down all covered PCBs at fast switching. This high breakdown strength is a promising sign for the objective of insulating subsea converters, which will require high reliability.

SAMMENDRAG

For å realisere fremtidens kraftsystemer med frekvensomformere på havbunnen, er det et mål å utvikle trykk-kompensert kraftelektronikk isolert med flytende dielektrisk isolasjon. Den flytende isolasjon har høyere elektrisk holdfasthet sammenlignet med luftisolerte systemer og gir naturlig kjøling. Forurensninger kan midlertidig forårsake høye lokale elektriske felt som kan forringe isolasjonen. For å unngå påvirkning av forurensninger, kan man dekke elektrodeoverflatene med f. eks Parylene.

Skarpe kanter i elektrodegrøfter i kraftelektronikken kan gi opphav til høye lokale elektriske felt. Elektriske feltverdiene på 10^8 V/m kan initiere delvise elektriske utladninger eller i verste fall gjennomslag. Utladningsaktiviteten og gjennomslagstester, ved høye elektriske felt i slike elektrodegrøfter, har blitt undersøkt i progressive gjennomslagstester på spesiallagde kretskort. Målinger med både sinusformet og rask påslått bryterspenning (100 ns stigetid) har blitt utført for tre forskjellige dielektriske væsker. En mineralolje (Nytro 10XN), en syntetisk olje (Midel 7131) og en fluorinnholdig væske (Galden HT230) har blitt testet for å få et utvalgt av ulike væskegenskaper. Kretskortene har blitt nedsenket i væske er testet både med og uten et overflatelag av Parylene.

Aktiviteten av delvise utladninger er registrert i et forsøk på å fastslå hvilket spenningsnivå som kreves for å initiere utladninger. Utladningene er målt ved hjelp av elektriske, optiske og akustiske metoder i testoppsett med lavt støynivå. Oppsettet hadde peak-til-peak støy på mindre enn 2 picocolomb [pC]. Testresultatene viser at utladningene var mulige å detektere for sinusformet spenning.

Optiske og akustiske metoder for deteksjon av utladninger burde være immun mot transient støy fra den raske bryteren, men resultatene tyder på at transienter fortsatt påvirker metodene. I testene utført med rask påslått (impuls) spenning var det ikke mulig å måle elektriske utladninger. Bare i den vanlig brukte transformatoroljen, Nytro 10XN, ble noe optisk og akustisk utladningsaktivitet registrert rundt 20 kV i løpet av gjennomslagstestingen. For motsatt polaritet på likespenningskilden og minuskoblet bryter, ble delvise utladninger observert hyppigere. Dette er på grunn av effekten av romladninger.

Sammenligning av sinusformet og rask påslått spenning, begge på lav effekt-frekvens (38.5 Hz), ble gjort ved å regne ut gjennomslagsspenningen gitt av tilhørende Weibullfordeling. Påtrykt impulsspenning gav litt høyere holdfasthet for Nytro og Midel, med en økning på henholdsvis 21.8 til 23.1 kV (5%) og 20.6 til 23.7 kV (15%) sammenlignet med sinusspenning. Impulsspenning gav en signifikant høyere holdfasthet for Galden på 34,2 kV, noe som tilsvarer en økning på 58%. Grunnen kan være at det bare er romladninger med samme polaritet som kan genereres ved unipolar impulsspenning.

Parylenelaget økte holdfastheten med opptil 65% sammenlignet med samme betingelser uten Parylene. Testspenningen var begrenset til 40 kV som vist seg å ikke være tilstrekkelig til å oppnå gjennomslag av dekte kretskort med impulsspenning. Denne høye holdfastheten er et godt tegn med tanke på formålet med dielektrisk isolasjon til frekvensomformere, som vil kreve høy pålitelighet.

NORGES TEKNISK-NATURVITENSKAPELIGE UNIVERSITET

NTNU

M A S T E R   T H E S I S

Candidate name   : Malin Drevedal Borge

Field of Study   : **ELECTRICAL POWER ENGINEERING**

Oppgavens tittel (Norsk)   : Testing av isolasjon for undervanns frekvensomformere

Thesis title (English)   : Testing of insulation liquids for subsea power converters

Description:

For subsea process plants for oil and gas production, power converters are needed at the seabed. Current technology applies converters placed in one bar pressure vessels. These are heavy and costly for large water depths. ABB and OneSubsea have earlier developed a 3MW subsea converter of this type. The converter is placed in a vessel filled with a dielectric liquid and pressure compensated. The objective is to do experimental tests in order to evaluate the performance and suitability of different dielectric fluids as insulant in the power electronic converters.

More specifically the work shall focus on:

- Design and assemble a low noise HV test cell for Partial Discharge (PD) detection
- Install and evaluate the use of optical and acoustic PD detection methods
- Perform dielectric tests with Printed Circuit Boards (PCBs) model with sinusoidal voltage for different candidate liquids.
  - Compare PD inception voltage (PDIV) and breakdown voltage of the PCB trench
  - Compare the statistical analysis of breakdown strength of the trench with different liquid.
- Test the effect of Parylene coating on the PD inception and characteristic breakdown strength of the PCB trench.
- Evaluate the PDIV and the breakdown strength of the test object under a fast switching voltage source.
- Compare PDIV and breakdown strength for the two voltage sources. Use optic and/or acoustic detection method if needed.

Further details of the work are to be discussed with the supervisors during the project period.

Thesis given	:	1st of February 2015
Thesis revised	:	18th of June 2015
Submission deadline	:	5th of July 2015
Date of Submission	:	
Carried out at	:	Department of Electrical Power Engineering at NTNU
Professor and supervisor	:	Professor Arne Nysveen
Co-Supervisor	:	Postdoc Abdelghaffar A. Abdelmalik

Trondheim, 18th of June 2015

Arne Nysveen

Professor

PREFACE

This master thesis is conducted as the final part of a five-year study at Energy and Environmental studies at NTNU.

I would like to thank my supervisor Arne Nysveen, for his good guidance and discussions. A special thank must also be given to my co-supervisor Postdoc Abdelghaffar Amoke Abdelmalik, for all the help I have received throughout my thesis. I am also very greatful for all the help from Lars Lundgaard, Dag Linhjell and Knut Liland at SINTEF Energy Research, who both have so much experience and knowledge in the field. I would like to thank the Service Lab at the 3rd floor, for helping me find all equipment needed and making numerous electrical plugs for me. Thanks are also granted to the workshop in the basement for helping me make many different parts to the laboratory setup.

Finally, I want to thank my girls Anja, Ingvild, Britt and Mai-Linn, for all the good times, memories, laughter and support throughout the last five years, and especially this last year. I am forever grateful for the effort made to motivate me through both the specialisation project and master thesis. I also need to thank the rest of "Gullrekka", which is a unique bunch of cheerful people, whom I all regard highly. Thanks to my "big brothers" in Snorres gate 9 for late-night reflections over life, extensive tea-drinking and Netflix binge-watching.

Trondheim, July 2015

Malin Drevdal Borge

CONTENT

ABBREVIATIONS

AlN	Aluminium Nitride
BDV	Breakdown Voltage
Ch	Channel
EHD	Electrohydrodynamic
EMI	Electromagnetic Interference
FR-4	Flame retardant glass-reinforced epoxy laminate sheets
HT	Heat Transfer
IP	Ionization Potential
PD	Partial Discharge
PDEV	Partial Discharge Extinction Voltage
PDIV	Partial Discharge Inception Voltage
PFPE	Perfluorinated polyether
PMT	Photon Multiplier Tube
PTPE	Pressure Tolerant Power Electronics
S/N	Signal to Noise
TTL	Transistor-Transistor Logic
VSD	Variable Speed Drive

1 INTRODUCTION

The OG21 subsea cost report from April 2015 present how Norway can reduce costs of subsea construction with up to 50% by utilizing the knowledge and research developed over years [1]. To achieve cost reduction, an all-electric subsea system with simplified subsea power converters can be developed. Having one power umbilical to supply the electrical equipment at subsea is cost effective and reduces the connection points and the complexity, which further reduces the weight and space required.

One of the most important sophisticated electrical components in the future subsea farm is the variable speed drive (VSD). The VSD can efficiently control pumps and compressors by the use of power electronics, varying the supplied voltage and current frequency. However, there are great challenges to overcome in order to place the VSD at subsea level. They should have the ability to run for five years without maintenance and be of a much more compact size compared to the larger VSDs normally used onshore [2].

The master thesis is connected to a SINTEF project called Presspack. The research in Presspack investigate issues related to realise subsea VSDs where the pressure inside the equipment vessel equals the surrounding water pressure. The main objective for Presspack is to "*provide fundamental material and packaging knowledge for supporting realisation of reliable Pressure Tolerant Power Electronic (PTPE) components and circuits for operation depths down to 5000m* [3]."
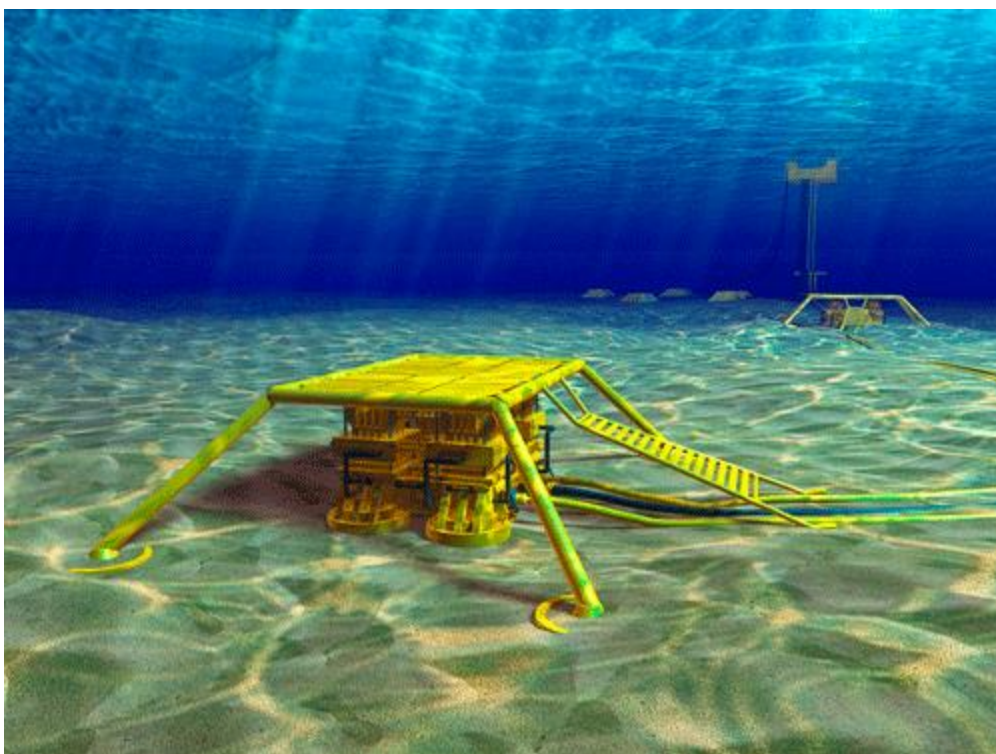

Figure 1 - Subsea Power System illustration by Statoil [1]

This thesis will investigate the breakdown strength of the dielectric high voltage insulation required together with the PTPE. Furthermore, the influence of surface covering to improve the breakdown strength will be tested. Condition assessment of such subsea VSDs will be important to ensure high reliability. The occurrence of partial discharges (PD) in local high field areas like the electrode trench in IGBTs with sharp edges can deteriorate the insulation and could eventually lead to breakdown. PDs are stochastic phenomena, and can be occur due to bad design, contaminations, or air bubbles. By detecting and monitoring PD activity, one can avoid failure by performing maintenance or replacement at a suitable time.

To ensure a long life-time, a reliable insulation material with high breakdown strength should be chosen. Liquid insulation has been chosen as the best alternative because of its natural cooling and self-healing effect [3]. To determine which liquid is best as power electronics insulation material, different liquids are to be tested in conditions similar to when power electronics are operating. Today there exists no standard way of testing high power electronics submerged in liquid insulation, only standards for transformers. This requires that a test procedure have to be suggested.

There exist virtually no studies showing PD activity in the trench between electrodes in Power Electronics submerged liquid insulation. The fast switching used in Power Electronics introduce severe electrical transients, which exclude the possibility of using the convention electrical PD detection method. The PDs will not be detectable behind the noise originating from switching. In order to detect the PDs despite the transients, alternative detection methods are required, e.g. optical and acoustic methods. Detecting PDs by acoustic detection can be performed with a piezoelectric transducer picking up vibrations from the sound accompanying the discharge. Light emission from PDs is sent out from the streamer and can be detected with a Photon Multiplier Tube (PMT).

1.1.1 Specialization project summary

In the specialization project leading up to the master thesis light emission by the use of a PMT was detected [4]. Detecting the light with a photomultiplier tube will give an indication on PD activity and PD size. To evaluate the reliability, a low noise test setup a with point to plane gap measuring both light and electrical signals was set up. The light emission was compared to electrical detection and the correlation was evaluated. Three different liquids were tested with AC voltage applied: Nytro, Galden and Midel. In general, small negative discharges and large positive discharges were detected. Galden HT200 and Nytro 10XN showed light emission that correlated well with the electrical PD signal detected. Midel showed barely any light at all, and not much correlation. The reliability of light detection is shown to be highly dependent upon the liquid, and this must be kept in mind moving over to further testing.

2 THEORY

This chapter is an attempt to summarise the relevant theory and terminology of electrical breakdown and partial discharges in liquid insulation. A large part of the theory is taken from the specialisation project [4]. The chapter starts with explaining the basic physical terms of conductivity and permittivity as properties of a dielectric media. Furthermore, the properties of partial discharges and the breakdown mechanisms in liquids are explained.

2.1 ELECTRIC FIELD IN DIELECTRIC MEDIA

The conductivity σ of an **ideal *dielectric*** or insulator, is zero. The value σ describes the material's ability to carry current, thus an ideal dielectric will have no current carrying abilities. However since no materials are ideal in nature, even insulators will have a certain, but very low, conductivity. When applying voltage across a dielectric, it experiences an electric field and different polarisation mechanisms will be present. The electric field response can be explained by **four different mechanisms of polarisation** [5]:

1. <u>Electronic:</u> Displacement of the electrons orbiting the nucleus of the atom according to the field, creating temporarily dipoles.
2. <u>Ionic</u>: Positive and negative ions are pulled to their opposite charged electrode.
3. <u>Orientation</u>: Molecular shift of the permanent dipoles.
4. <u>Interfacial absorption of charge:</u> Surfaces and interfaces near the electrode acquire the opposite charge and increase the total field locally due to charge super positioning.

The first two mechanisms happens instantaneously at the applied field and disappears if the field is removed. The latter two require some time to be completed, which can cause dielectric losses. All dielectric media have a certain relative permittivity, ε, which describes how they act when they are placed in an electrical field. The permittivity of the material is frequency dependent, ε_r (f) as the material requires some time to adjust according to the effect of the electric field. At high frequencies, the dipoles might not complete their polarisation, which causes a reduction in permittivity. Typically, in liquids the value of the relative permittivity is in the range 2-5 [6].

The electric field, E, can be described by Gauss law as the superposition of all charges ρ, free or bounded in the dielectric material [7].

$$\nabla \cdot E = \frac{\rho}{\varepsilon}$$

Eq. 1
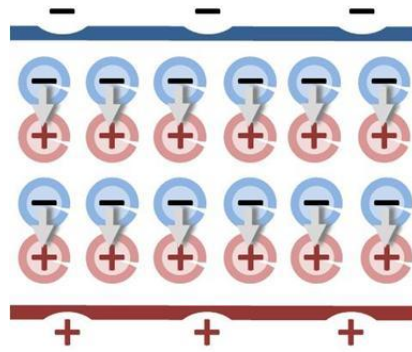
Figure 2 - Dipoles equally oriented to the homogenous field in a plane-to-plane gap

The electric field is initialized by the voltage difference between the two electrodes, with one high voltage side and one lower voltage or grounded side. A fulfilled dipole shift with an applied electric field is illustrated in Figure 2.

It is common to distinguish between homogeneous and inhomogeneous fields. An ideal homogenous field can be found between two plate electrodes with a potential difference, U, and a distance, d, separating them as in Figure 2 and the relation is given by:

$$E = \frac{U}{d} \ [\frac{kV}{mm}]$$

Eq. 2

If the potential difference becomes very large or the distance between the electrodes is very small, the electric field get sufficiently large for breakdown to occur.

Inhomogeneous fields have uneven charge distribution, which can be due to a non-homogeneous geometry, or because of local effects like space charges, which will be explained in 2.2. An example of a highly divergent field is the point to plane electrode configuration in Figure 3. An inhomogeneous field distribution is seen along the distance axis, where x=0 is at the tip of the electrode. Other sharp edged electrodes will have similar field distributions as the point to plane gap depending on the electrode geometry. Interfaces with different permittivity also gives rise to high local field.
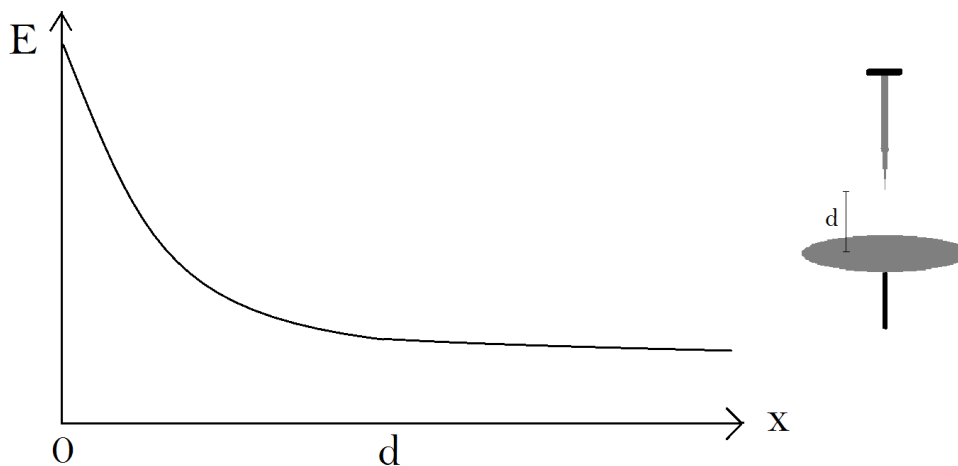

Figure 3 - Field distribution of a point to plane gap

The local electric field strength in a pointy configuration will be highly dependent on the radius of curvature of the tip and is approximated by:

$$E_{tip} \approx \frac{2 \cdot U}{ln\left(4 \cdot \frac{d}{r} + 1\right) \cdot r}$$

<div align="right">Eq. 3</div>

From the formula, one can see that a small radius of curvature causes very high electric field around the tip. The *active volume* is defined as where more than 90 % of the applied field is present. With increasing tip radius, the active volume also increases, as shown in Figure 4:
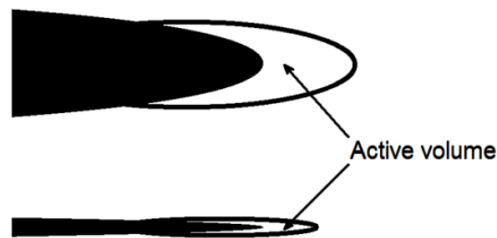

Figure 4 - Active volume decreasing with smaller tip radius [8].

2.2 SPACE CHARGE EFFECT

The normal field distribution for a point to plane gap was shown in Figure 3. There will be another inhomogeneous effect present; the so-called *space charge* or *polarity* effect. Space charges are charges where the location and concentration will influence the electric field locally. Space charges can be negative in form of for instance an electron or a negative ion, or positive in form of a positive ion (cation). Normally it is referred to as homo charges and hetero charges, which describes whether the charges are equal or opposite to the polarity of the nearby electrode. Homo charges will enhance the field strength close to the electrode, while the hetero charges will react with the opposite charges and weaken the total electric field.

With AC voltage applied, the field will change polarity every period, so that the local field is constantly changing. Electrons are very small compared to the ions so they have much higher mobility and will move much faster to the opposite polarity electrode. The distance dependent field, E(x), is shown in Figure 5 for positive and negative point electrodes. During the positive half period the electrons will move quickly to the anode and react with the positive ions around the tip, weakening the total field. The remaining cations in the bulk will locally increase the field, where they are left with low mobility, after the electrons have fled to the positive tip electrode. During the negative half period the most extreme field will occur as the electrons move away quickly, lowering the field far away from the cathode. The ions are then drawn to the negative tip resulting in a high local field.

In general, the polarity effect causes the electrons to either be repelled from or attracted to the high field region.
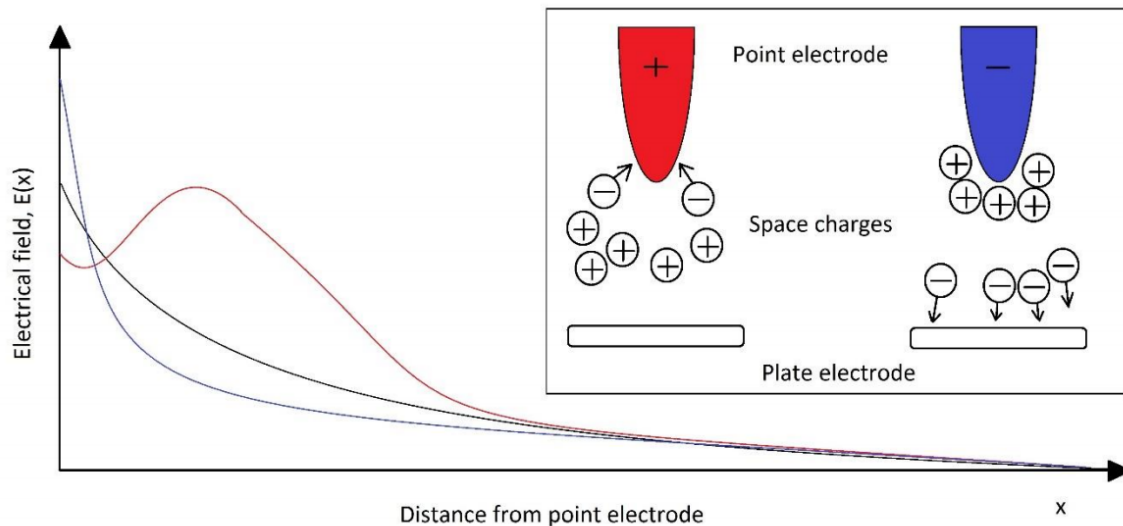
Figure 5 – The space charges effect on the field in AC point to plane electrode configurations [9]

2.3 WHAT IS A PARTIAL DISCHARGE?

Partial discharge (PD) is a local micro breakdown of a small portion of an electrical insulation system under high electric field stress. The discharge does not connect the two electrodes electrically, but bridge parts of the space between the conductors with a leading channel, lasting a very short period of time. Extreme electric fields, caused by for instance inhomogeneous geometries or contamination, lead to locally high electric field concentration. When increasing the voltage to a certain level normally called the Partial Discharge Inception Voltage (PDIV), the electric field becomes sufficiently large for initiating PD activity. Accordingly, reducing the voltage to a certain level called the Partial Discharge Extinction Voltage (PDEV), the partial discharge activity is substantially reduced or ceases completely. The PDIV and PDEV are dependent on the electrode and insulation setup, and have been defined in relation to PD measurements and test procedures [10]. The PDIV is of special interest as PDs will start weakening the insulation properties of the system and can reduce its lifetime.

It is important to note that PDs only occur when inhomogeneous fields are present. If a discharge is initiated at perfect homogeneous field conditions, it will cause full breakdown every time. With uneven field conditions, the discharge will be quenched when it spreads to where the field is lower than what is required for continuing the elongation. No electric field is completely homogeneous, so there will always be a chance of initiating PD. However, PDs are highly stochastic phenomena, conditioned on probabilistic events such as generating a starting electron required to initiate a PD.

2.4 DETERMINING FACTORS OF PARTIAL DISCHARGE OCCURRENCE IN LIQUIDS

The following is an attempt to sum up some theories and explanations of electric breakdown in liquids. Over the last few decades, the electric breakdown in liquids have been investigated, attempting to explain the mechanisms leading to breakdown. Due to the lack of a

6

comprehensive physical theory of liquid behaviour, findings and conclusions seem have contradicted each other [11]. Even the purest liquids will have some trace of contamination, which makes it difficult to isolate the mechanisms leading to breakdown [12]. The discharges in liquids are a complex mixture of processes combining gas discharge physics, fluid thermodynamics and fluid/interface motion [6]. As the discharges in liquid insulation have somewhat similar characteristics as gas discharges they are usually termed "streamers" or "leaders" from gas discharge theory [6]. It is common to name the processes after where they happen:

- Bulk processes (inside the liquid)
- Surface processes (at the electrode/liquid interface)
- Interface processes (at the discharge/liquid interface)

The road to full breakdown can be divided into three steps [13].

1. **Pre-breakdown phenomena**
   - Dissociations of ions
   - Field emission
   - Field ionization
2. **Propagation of the streamer channel**
   - Photo ionization
   - Impact ionization
   - Suspended Solid Particle
   - Cavity/bubble breakdown

3. **Breakdown**
   - The transition into an arc, which bridges the electrodes.

2.4.1 Initiation of pre-breakdown phenomena

To initiate a discharge a starting electron is required. A successful free starting electron will eventually form a conductive channel in dielectric insulation where the discharge occur. The main charge carrier is the free electrons, giving the dielectric a certain conductivity.

Once an electron has been freed up, it will be accelerated by the electric field until it collides with a molecule. The avalanche initiating conditions is when the energy obtained by the average free path length of an electron is equal to the ionization potential (IP):

$$eE \lambda = ch\nu$$

<div align="right">Eq. 4</div>

,where c is a constant, $h\nu$ is the photon energy lost due to ionization, h is Planck's constant, e is the electron charge, E is the applied electric field and λ is the average free path length of the electron.

The initiation of breakdown in liquids can roughly be split into two theories:

1. Electronic breakdown caused by the processes of photoionization, impact ionization, field emission, and field ionization.
2. Suspended particle or cavity breakdown due impurities like particles, fibres, bubbles, etc.

In general, a large electric field is what is required to initiate the processes that lead to PDs and breakdown. Factors found to cause large fields are contaminants and imperfections in the insulation material like cavities, particles, interfaces with difference in permittivity, or sharp pointed electrodes that gives high local field around the tip. Also the generation of the **space charges**, explained in 2.2, affects the local field strength [13], and is likely to be caused by **field emission** and **field ionization**, explained in 2.6. Breakdown can also occur due to combinations of electrical mechanisms and particles present inside the liquid.

Both dissociation of ion pairs and recombination of the ions occur, when no field is applied to the liquid. By applying an electric field, the dissociation rate will increase exponentially because the work required to separate the ion pair is lowered due to ionic polarisation.

Electrolyte content, which increases with increasing permittivity of a liquid, cause ion dissociation where the equilibrium reaction is [13]:

$$A^+B^- \leftrightarrow A^+ + B^-$$
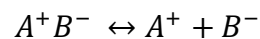
At local electric fields above 50MV/m, classified as large electric fields, the dissociation of ions in the bulk or interface is not enough to explain the fields' enhancement. Other physical phenomena like field emission, field ionization, impact ionization and electrochemical reactions must then be considered to explain the increased field [13].

2.4.2 Propagation of streamer channel

The streamer process is the formation of an avalanche which exponentially increases the electron concentration. The streamer formation can be explained by the percolation theory as described in Küchler [14]. The percolation theory is how the streamer follows a preferred current path, as some areas in the oil are disordered and more easily polarised. The combination of weakest-link breakdown in solids and the streamer mechanisms found in gas breakdown could possibly explain the breakdown in liquids. The streamer form in low-density conductive structures in the oil that are experiencing field stresses in order of 10^8 V/m or greater [15]. Only the initial part of the breakdown process, where a high field is built up prior to streamer formation, is due to the pure electronic processes of field emission, field ionization or impact ionization. Once this critical field stress is reached the streamer initiates. For the streamer to propagate once it has started only requires fields of 1-10MV/m [13]. Other field enhancing effects like photo ionization and impact ionization follow after the streamer initiation.

The streamer moves quickly through the insulation liquid. The duration and length of propagation is dependent on its energy gained from the electric field. The streamer grows

from the point of initiation towards a grounding point, and if it reached the grounding point an electric breakdown arc will form. If the streamer quenches before it reaches the grounding point, the term partial discharge is used.

Additives to the liquid, like water, electrolytes etc. might also affect the electric field conditions, but are not explained further in this project as it is not an object of discussion so far [6]. Pressure will also influence the PD activity; experiments in [16] show that fewer PDs are observed when increasing the pressure. Higher pressure increases the breakdown strength in liquids as it does in gases [5].

2.5 IONIZATION PROCESSES AND LIGHT EMISSION
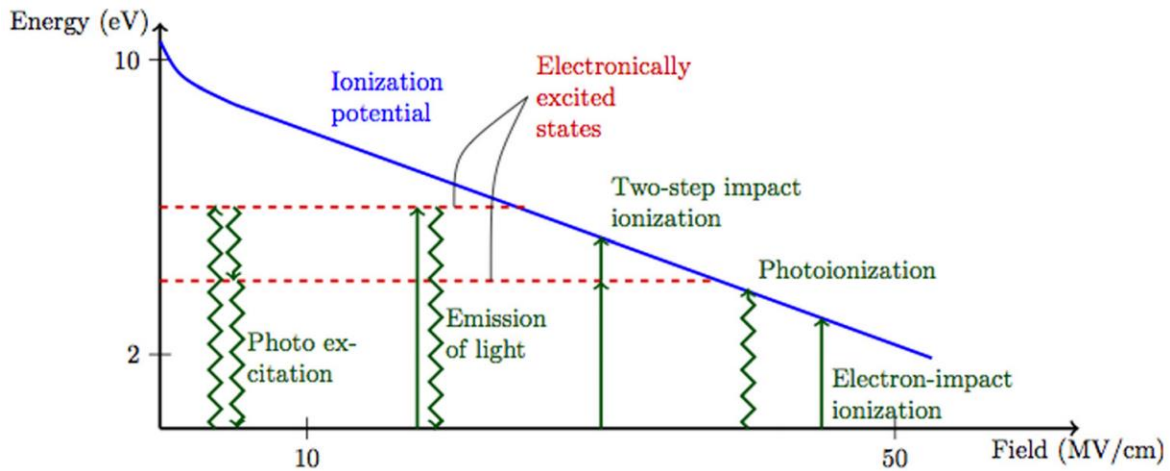
Figure 6 - Ionization processes and potential versus electrical field [17]. Wavy arrows represent photons while solid arrows are impact ionization.

The ionization potential (IP) describes the energy required to free up an electron from an atom or molecule:

$$IP = U_{A^+} + V_e - U_A$$

In general, ionization is defined as the freeing of an electron creating an ion from an atom or molecule. When an electron with a certain kinetic energy larger than the IP hits the atom the electron will be freed up. If the electron has less energy than the IP the kinetic energy will excite the atom, A, to a higher energy level inside the atom, A*. In this atom the electron is further away from the atomic nucleus, which is an unstable state. Hence, the electron will return to its original orbit, resulting in excess energy sent out in form of a quantum energy of photon (*hv*), and light emission occurs. [11] During PD-elongation, there will be many collisions with insufficient energy resulting in light emission. The photons might have enough energy to exceed the IP of another atom or molecule and ionize it, which in turn is called photoionization. The reactions can be explained by these formulas:

$$A + e + Kinetic\ energy \rightarrow A^* + e \qquad \textbf{Impact + excitation}$$

$$A + hv \rightarrow A^* \qquad \textbf{Photon excitation}$$

9

$$A^* \rightarrow A + h\nu \qquad \textbf{Photon emission}$$

$$A + h\nu \leftrightarrow A^+ + e \qquad \textbf{Photoionization}$$
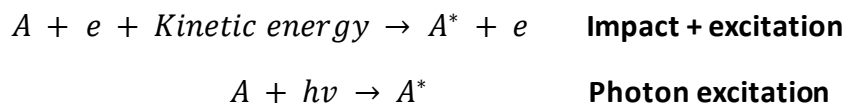
The opposite reaction of photoionization is called recombination. It involves recombination of electrons and ions, which will cause a quantum of radiation to be emitted.

The IP is related to all the ionization mechanisms, and is shown to be field dependent:

$$IP = IP_0 - 2\sqrt{\frac{E}{\varepsilon_r}} \qquad \textit{Eq. 5}$$

Figure 6 summarises the ionization mechanisms, but the mechanisms can also happen at other electrical field conditions than illustrated. At lower fields, ionization in two steps occur when an impact or photon absorption happen to an excited atom before it gets the chance to return to its ground state.

Above a certain electric field stress, an excitation state is no longer possible because all collisions with electrons and photon absorption will exceed the IP, so the only two states will be the ground state or complete ionization. There is a theory stated in [17], that when the number of excited states the atom or molecule can obtain are reduced, the insulation properties are altered and the transition of a slow streamer to a fast mode streamer occurs. Fast and slow streamers are explained in 2.8.

None of the pre-breakdown phenomena can excite atoms and cause light emission directly. Only when the propagation of the streamer has started, there will be recombination of ions which sends out the excess energy in form of a photon. Light emission can also occur related to excitation and subsequently photon emission.

2.6 FIELD EMISSION AND FIELD IONIZATION

Field emission is the event where an electron is emitted directly from a metal surface of the cathode due to high electric field. The potential barrier of such an injection of electrons to happen would require extreme local field; $1.4 \cdot 10^{10}$ V/m for copper [18]. Some amplification of the electric field will occur due to asperities or "micro rods" at the electrode surface, which increases the field locally. Another local effect called "tunnelling", lowers the potential barrier to the so called Fermi-level, so that electron emission can happen at lower fields [19]. In the late 1920s the physicists Fowler and Nordheim explained the effect that some electrons in the metal will have an energy above the Fermi level. There will be a certain probability of some electrons tunnelling through the energy barrier, leaving the negative electrode resulting in a field emission current [11]:

$$j = CE^2 e^{-\frac{D}{E}} \qquad \textit{Eq. 6}$$

,where E is the electric field and C and D are suitable constants. The tunnelling effect, injecting electrons into the liquid can make a small area around the electrode conductive. The formula is valid for low temperatures, but for higher temperatures, thermionic effects will work together with field emission as the electron's kinetic energy is increased due to the heat.

Field ionization are bulk processes happening close to the electrode. It occurs in an inhomogeneous field with a point or sharp anode. A large field causes an applied force strong enough to free up electrons from the bulk molecules. The electron will be withdrawn into the metal of the positive electrode, leaving positive ions behind and enhancing the field even more [16]. The injection of charge carriers will transfer momentum in the liquid causing a motion which is termed Electrohydrodynamic motion (EHD). Using the conservation of energy, one obtains an expression for EHD mobility:

$$\mu_{EHD} = \frac{v}{E} = \sqrt{\frac{\varepsilon_0 \varepsilon_r}{\rho}} \qquad [\frac{m^2}{Vs}] \qquad\qquad Eq.\ 7$$

For a typical hydrocarbon with $\varepsilon_r = 2$ and $\rho = 600\ kg/m^3$, the mobility becomes $\mu_{EHD} = 1.7 \cdot 10^{-7} m^2 V^{-1} s^{-1}$.
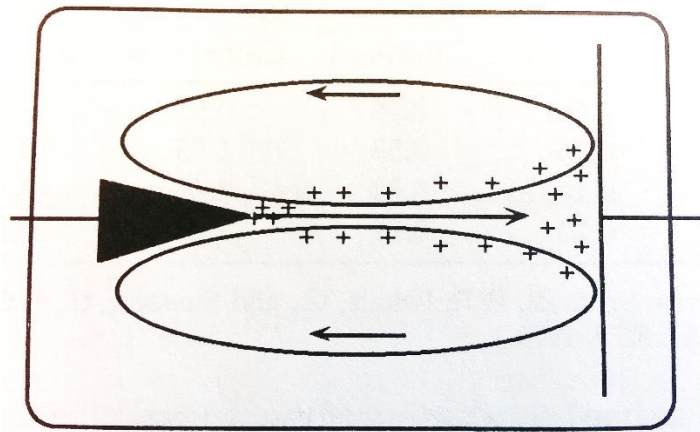
Figure 7 - Electrohydrodynamic motion induced by ions from field ionization [20]

2.7 SUSPENDED SOLID PARTICLE MECHANISM AND CAVITY BREAKDOWN

Contaminations like fibres and solid particles might be present in the liquid. The particle will be interface polarised, causing an electric field force that depends on the permittivity difference between the contamination and surrounding liquid. If the particle is spherical with radius r and permittivity ε, it experiences a force given by the formula:

$$F_e = \varepsilon_{liq} r^3 \frac{\varepsilon - \varepsilon_{liq}}{\varepsilon + 2\varepsilon_{liq}} E \cdot \nabla E \qquad\qquad Eq.\ 8$$

The direction of the force depends on whether if the permittivity is larger or smaller than the liquid's.

If $\varepsilon > \varepsilon_{liq}$ the particle will move toward where the E-field is highest with a velocity limited by properties including the viscosity of the liquid, and for lower permittivity (gas) the force will be opposite. Homogeneous field will cause particles to align, enhancing the field strength until it bridges the whole path between the electrodes. For inhomogeneous fields the particle will be attracted to the high field areas, increasing the stress, and improving the conditions for initiating PD activity.

Gas bubbles is another impurity phenomenon in liquid insulation that can cause breakdown inside the local cavity. The permittivity difference gives a larger electric field inside the cavity E_b [11]:

$$E_b = \frac{3E_0}{\varepsilon_{liq} + 2}$$

Eq. 9

,where E_0 is the applied field and ε is the liquid permittivity. PDs will occur when E_b reaches the PDIV of the gas, which occurs for lower fields than for the surrounding liquid. The presence of gas inside the liquid can be because of gas pockets on the electrode surface and generated by temperature and pressure changes. After the dielectric obtains a conductivity at a large field, corresponding effects like partial discharges, light emission and phase change, from liquid to a gaseous state, will happen. The collisions in the ionization process can also produce gas.

2.8 Dependence on the applied voltage

The applied voltage causing the large electric fields will influence the streamers and breakdown voltage depending on:

- Magnitude
- Polarity
- Wave shape (sinusoidal, impulse, etc.) with a certain duration, rise time and fall time

The magnitude of the applied voltage is proportional to the electric field. The discharge phenomenology is quite different for positive and negative applied voltage [6]. At AC, the voltage will change between positive and negative polarity each period changing the conditions and space charges. The space charge effect will cause PDs to happen first at negative polarity, but complete breakdown happens first for positive polarity. This is because the mean electric field for positive point polarity is higher than for negative polarity as illustrated in Figure 5. The positive streamers are accelerated over a longer distance and can travel longer into the insulation material.

The electric field distribution for negative electrodes will have a large maxima close to the electrode, due to direct free electron injection. However, once it leaves the large-field area it will slow down quickly as it has had a too short distance to build up high velocities. In general,

the negative streamers have a velocity of one order of magnitude smaller than the positive streamers. Both polarities can have fast (supersonic) and slow (subsonic) modes for sufficiently high fields [13].

Dependent on the applied voltage one can distinguish between four different positive streamers: primary, secondary, tertiary and forth mode streamers, shown in Table 1 . The fast discharges will propagate a longer distance, corresponding to a higher charge injected in the discharge and higher energy. The energy is given by $W = Q \cdot V$, where Q is the apparent charge and V is the magnitude of the instantaneous voltage.

How the discharges spread in the dielectric will depend on polarity. The positive discharges are generally spread in a filamentary "tree-like" way, and the negative discharges are bushier and bubbly shaped. The filamentary streamers seem to start from the same place [21]. In a point-plane electrode the bushy discharges are the result of the streamer channel initiation several places. This is related to field emission with several injections of electrons from the cathode. At negative polarity more gas is generated which cause many discharges close to each other. For a negative point electrode, the resulting conductivity experienced is mainly due to field emission. For positive point electrode the conductivity is mainly explained by field ionization, with absorption of an electron to the metal electrode from the bulk.

Table 1 – Positive and negative discharge modes and shapes [6], [12]

Polarity	Propagation velocity	Classification 1	Classification 2	Classification 3	Description
Positive	Slow	Subsonic	Bubbling		
	Fast <1 km/s	Supersonic	Primary	1st	
	~1 km/s		Secondary	2nd	Filamentary voltage independent
	~10km/s		Tertiary	3rd	Filamentary voltage dependent
	~100km/s		The fourth mode	4th	Filamentary ultrafast
Negative	Slow				Bubbly shape
	Fast				Filamentary

Experiments done in transformer oil have identified the four different propagation modes for positive streamers. The positive streamers are the most critical ones as they tend to initiate at lower voltages and propagates faster. Therefore mainly positive streamers are studied in experiments [12].

The positive, **primary** streamers are slow, 100 m/s to some km/s, and appear at modest voltages [6]. They are usually bush-shaped and hemispherical. The **secondary** streamers can travel much faster, many km/s depending on the liquid. They initiate at breakdown voltage, V_b, that indicates 50 % probability of breakdown. Their shape is filamentary and sometimes cylindrical at the end as they stretch over a longer distance. The **tertiary** streamers have more filaments and the velocity is voltage dependent. They are initiated at a certain acceleration voltage, V_a, where the velocity of the streamer radically increases [22]. The **fourth mode** is ultra fast and also voltage dependent where further acceleration quickly bridges the remaining electrode gap. The subsonic streamers start to form between initiation and breakdown level and the supersonic ones initiate above breakdown voltage level [17].

2.9 ACOUSTIC EMISSION

In this section, some of the theoretical background of acoustic emission detection is explained. This is done in order to be aware of the physical limitations and to understand how to design the detection system.

An acoustic signal can be explained as a densification and dilution of pressure propagating as a motion through a medium where the acoustic source is mechanically vibrating. The occurrence of a PD will be a vibrating point source to acoustic waves [23]. The PDs in oil cause sound waves in the ultra-sonic range from 20kHz to 1MHz [24]. The acoustic wave motion can be expressed by the elastic wave equation:

$$\nabla^2 p = \frac{1}{c^2} \frac{\partial^2 p}{\partial t^2}$$

Eq. 10

, where p is a harmonic function varying with time and location; $p(x,t) = p_0 \sin(\omega t \pm \frac{\omega x}{c})$ and c is the velocity of sound. The harmonic variation, models the repetition rate of the excess pressure with a period of $T = 1/f$ along the propagation path with wavelength given by $\lambda = \frac{c}{f}$. The speed of sound is determined by the physical properties of the media in which the sound wave propagates, and will be different in gas, liquid and solids. Analogous to electrical impedance, the medium has a characteristic acoustic impedance vector determining how fast the sound propagates. For planar waves, the impedance is a scalar; $Z = \rho_0 c$, where ρ_0 is the medium density.

An acoustic wave will attenuate as it propagates due to several mechanisms:

- Geometrical spreading of the acoustic wave
- Acoustic absorption due to the acoustic impedance resulting in heating losses
- Scattering at the wave front due to inhomogeneity

The intensity of the acoustic wave is inversely proportional to the square of the distance, r^2 from the source. Analogous to how electrical permittivity decrease for high frequencies, the

sound wave velocity depends on frequency. This frequency dependency, called **dispersion**, is how a sound wave split up into different frequencies when it passed through a material.

In gas and liquids, the pressure wave motion causes the acoustic wave motion. In solids, shear motion expressed by Hookes law can also create sound waves, so there will be one pressure velocity and one velocity caused by the shear force. Accordingly, speed of sound is different in different media. For instance, the velocity in air is 340 m/s, while tests in transformer oil show a speed of 1415 m/s. In solids like steel, the shear and pressure force will work in both longitudinal and transverse direction causing the speed of sound to be approximately 6000 m/s [23].

2.10 ELECTROSTRICTION

Electrostriction will be present when the liquid is exposed to strong-pulsed fields. Electrostriction is the mechanical strain resulting from a combination of the different polarization mechanisms causing a slight displacement of ions in a dielectric material. The strain is proportional to the square of the polarization [25].

An electrostriction pressure is formed in the liquid in relation to the strain and can be expressed by:

$$\Delta P_{es} = \varepsilon_0 \rho \frac{\partial \varepsilon}{\partial \rho} \frac{E^2}{2}$$

Eq. 11

,where the permittivity ε dependence on the density ρ of a liquid will affect the electrostriction [26].

2.11 DIELECTRIC STRENGTH OF LIQUIDS AND CHEMICAL PROPERTIES

The main objective of an insulation system, is to avoid breakdown and failure [27]. Insulation materials can be in the gaseous, liquid or solid state. To choose which form of insulation material is suitable, the whole system has to be evaluated. Breakdown mechanisms and partial discharge activity in liquid insulation has been investigated over the last decades, as liquid insulation has become more frequently used.

Because of a liquid's density, **the average free path length** of an accelerated electron is a lot smaller in liquids than in gases for the same field [6]. The initiation of an electron avalanche in liquid will require higher field, so the breakdown strength of liquids are approximately one order of magnitude higher than for air. Air has typically a breakdown strength of 2.5 kV/mm while liquids need 25 kV/mm or higher [18].

Choosing a liquid insulating material has the advantages of a natural cooling effect due to the circulation of the liquid because of temperature differences. In addition, voids can be avoided since the liquid fills the whole vessel. The viscosity of a liquid will determine how efficient the natural cooling is. Viscosity is defined as the amount of friction between adjacent layers of

liquid moving at different speed. The viscosity decrease exponentially with increasing temperature [20].

Liquids are approximately incompressible and can be used in pressurized environments giving a pressure compensated system when used at subsea with low risk of explosion. In addition, the pressure in the vessel can be used at a slight over-pressure to ensure that the oil will leak out before water can penetrate. Liquids are normally cost efficient which is important because high volumes are required. It is also important that the chosen liquid dielectric can handle the extreme conditions of pressure and temperature.

There are two main types of liquid insulation oils used in insulation systems; Mineral oils and synthetic oils. Mineral oils are normally clear and colourless distillates of petroleum containing hydrocarbons. Synthetic oils are often coloured and viscous and they consist of artificially compounds made in the laboratory.

When testing PD activity in different dielectric liquids a lot of the parameters change due to different material properties, so it is challenging to find correlations with respect to molecular structure [6]. Some molecular properties can however increase the probability of PDs. The longer the carbon chains in organic oils are, the less soluble it is, so the ion concentration is low. Low ion concentration decreases the chances of large local fields unless high voltage is applied. Hydrocarbons containing double or triple C-connections can capture electrons, so the mobility of the free electrons are reduced, increasing the dielectric strength [6]. In liquids containing electronegative atoms like fluorine, the electronic polarizability will be decreased compared to hydrocarbons since fluorine has a much stronger electron-withdrawing effect than the hydrogen atom [28]. The electron affinity and ionization potential of atoms and molecules in a liquid are easier parameters to check for correlation. The electron affinity is the amount of energy released after an atom gain an electron, for instance due to its electronegativity. Low IP and low electron affinity increase the chance of PD activity.

A hypothesis from [12] states that the streamers initiated at large electric field will depend on the molecular composition of the liquid. As an example the commercially used transformer oil Nytro 10XN contains some aromatic, but mainly naphthenic and paraffinic molecules which will have different IP. The transition from small PDs to breakdown can happen when the field stress suddenly becomes high enough to polarize a certain molecule type in the liquid. In Nytro the aromatic molecules have lower IP than the naphthenic and paraffinic molecules. When the field stress is high enough to polarize the main molecules can be compared to when the streamer transition from 2nd to 3rd mode streamers happen. It is clear that increased ability to ionize the high-density molecules will increase the amount of space charges generated, which in turn will enhance the electric field.

2.12 STATISTICAL BREAKDOWN ANALYSIS
The result from breakdown testing on insulations systems will give a data set that can be analysed using statistics. The intention of finding a mathematical model to fit the data set is

to be able to predict time breakdowns. Statistics also helps with analysing trends and trying to link it to the physical processes leading up to breakdown. A guide for insulation breakdown analysis is proposed by IEEE Dielectrics and Electrical Insulation Society in [29]. This guide is for sinusoidal voltage testing, but can be used for impulse testing if the failure mechanisms are known. The method in the guide is summarized in Appendix 9.4.

Typical failure distributions are the Weibull, Gumbel and lognormal distributions. Especially the Weibull distribution has shown to have a wide applicability for failure analysis. The distribution models weakest-link failure well. The Gumbel distribution models failures related to percolation theory where location of fault initiation is exponentially distributed. Therefore, it might be able to accurately describe breakdown insulation liquids.

The three-parameter Weibull probability density function is given by

$$P(U) = 1 - \exp[-\left(\frac{U - U_{min}}{U_{63} - U_{min}}\right)^b]$$

<div align="right">Eq. 12</div>

, where U_{min} is the lowest possible voltage causing breakdown, b is the shape factor and U_{63} is the scale parameter. The U_{63} − value denotes the expected breakdown value, analogous to the means value in the Gauss distribution. It corresponds to a $(1 - e^{-1}) \cdot 100\ \% = 63.21\ \%$ probability of breakdown.

U_{min} is normally difficult to determine and several combinations of the three parameters can give sufficiently fitting results. It is normal to use a simpler two-parameter model where U_{min} is assumed to be zero:

$$P(U) = 1 - \exp[-\left(\frac{U}{U_{63}}\right)^b]$$

<div align="right">Eq. 13</div>

Large values of b means that the variation between each breakdown strength is small. A large b can mean that physical flaws in the object are distributed uniformly throughout the material, whether inherent to the material itself or resulting from the manufacturing process. A low b can mean that the flaws are distributed unevenly and that one single test object is not a good representation for the breakdown strength.

The Gumbel distribution is closely related to the Weibull distribution where if U has a Weibull distribution, then y = ln (U) has a Gumbel distribution. The relation is expressed with a location parameter u = ln (U$_{63}$) and a scale parameter β which is the inverse of the shape factor $\beta = 1/b$ for Weibull giving:

$$P_G(U) = 1 - \exp[-\exp(\frac{U - u}{\beta})]$$

<div align="right">Eq. 14</div>

3 METHOD

Observing PDs at the PCB electrodes are a challenging task due to their stochastic nature. Figure 8 shows the electrode cross section of the main test object used in this experimental work. The critical triple junction is indicated in the figure at the tip of the high voltage electrode. A highly divergent field will be present at high voltages across the 1.73 mm electrode trench. Despite the divergent field nature of the board, once a streamer has initiated it might lead to breakdown straightaway. In the following the methods used for reliable PD detection and performance of breakdown tests are explained.
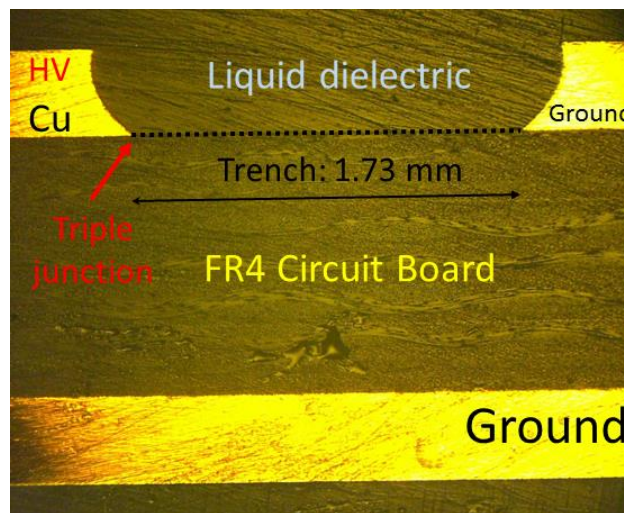

Figure 8 - Cross section of PCB Trench marking the triple junction between board, electrode and liquid insulation

The dielectric strength tests and PD detection performed in the laboratory has been performed in in three different setups:

1) Setup with light-sensitive high-speed camera
2) Low-noise setup with sinusoidal voltage source
3) Low-noise setup with fast switching voltage source (modified from setup 2)

A lot of the same detection equipment have been used in the setups.

3.1 TEST SETUP 1 – PRE-TESTING

To get familiar with the system response and the sensitivity of different detection methods of partial discharges preliminary tests were performed in the test setup shown in Figure 9. The PDs were observed by a high-speed light-sensitive Phantom Camera. Observing PDs in such a camera gives the certainty of PD occurrence and provide the location of the PD. Test setup 1 had a high electrical noise level above 5 pC, hence the optical and acoustic detection had to be utilized to check for PD.
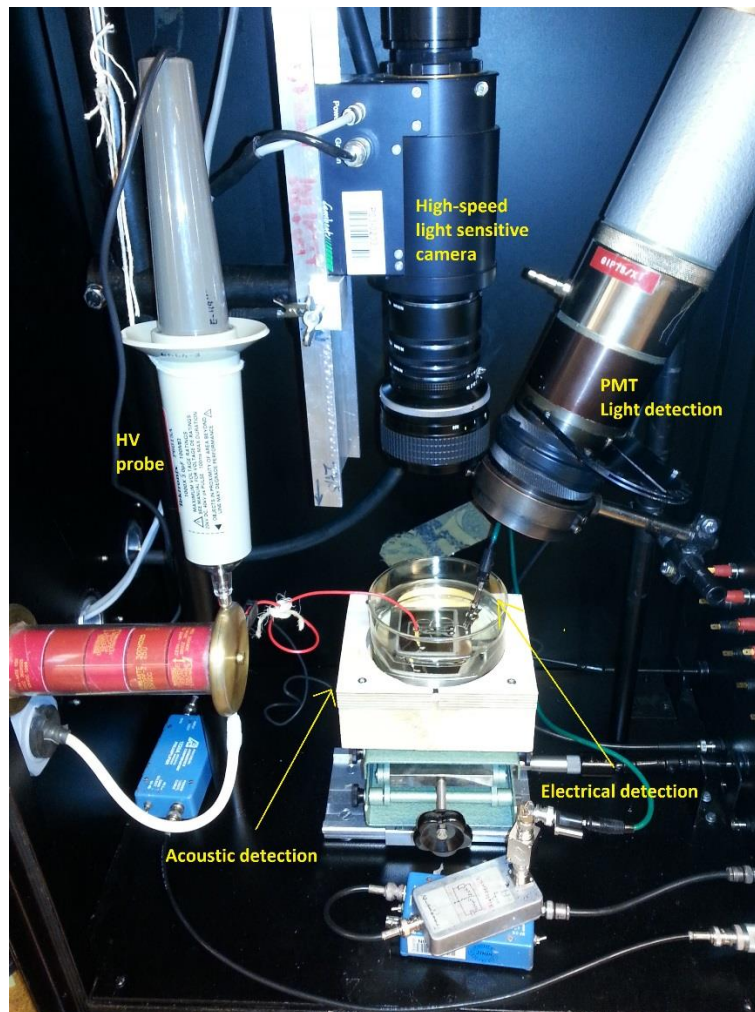
Figure 9 - Test setup 1, with high-speed camera, but high electrical noise.

IGBTs normally have circuit boards where the electrodes are mounted on a substrate of Aluminium Nitride (AlN). This AlN-substrate have been observed to have electroluminescence [30]. Such AlN-boards are the ones tested in other experiments within the SINTEF Presspack project. If a PMT is used to detect light from PDs on this board, it will give light impulses that does not origin from discharges. The PCBs have been designed with FR-4-substrate, which does not have electroluminescence. The PCB-design have a trench with the same dimensions as the AlN-board, so the electrical field conditions should also be similar. The breakdown behaviour of PCBs should be representative to how AlN-boards would behave, except when it comes to light emission.

In the pre-testing, different test objects were used and has been summarized in Table 2.

Table 2 - Test objects tested in Test setup 1

a) **Point-to-plane gap integrated in a circuit board**
- To ensure high field conditions and a high PD activity easy detectable
- Used PC activity verification

b) **IGBT module electrodes with Aluminium Nitride (AlN) Substrate**
- Close to real conditions
- To check for PD location
- Electroluminescence from the substrate showing light in the PMT, which does not originate from PDs [30]
- Inserted BG18 light filter excluding most of the photons outside the range of 350-650 nm wave length λ
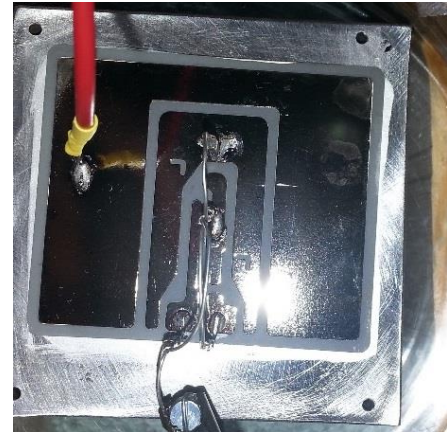
c) **Printed Circuit Board Electrodes at FR4 substrate**
- To avoid electroluminescence from substrate
- Similar, but cheaper and smaller than IGBT electrode boards
- Main test object
- Both with (right) and without (left) 27 µm Parylene surface cover shown in the picture

3.2 TEST SETUP 2 - SINUSOIDAL

The low noise test setup used in the project thesis [4] and in a previous master thesis [9], is shown in Figure 10. The high voltage supply is generated from an independent AC source to avoid the line voltage's variation to influence the test results. A stable sinusoidal voltage is obtained from a small **Goodwill Signal Function Generator**. To reach high voltages, two transformers are used. The function generator itself cannot deliver enough current to overcome the power losses in the first transformer. To solve this problem, a stereo amplifier is placed in front of the transformer. For the first sinusoidal tests a **NAD Stereo Amplifier** was used, but was replaced by a **Cewin Vega Home Audio CX-10 Power Amplifier** due to problems

with overheating. The overheating was caused by energy dissipation in the amplifier, as the circuit input impedance it experienced was too low. The frequency is set to 38.5 Hz as it gave a perfect resonant circuit, measured with a **Fluke Power Quality Analyzer** at the output of the amplifier.

For further noise reduction, the setup was placed inside a Faraday cage. A current limiting resistor, R, of 35.15 kΩ was connected in series with the test cell to avoid high peak current and excessive decomposition of the liquid if breakdown should occur [10].
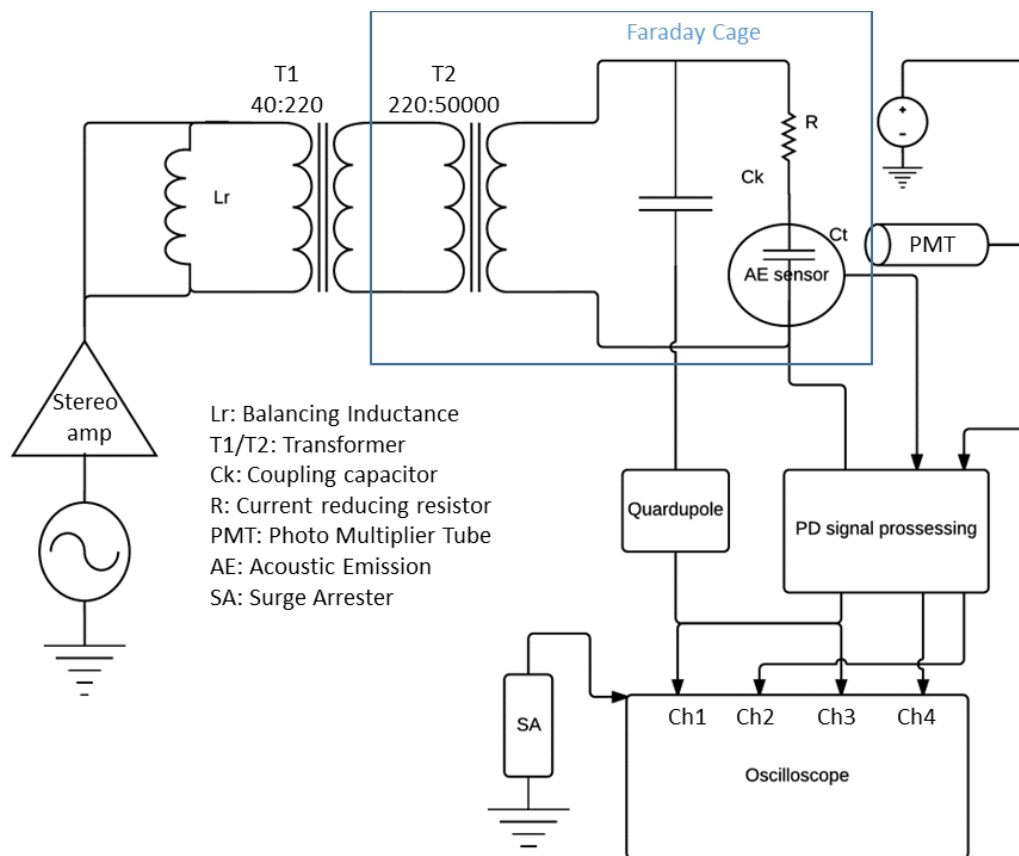
Figure 10 - Test setup 2

3.3 TEST SETUP 3 – FAST SWITCHING

The switching test setup is the same as for sinusoidal voltage, only that the voltage source and the circuit inside the Faraday cage is modified, as shown in Figure 11.
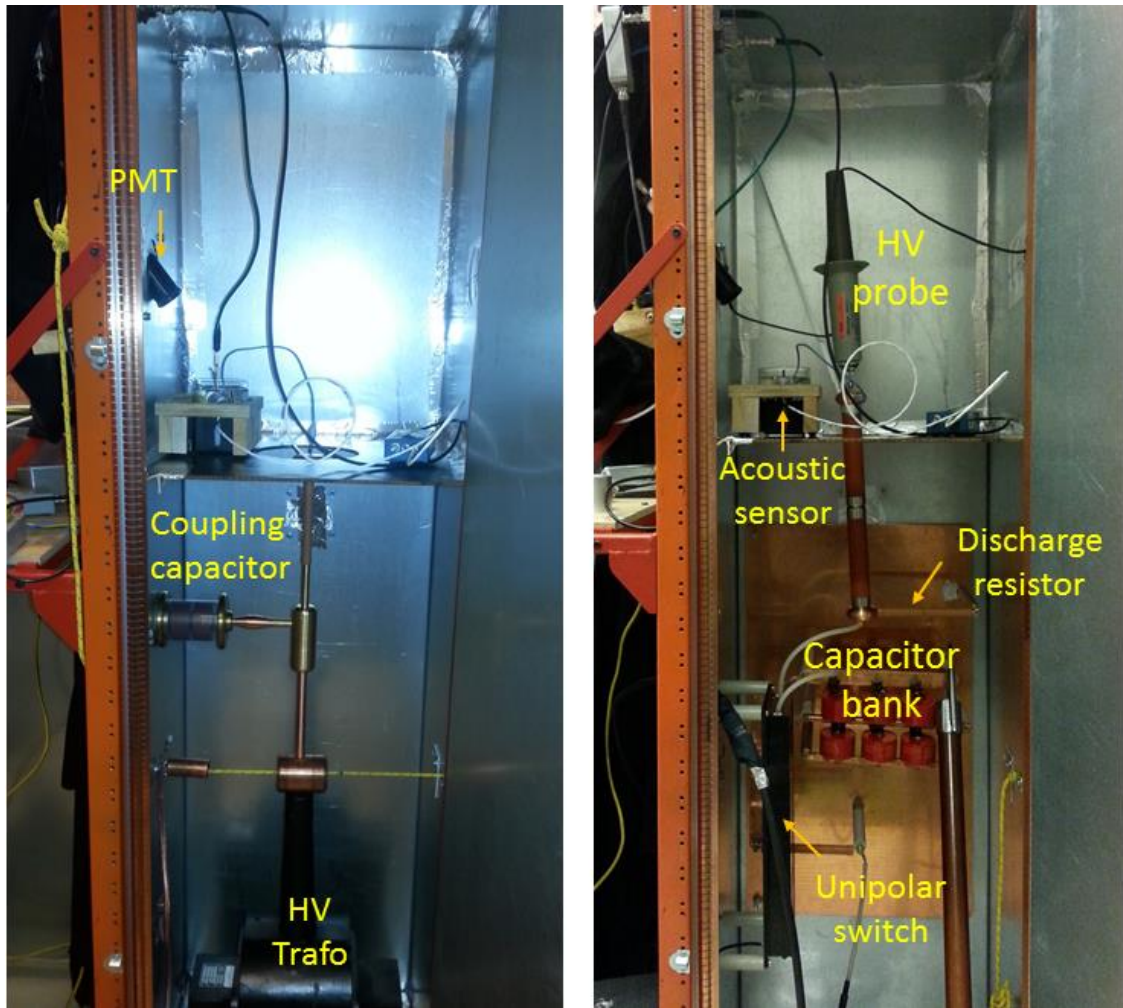
Figure 11 - Test setup 2 (left) and test setup 3 (right) showing some of the main components

A fast turn-on switching circuit has been designed in order to perform measurements closer to the fast switching frequency in an IGBT. The circuit design is shown in Figure 12. Here the high voltage DC source charges up a capacitor bank, C_k, consisting of three pairs of a high voltage capacitor in parallel. Each capacitor has a capacitance of 3300 pF, giving a total capacitance of 4.95 nF. The capacitor bank is charged with a time constant τ_1. Once the switch closes, the voltage is applied from the capacitor bank across the test object, C_t, nearly instantaneously, with a small time constant τ_4.

The circuit consists of several RC time constants explaining the charging and discharging occurring in advance and right after each switching operation. R_1 is a large resistor that should limit the current from the DC source to maximum 1.5 mA. R_3 is also a current limiting resistor in series with the test object, which should keep the current below the rated current of the switch. A large resistor, R_2, is placed in parallel with R_3 and the test object. This will cause nearly all the current to pass through the test object. The capacitor bank also gets discharges with a time constant τ_2 because of the resistor R_2. The capacitor bank should be large to supply the test object with sufficiently high voltage. When the switch opens again, the test object is discharged through R_2 and R_3 with a time constant τ_3.

23
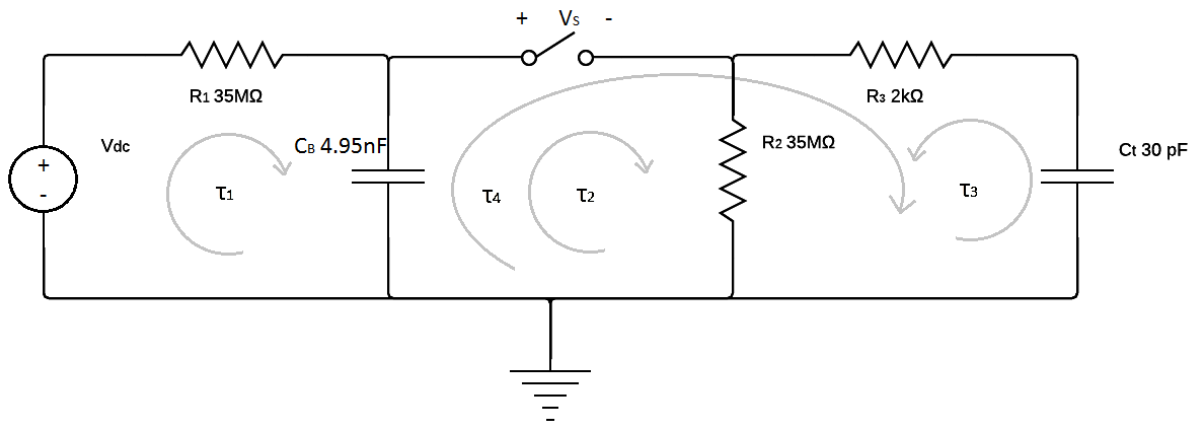
Figure 12 – Circuit design for fast turn-on voltage across test object

Table 3 - Time constants for charging and discharging

τ_1	τ_2	τ_3	τ_4
0.173 s	0.173 s	1.05 ms	6 ns

The switch used in the experiments is a fast, unipolar high voltage transistor switch from Behlke with a rating up to 65 kV/30 A. A controlled turn-on is achieved by a positive square wave voltage of 5 V coming from a Goodwill Signal function generator. The 5 V signal is converted in an electrical-to-optical signal converter and the optical signal goes to a low voltage TTL (Transistor-Transistor-Logic) controlling the switch.
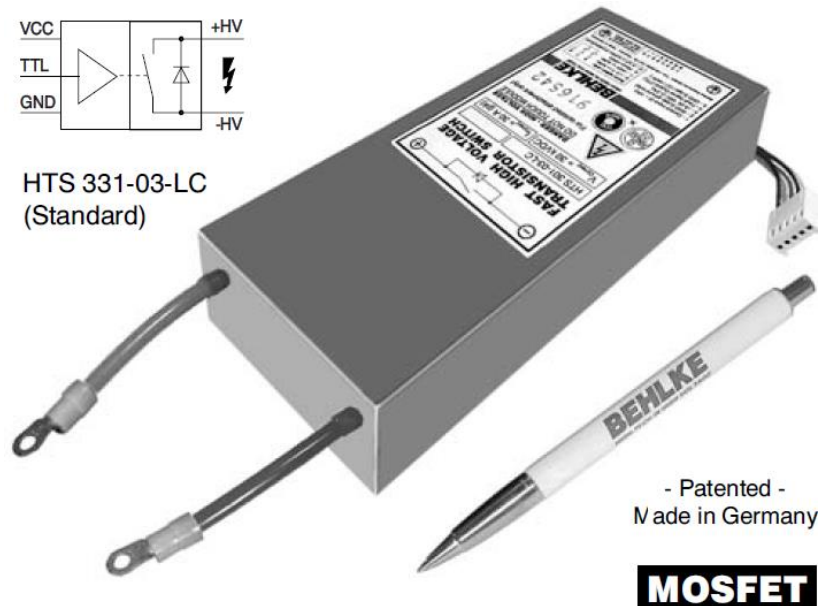
Figure 13 - Behlke (65 kV/30 A) Fast High Voltage Transistor Switch [31]

3.4 PD Detection Method

3.4.1 The Oscilloscope

A DPO5104 Textronix Oscillosope is used in all setups. All four input channels are used for the three different PD detection signals and the voltage measurement. These channels have been used with the same signals throughout the experimental work. The channels will appear in several screenshots in the results and is given as:

Ch1: Electrical PD signal

- Ch2: PMT PD Light Signal
- Ch3: Voltage waveform. Approximate voltage across test object
- Ch4: Acoustic PD signal

A surge arrester is connected to the oscilloscope's fifth channel for overvoltage protective reasons.

3.4.2 Calibration

Before starting the electrical PD measurements the measuring system needs to be calibrated. A PD Calibration apparatus is placed in parallell with the test object and injects a known charge in either polarity in the range of 1-100 pC.

3.4.3 Electrical PD Signal detection

Detecting the occurrence of PDs can be a rather complicated task as they are fast, small and have broad frequency spectra. Since the duration of each current pulse from these discharges is normally much less than 1 μs, closer to nanosecond range, the detection equipment needs a short sampling time [32]. The sample rate can be varied at the oscilloscope and is set to 2 Giga samples per second (Gs/s).

PDs are broad banded pulse phenomena, which implies that the pulses can have frequency components at many different frequencies [33]. The PD detection system should therefore include a broad band of frequencies. Narrow bandwidth can be used if the PD is prominent in a certain frequency area. Normally, large frequency ranges are used for PD detection, as for oscilloscopes with bandwidths of typically 1 GHz.

The measuring impedance, capacitors, and inductors in the measurement system will affect the frequency response of the discharge. The circuit can be both capacitive and inductive, dependent on which components are used. It is important to note that the output signal's shape, duration and peak value are formed by all the individual parts in the total system impedance of the measuring circuit.

Many PD detection systems utilize the measurement of the apparent charge. Apparent charge denotes the charge that could have been injected at the terminals of the test object and give the same output on the measurement system as the PD pulse. The apparent charge is normally

measured in picocoulombs [pC]. 1 pC is a small unit indicating that PDs have low magnitude. PD measurement circuits require high gain amplifiers to increase the low magnitude.

A custom-made LCR-filter is placed in series with the test objects to create a critically damped PD pulse. The circuit parameters of 100 pF, 2.5 H, and a variable resistor manipulates the PD signal to be nearly without oscillation.
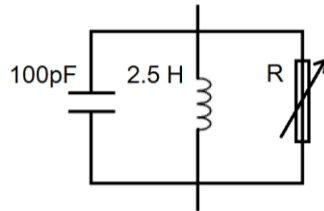

Figure 14 - LCR-filter

Furthermore, a preamplifier and a measuring shunt is connected in series after the LCR-filter. The capacitive measuring shunt and the pre-amplifier, set to 40 dB amplification, is shown in Figure 15. Operating the preamplifier and shunt together, requires a DC source of 28 V or three 9 V batteries.

a)   *b)*

Figure 15 – Preamplifier (a) and capacitive measuring shunt box (b)

High sensitivity can be obtained by utilizing a coupling capacitor with a higher capacitance than the test object as recommended in [32]. The coupling capacitor in Figure 10 consists of two capacitors in series, each of 2 nF, with a total capacitance of $\approx$ 1023 pF. This is sufficiently large compared to the small test object capacitance of 30 pF.

3.4.4 Optical PD detection

The photon emission from PD-activity causes photons to be sent out in every direction. Some of the photons will hit the Photomultiplier Tube (PMT), which is directed with an angle down at the test object. A Hamamatsu R1635 PMT is used in this project and is shown in Figure 16. Photons are normally too small to be measured, but the PMT is designed to amplify the signal.

The R1635 tube consists of eight dynodes. A photon will kick loose an electron from the cathode, which will be sent to the first dynode in the tube, knocking loose more electrons due to its kinetic energy. These electrons will again hit the second dynode and each knock loose more electrons. The voltages applied at the dynodes Dy1-Dy8 are increased throughout the tube to accelerate the freed electrons to move further until the end of the tube at the anode. The total multiplication leads to a current amplification of approximately $1 \cdot 10^6$ [34].
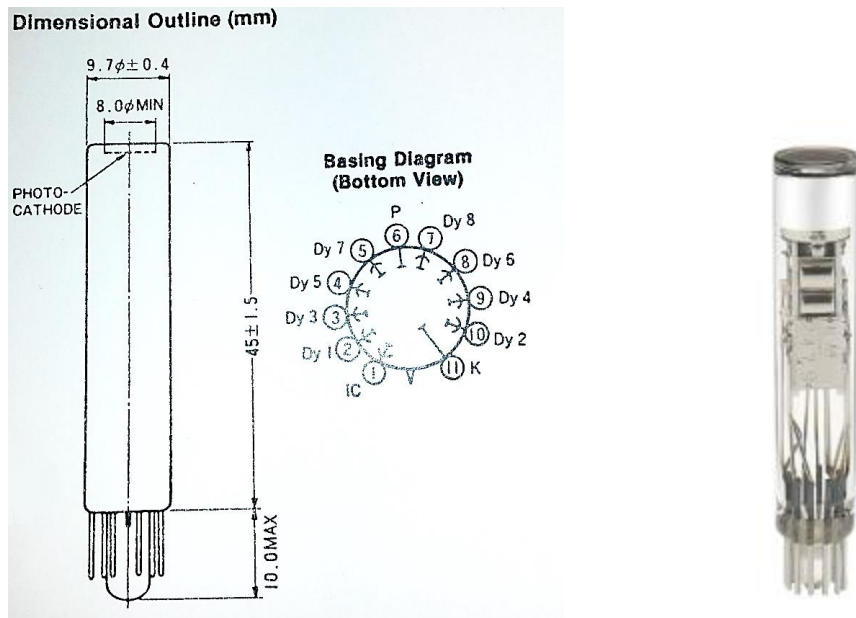
Figure 16- Photomultiplier Tube R1635

The photomultiplier tube will always have some random noise pulses, which are often called dark currents. Dark currents are not caused by photons hitting the cathode of the PMT, but by random free electrons at the cathode of the photomultiplier hitting the dynodes and amplifying themselves. Dark currents are unwanted noise, since they are not a result of light emitted. The PD light pulses measured are in range with the amplitude of the dark currents, so it can easily lead to problems by differentiating between the pulses caused by light emission from PDs and dark currents. The PMT requires a DC-supply of 1250 V for normal operation, and an Oltronix stabilized rectifier is used.
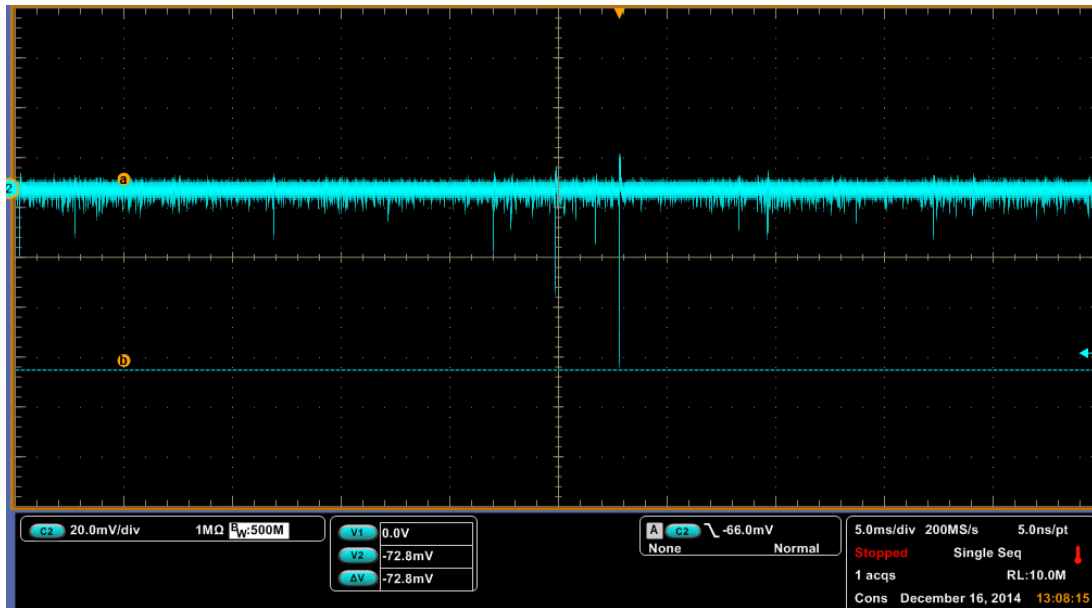
Figure 17 – Showing typical dark current signals in the PMT showing with random amplitudes ranging up to 73 mV or higher. However, most dark current signals are smaller than 73 mV [4].

3.4.5   Acoustic Emission detection

One of the greatest advantages of acoustic partial discharge detection is its immunity to electromagnetic interference (EMI). At on-site field conditions, the EMI will make it difficult to detect PD by the conventional electrical methods, as it will be hidden beneath a noise level higher than the discharge magnitude [35]. The technique of Common Mode Rejection (CMR) is used in acoustic detection, where two simultaneous acoustic signals are measured and compared in a differential electrical configuration so that fake signals and noise can be omitted.

Choosing a suitable acoustic sensor will be a trade-off of between bandwidth and sensitivity. To ensure a wide frequency band the size of the sensor must be small compared to the wavelength of the signal. Reduced size will on the other hand reduce the sensitivity. Usually, for PD detection, acoustic emission transducers are used. They are resonant sensors with damping materials at the back, shown in Figure 18. Such sensors have been developed for different frequency ranges from 30 kHz to 1 MHz. The sensor produce an electric signal proportional to the velocity of the acoustic wave travelling through it.

A thin layer of grease is applied in order to ensure that the sensor is sticking to the test object, reducing attenuation, increasing the sensitivity. A magnetic hold down or elastic band can be used to keep the sensor in place.
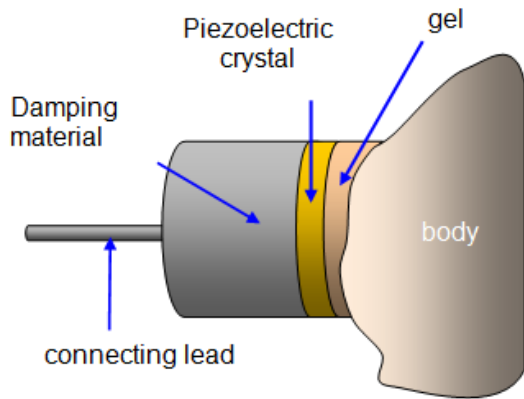
Figure 18 - Piezoelectric transducer drawing from [3] to the left and the acoustic sensor used in the thesis to the right.

The acostic signal will have a detection time lag dependent on the media it propagates in before it reaches the sensor. The acoustic wave will travel through the liquid, glas, grease and steel with different speeds, which will cause some attenuation and time lag.

One preamplifier and one measuring shunt with DC supply are connected in series with each of the detection sensors (electrical, optical, and acoustic) before entering the oscilloscope.

3.4.6   The main test object
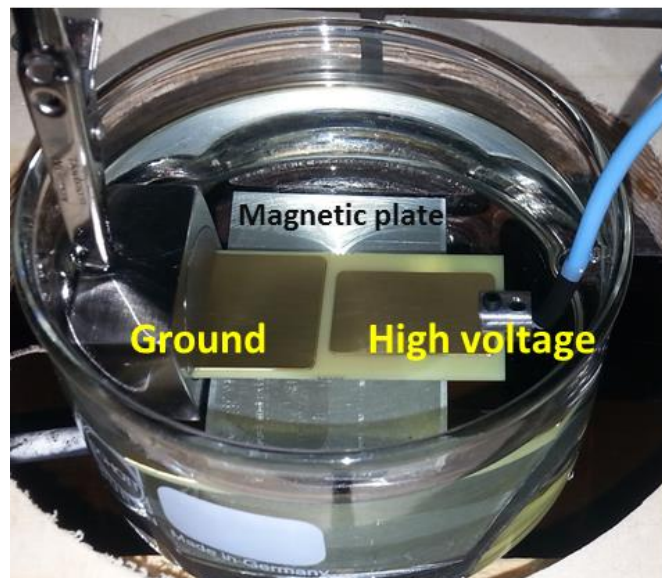
Figure 19 - Test object submerged in dielectric liquid

The complete test object with board and liquid is shown in Figure 19. The capacitance between of the test object is measured with a Escort Dual Display LCR Meter and found to be 30 pF. It was measured between the high voltage side and the two ground plates on the PCB, when

submerged in transformer oil. The right electrode in Figure 19 is connected to the high voltage side of the circuit. The left electrodes, one on top of the PCB card and one at the bottom, are connected to ground. The whole board, with the connections, is placed in a 150 mL glas cup filled with ≈ 100 mL dielectric test liquid. A 3 mm thick, 8 x 5 cm, steel plate is placed at the bottom of the cup. This plate is magnetically connected to an magnetic casing for the acoustic senor which is placed directly underneat the cup. Additionally, the ground side of the board connection is magnetically connected to the steel plate, grounding it.
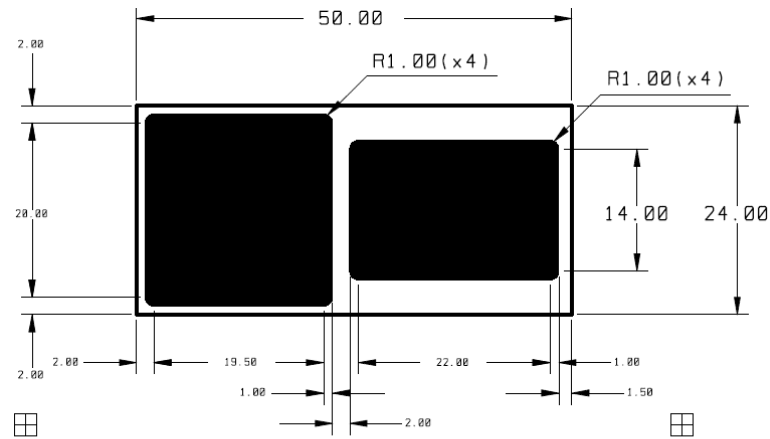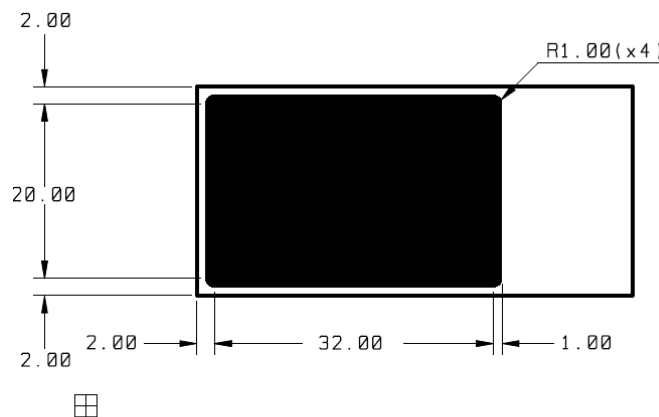
Figure 20 - PCB test board dimensions showing top side and bottom side of the board

Three dielectric test liquids with different chemical properties are tested:

- Nytro 10 XN
- Midel 7131
- Galden HT230

The dielectric liquids are referred to as just Nytro, Midel and Galden as a simplification. The liquids have been chosen to get a variety of different dielectric liquids. Nytro is the mineral oil, Midel is a synthetic oil and Galden is a heat-transfer perfluorinated polyether (PFPE). The water in the oils are obtained 16th of June from employees working at SINTEF Energy Research. The water content for Nytro and Midel reported to be is approximately 2 ppm and 25 ppm respectively. The values have been measured using the Karl Fisher Method and are obtained from former experiments. Keeping the oils in closed containers up until testing, will keep the water content approximately unchanged. The water content is therefore assumed to not affect the breakdown strength considerably.

Nytro 10XN

Nytro is a commonly used transformer oil with a mix of several molecular structures. Three structures are prominent in the liquid; naphthenic, paraffinic and aromatic hydrocarbons. Napthentic and aromatic molecules both have ring structures. Napthentics have only single bonds, while aromatic molecules have some double bonds and are thereby unsaturated. The paraffinic molecules are linear and saturated alkanes with the typical chemical structure of C_nH_{2n+2}. Nytro has a high dielectric strength, good heat transfer abilities, oxidation stability and it work well also at low temperatures due to its naphthenic content [36].

Naphthenic (Cyclohexane)	Paraffinic /Alkane	Aromatic (benzene)
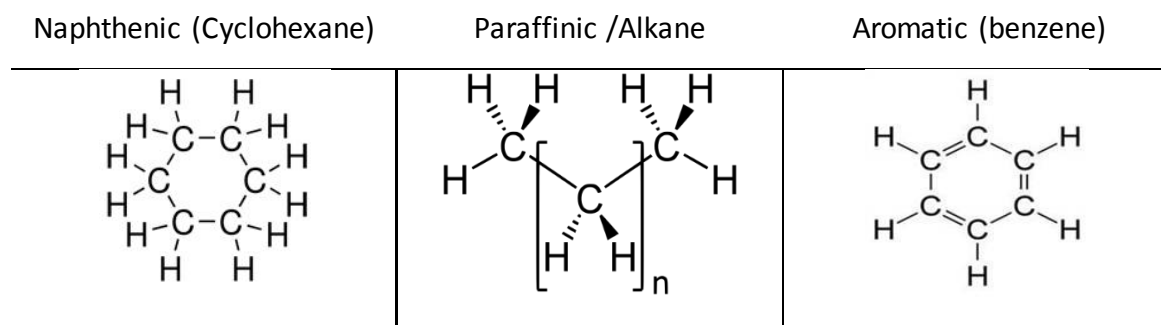
Figure 21 - Chemical content of Nytro

Midel 7131

Synthetic oils like Midel 7131 are ester oils that have the important property of low flammability with a higher flash points than mineral oils. The oil is based on a pentaerythritol tetraester shown in Figure 22 , where R is an alkyl group ranging from C_5H_{11} to C_9H_{19}. Midel 7131 contains the characteristic carbonyl group, which is a double binding between carbon and oxygen. Midel 7131 has already been used in many applications e.g. transformers, for over 30 years [37]. Synthetic oils are used increasingly because of environmental concerns and due to growing prices of mineral oils [38].
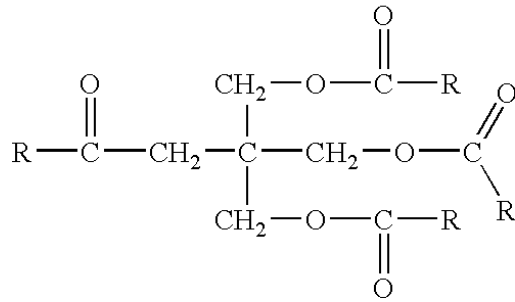
Figure 22 - Pentaerythritol tetraester base components in the synthetic ester oil, Midel 7131 [39]

Galden HT230

Galden HT (Heat Transfer) is a line of Galden dielectric liquids with a high boiling point. The Galden used in the following tests has a wide operating range from 0-230 °C [40]. The fluid is a perfluorinated polyether (PFPE) which gives it good dielectric properties at hostile high field conditions found in semiconductors. The molecular structure of Galden in Figure 23 shows that Galden consists of only single bonded carbons, and have strong bonds of fluorine-carbon.
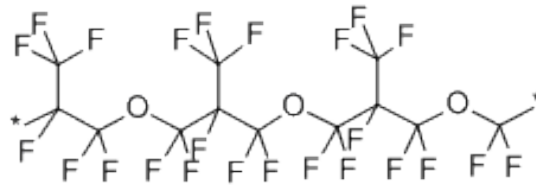
Figure 23 – Chemical structure of Galden HT70 [41]

3.4.7   Parylene coating

Parylene is a thermoplastic film polymer which is based on para-xylylene and made by vapour phase polymerization [42]. The cover is applied by condensing a polymer from the vapour onto the substrate and electrodes in the PCB trench. The thickness of the layer is 27 µm.

3.4.8   Voltage measurement device

For measuring the voltage across the test object at the oscilloscope, a low voltage copy of the HV is required. For sinusoidal testing, a PD Quadrupole that reduces voltage by a factor of 1000 is used.

For fast switching, a high voltage probe is used to measure the voltage at the test object. Due to protective reasons, the high voltage probe should not be used at voltages above 20 kV, so it could not be used during the testing. The DC source voltage is read from the scale at the source and the corresponding voltage at the test object is measured with the high voltage probe. The voltage at the DC source corresponded to 1.5 times the voltage at the test object.

3.5   NOISE REDUCING MEASURES

Noise is inevitable, but can be reduced to a tolerated level. The acceptable noise limit is given by the signal to noise ratio, and it is desired to have this ratio as high as possible.

Typical sources of noise can be Electromagnetic Interference (EMI), which includes both electromagnetic induction noise and radiation summarized [43]. Noise can also originate from poor contact, corona discharges or even PDs at other locations inside the system. The IEC standard 60270, test method for AC partial discharge measurements, states that the test circuit should be discharge free except for at the test object at the highest test voltage applied [44].

The connections in the test setup should not have sharp corners and edges, as this will cause charges to assemble at these edges, leading to a high electric field strength [45]. The electric stress will lead to unwanted discharges that are not interesting to measure. To avoid this effect, a good design is rounded and symmetrical. This will provide an evenly distributed stress at all parts of the setup with high voltage potential. Semiconducting tape or a toroid can be used at critical points to smooth out the electrical field.

Screened walls can be used to otained a reduction in the noise. This will create a Faraday cage around sensitive components preventing the noise from being picked up. Test equipment with electric circuits are generally placed inside a metal box as in Figure 15, shielding the components from external influence.

3.6   CLEANING AND FILTERING PROCEDURE

To minimize the amount of contaminations present in the test, the glass cup, test boards and connections should be cleaned to avoid dust and oil remains influencing the breakdown strength. The aim is to have as similar conditions as possible for each test object to obtain trustworthy results. Contaminations like oil remains or fibre particles might distort the BD voltage. When changing the test board, the glass container and oil was always replaced with a clean cup and new oil. Chemical reactions in the oil and carbonized particles floating in the oil generated in the breakdown flash, can change the dielectric strength. Replacing the oil will help prevent this effect. The glass containers were cleaned properly with isopropanol, dried and blown dust-free with a pneumatic air gun blowing out clean, pressurised air. The objects were cleaned in a laboratory under an air extractor hood to minimize dust particles. The first cleaned test objects were examined in a microscope to confirm that the procedure gave sufficiently clean objects. When practically no dust particles could be observed in a VHX Digital microscope, the object was declared clean enough. To minimize polluting, the objects were placed in plastic zip bags during transportation from the cleaning lab and up until testing. Assembling test object in the cup right before testing, was performed under an air extractor pipe trying to avoid dust particles.

The Nytro oil used in the experiments, came from a large transformer tank in the high voltage lab at NTNU. The Midel oil was collected from a large barrel at SINTEF Energy Research. As the contamination conditions of the oils were unknown, the oils were filtered using a setup shown in Figure 24, with a filter with 0.22 μm holes. A vacuum pump was utilized for a more efficient draining of the oil through the filter. A thin layer of anti-seize vacuum grease was applied on the connecting parts between the vacuum suction chamber and the Erlenmeyer flask at the

bottom. Galden came in a 3 L sealed container and was hence assumed nearly contamination free. Due to time limitations the Nytro tested at fast switching was not filtered.
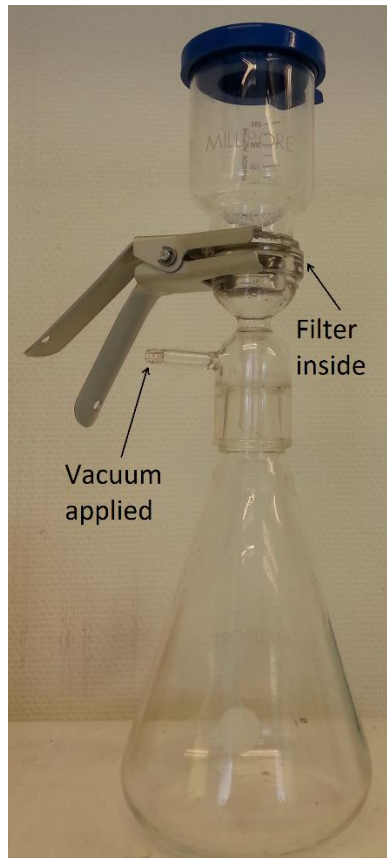
Figure 24 - Millipore filtering equipment

3.7   METHOD OF RECOGNIZING PARTIAL DISCHARGES

In order to be familiar with the PD signal shape, several test boards were investigated. This was to examine and make sure that the signals were discharges and not random noise. The shape of the signals and their phase response was also explored through pre-testing in test setup 1. The stochastic nature of PDs makes the signals look slightly different dependent on several factors e.g. origin, polarity and voltage level.

In general, the observation of PDs showed signals similar to the ones in Figure 25.
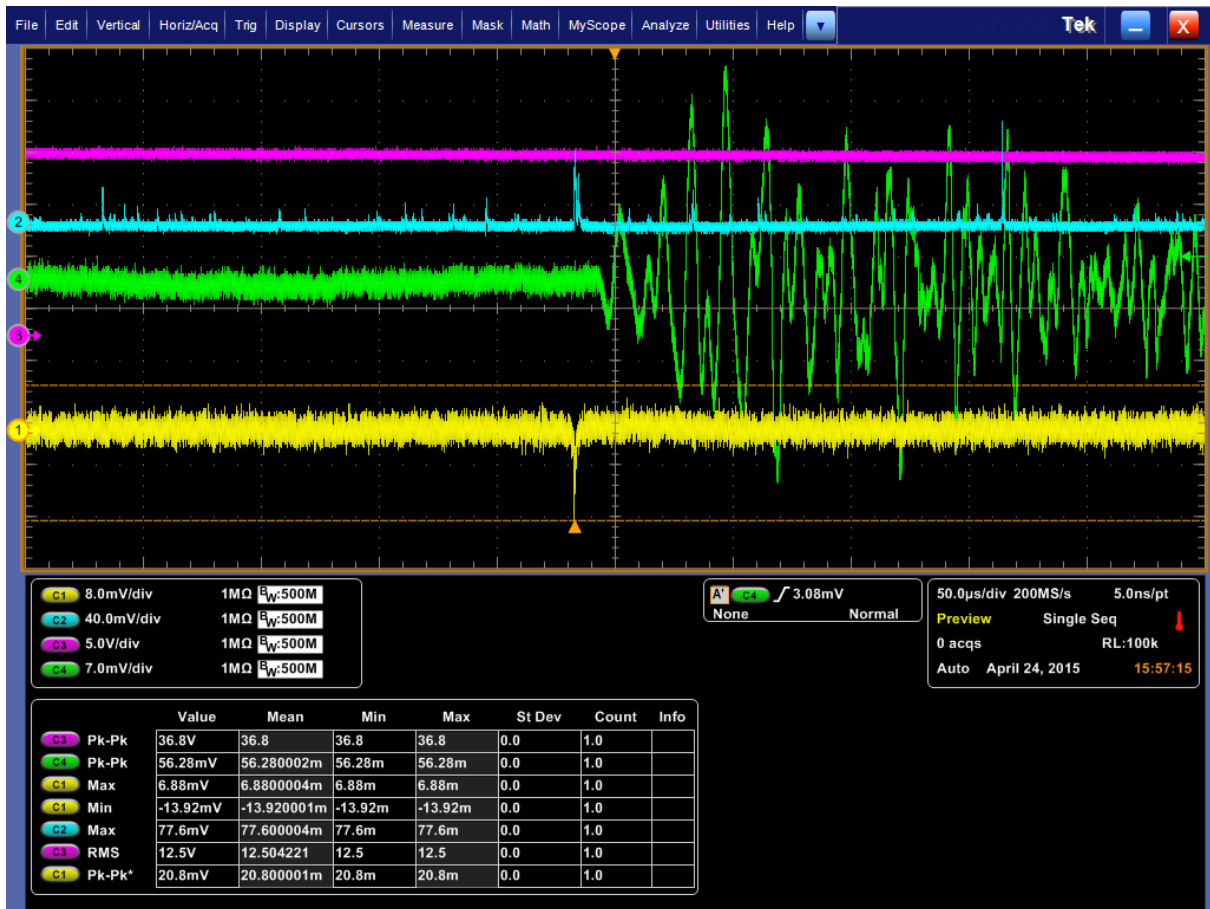
Figure 25 : Typical positive PD signal. Electrical signal (1), PMT Light Signal (2) and acoustic signal (4), occurring at 18.4 kV peak sinusoidal voltage (3)

The electrical PD signal in Figure 25 is observed during the positive half cycle of the 18.4 kV sinusoidal voltage applied, shown in Ch3. The pink voltage signal is sinusoidal, even though it looks constant, as the time resolution per division (dotted lines) is 50 µs. The PD has occurred on the rising voltage edge at approximately 17.5 kV. The electrical PD signal shown in Figure 25 have positive polarity even though it appears with a negative polarity. This is because the signal is inverted after passing through the measurement setup. The electrical PD signal will always have opposite polarity to the applied voltage.

The PD light signal at Ch2 has a fast rising edge, which is gradually damped. In general the light signals are unipolar, but can have some damping due to the capacitive measuring circuit. The small light signals in Figure 25 are dark currents. The test cell should be light proof so a blanket is placed over the cabinet in case there are any slips in the cabinet, polluting the PMT signal.

The acoustic PD signal has an uneven oscillating signal as it is a product of the vibrations originating from the discharge. The reason it is so uneven is because of its wide frequency spectrum. The signal is gradually attenuated. An important thing to note is that the acoustic signal happens with a time lag compared to the faster light and electrical signals. This is because the speed of sound is lower than the speed of light. The sensor should be placed as close to the PD location as possible, and is therefore placed at the bottom of the glass cup.

35

The PD sound wave must travel through the glass cup, the steel plate, the oil and the circuit board. The sounds will move very fast through the solid materials with a speed up to 6000 m/s. The glass, steel and circuit board will contribute to a small but negligible time lag. The main time lag comes from the 1.5 cm of oil between the board and the sensor. It will result in a time lag of 10.6 μs, calculated with the sound velocity in transformer oil of 1415 m/s [23].

3.8 BREAKDOWN TEST METHOD

Table 4 – Systematically test matrix for all oils with and without cover for sinusoidal and switching voltage

Test voltage	Surface	Oils		
		Nytro 10 XN	Midel 7131	Galden HT200
Sinusoidal	No cover			
	Parylene			
Switching voltage	No cover			
	Parylene			

The setup was first tested with sinusoidal voltage with the three different oils, both with and without surface covering. This is because it is easier to detect PD when a smooth sinusoidal voltage is applied. In the following a progressive voltage test is presented. The procedure has been made with guidance from supervisors and external sources in [46], [47] and [10]. The **progressive** breakdown stress test is performed by increasing voltages in small steps over equal time steps. Failure data of at least ten samples should be obtained. Less than five specimen can lead to serious errors [29]. The following procedure is used for the progressive breakdown testing with PD detection:

1. Slowly increase the voltage from zero with a maximum voltage increase of 0.5 kV/s.
2. Reach initial test voltage preferably below the PDIV. Note the initial voltage.
3. Rest 1 minute at initial voltage.
4. Increase voltage of approximately 1 kV.
5. Rest 1 minute. Note PD activity if observed in order to evaluate PDIV.
6. Repeat step 4 and 5 until breakdown occur. Note BD voltage.
7. Right after BD: Decrease voltage well below initial voltage or even to zero.

For the tests to be valid, there should be 2-12 voltage steps before breakdown [48]. To obtain this the initial test voltage can be increased or decreased.

The voltage is increased from zero to a level well below the BDV. To minimize the probability of individual manufacturing defects affecting the test result, several boards should be tested. Numerous of tests will give a more realistic result. If the boards are not wrecked after the first breakdown more tests can be performed on the same board. In [49] it is proposed to test each test specimen 5 times to obtain 5 BDVs per board. After the first breakdown test the voltage should be decreased well below the PDIV-level before the next breakdown test is initiated. It

was determined to test each board 5 times for the sinusoidal testing for PCBs without cover, as they were not wrecked after the first test.

3.8.1 Determining the PDIV

The voltage value of PDs inception was recorded when one or more PDs were observed during that voltage step in the progressive test. To rely on the PD observed, all three PD detection methods were compared. When they correlated, as in Figure 25, the voltage level was recorded as the PDIV. The acoustic signal was used as the triggering variable because it had the highest sensitivity. Another method used extensively in the thesis to capture PDs is the **Persistence Control**. If the persistence is set to infinite, it will track all the signals that are detected by leaving a history track at the graphic interface of the oscilloscope. The channel with test voltage is then used as the trigger channel, as it has a repetitive signal. Applying persistence at a constant voltage level and period will capture only the transient PD signals that will appear on the screen. Persistence screen shots will be illustrated in many of the screen shots from the oscilloscope in the results chapter 4.

3.8.2 Method of comparison

For sinusoidal voltages, the test object experiences two similar rising and falling edges during one time period, respectively one for positive and one for negative voltage. In the specialization project, the PDs were detected at the rising edges for each polarity of the sinusoidal voltage [4]. No PDs were observed for falling voltage level, hence the rising edge is considered the critical. For the fast turn-on circuit the rising edge is fast, but the turn off is much slower. The hypothesis is that the slow turn-off in the fast turn-on circuit is not that critical. The circuit could also have been designed to be a fast turn-off circuit, by placing the switch in parallel with the test object. Then the turn-on would be slow instead. Due to time-limitations only the fast turn-on setup is tested. Regardless, the fast switching circuit generates one critical voltage change per switching period. To compare square switching with sinusoidal voltages, the time between each voltage increase in the square wave testing, is set to 2 minutes. This way the number of critical voltage changes are the same in both sinusoidal and fast switching for each time step. The test procedure for progressive breakdown test at switching voltage will be as proposed for sinusoidal testing, except for a rest time of 2 minutes.

3.9 ELECTRICAL FIELD MODELLING IN COMSOL

The test object in Figure 20 was measured in a microscope to find all the dimensions of the shapes. This was done in order to make a COMSOL Multiphysics model of the board. The objective is to examine the electrical fields present in a typical test situation. The critical high electric field point is at the triple junction; the interface between board, electrode and the liquid. The triple junction is located at the lower part of the high voltage copper electrode. The electrodes were drawn by based on the radius of curvature of the electrodes. The smallest and hence the most critical radius of curvature at the lower part of the electrode was measured to be 3.8 µm. All dimensions measured are summarised in Figure 26. The HV electrode and the ground electrode is assumed to have the same radii of the curvatures.

The goal is to simulate the Electrical field distribution and magnitude. The electrodes were modelled by using super positioning of different shapes in COMSOL.

r_{upper}	10 µm
r_{lower}	3.8 µm
d_{upper}	2073 µm
d_{lower}	1730 µm
$r_{etching}$	650 µm
$t_{electrode}$	390 µm
t_{board}	1162 µm
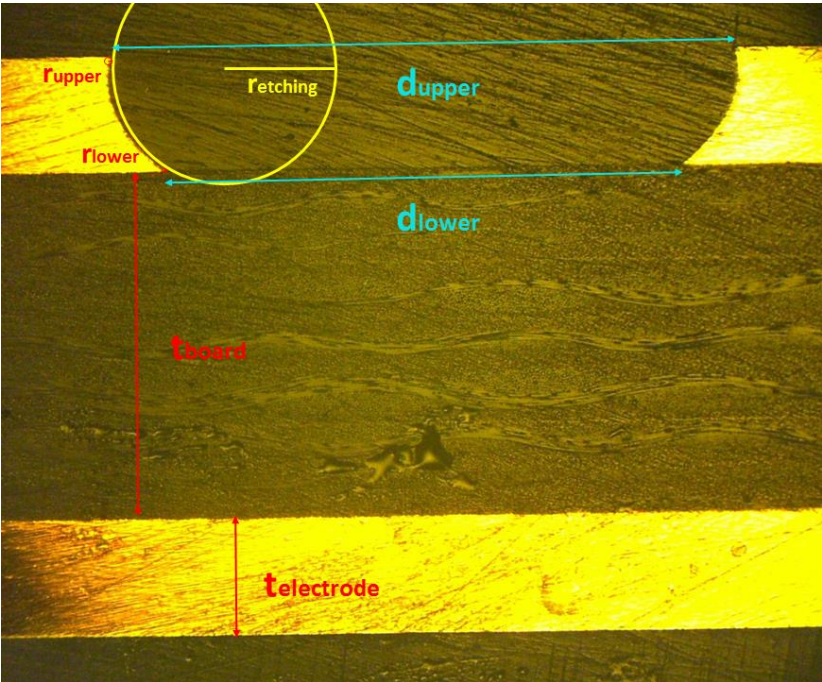
Figure 26 - Measurements done to build a COMSOL Model

4 RESULTS

This chapter presents the findings throughout the testing. All voltages are peak voltages with the amplitude given in [kV], unless otherwise specified. The BDV corresponds to the U_{63}-value.

4.1 CRITICAL ELECTRICAL FIELD STRESS IN COMSOL
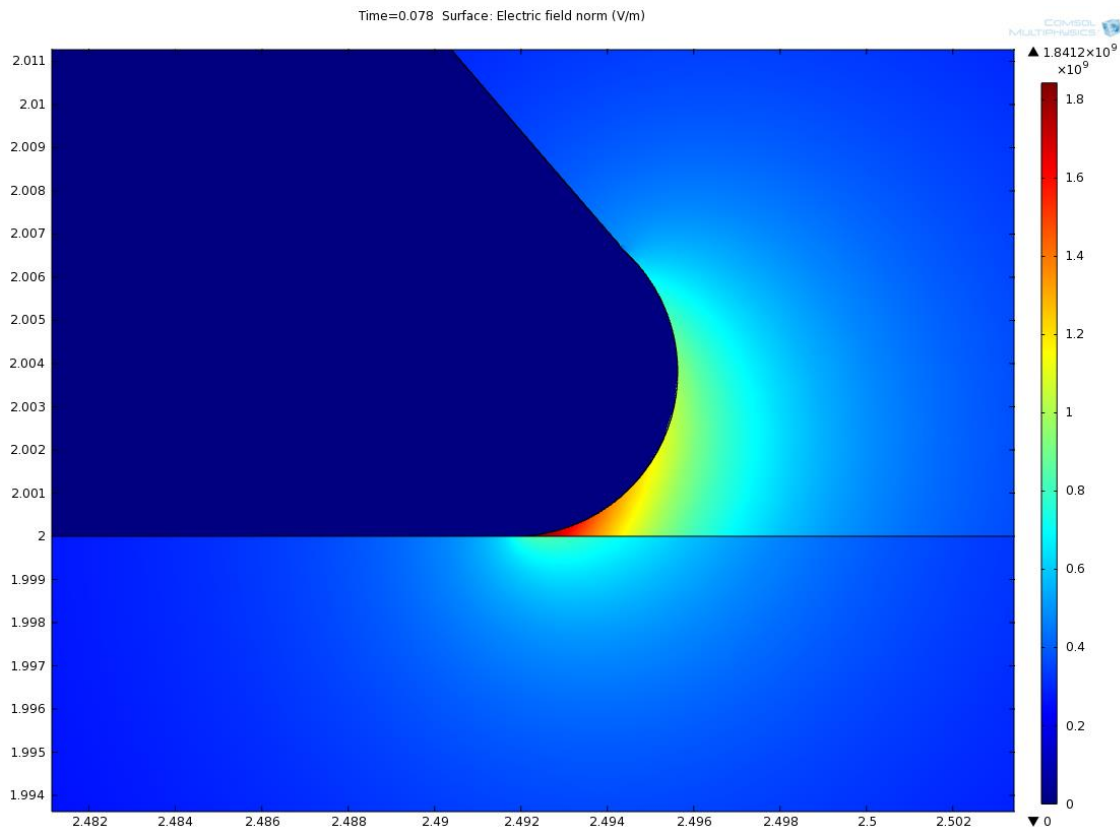
Figure 27- Sinusoidal 25kV AC applied showing high field region with maximum field stress of $1.84 \cdot 10^9$ V/m at 0.078 s.

The COMSOL model was analysed at 25 kV sinusoidal 50 Hz voltage. The electric field calculations in the triple junction based on electrostatics reached values up to $1.84 \cdot 10^9$ V/m. This field stress exceeds the level required to initiate PD. The effect of field emission and field ionization would result in even higher fields, but are not taken into account in the simulation.

4.2 PRE-TESTING

Calibration of the pre-testing setup gives 1 pC to correspond to 80mV. Hence, the noise level is above 5pC, which probably hid many of the PDs. The testing of the AlN-board showed extensive PD activity at 14.5 kV peak voltage. The high-speed camera showed light in the trench-area between HV and ground. Figure 28 shows, with one minute persistence, in particular the characteristic acoustic PD signals at Ch4. The PDs appear at the rising edge of the voltage in both half cycles as expected. Note that an optical filter has been used in the

PMT to avoid most of the electroluminescence. The light signals appear in the entire sinusoidal period but are larger and more frequent where the acoustic PD signals also appear.
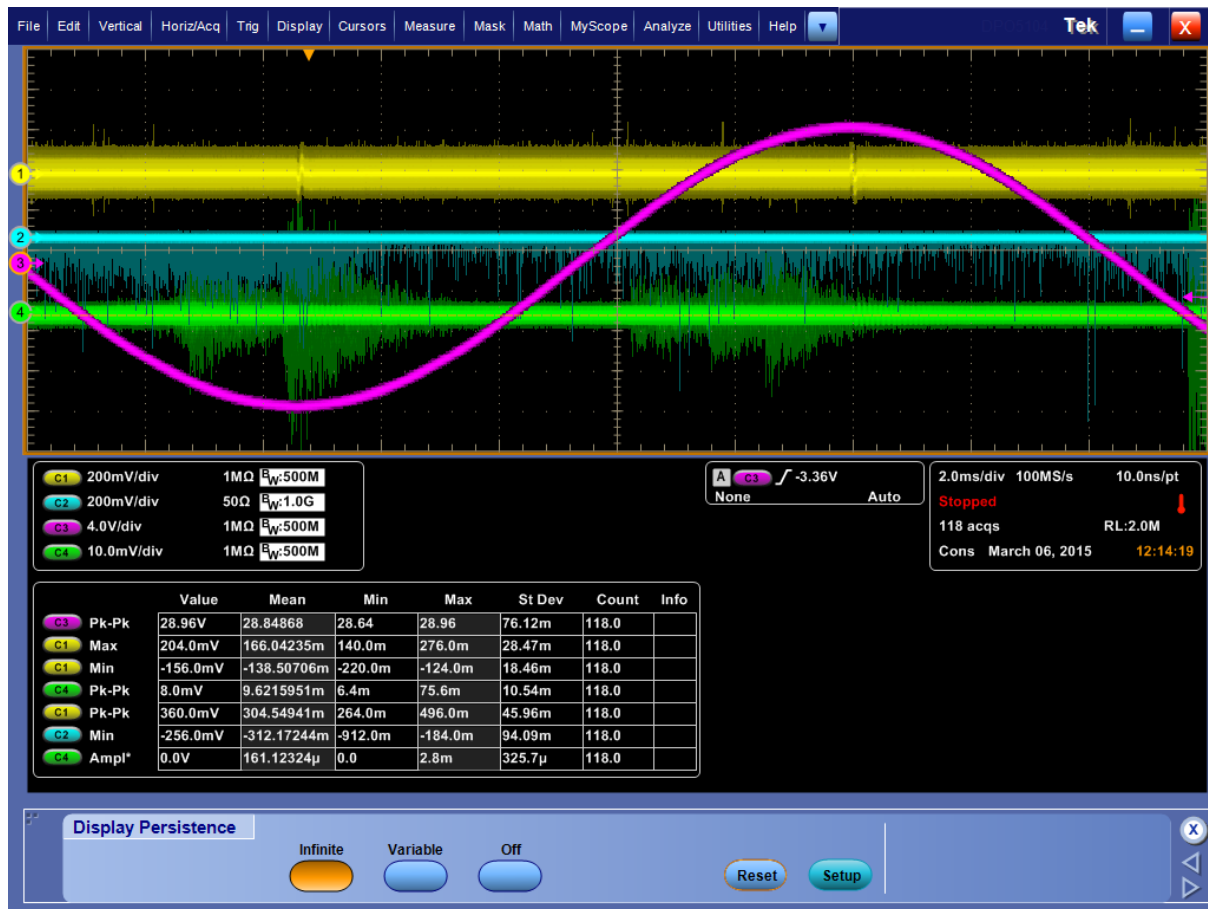
Figure 28 - 14.5 kV sinus applied (3) to the AlN-board with one minute persistence, showing acoustic PD signals (4), light emission (3) and high electrical noise (1).

4.3 SYSTEMATICALLY TESTING

4.3.1 Sensitivity

The calibration in test setup 2 and 3 gave that 1 pC corresponds to 3mV. The peak-to-peak noise level is measured to be almost 6mV corresponding to 2 pC.

All starting voltages during testing are recorded and presented in Appendix in 9.6. The starting point had to be varied dependent on the liquid. This is in order to have the ideal of 2-12 voltage steps before breakdown occurred. Varying the starting point did not seem to affect the BDV much. For tests with surface cover, the test starting voltage was around 24 kV. For boards without cover, the initial test voltage for the progressive tests was always in the range of 12-16 kV.

Nytro has shown to have a good correlation between light emission and electrical discharge in the specialization project [4]. Consequently, the discharge detection in this liquid should be quite sensitive. To evaluate the sensitivity, 20 PDs in Nytro without Parylene cover at sinusoidal voltages were recorded and compared. All three signals; **light amplitude**, **electrical**

40

amplitude and maximum **peak-to-peak acoustic signal** were all measured in millivolts, [mV]. The average signals of the 20 values shown in Table 5. The average light amplitude is five times bigger than the electrical signal, while the average acoustic peak-to-peak signal is three times larger than the electrical signal. The signal to noise ratio (S/N) calculation based on the twenty PDs in Nytro is shown in Table 5.

Table 5 - Signal to noise ratio at sinusoidal PD testing in Nytro without cover

	S: Average amplitude [mV]	N: Max noise level [mv]	S/N ratio
Electrical	14.5	≈6	2.42
Optical	70.1	≈70	1
Acoustic	44/2 = 22	≈5	4.4

In in the specialisation project [4] a typical shape correlation with multiple discharges was found for light and electrical discharges in Galden. The same correlation was found during tests at PCBs in Galden, shown in Figure 29. Note that the polarity of the light signal is inverted in this test setup compared to the test setup during pretesting.
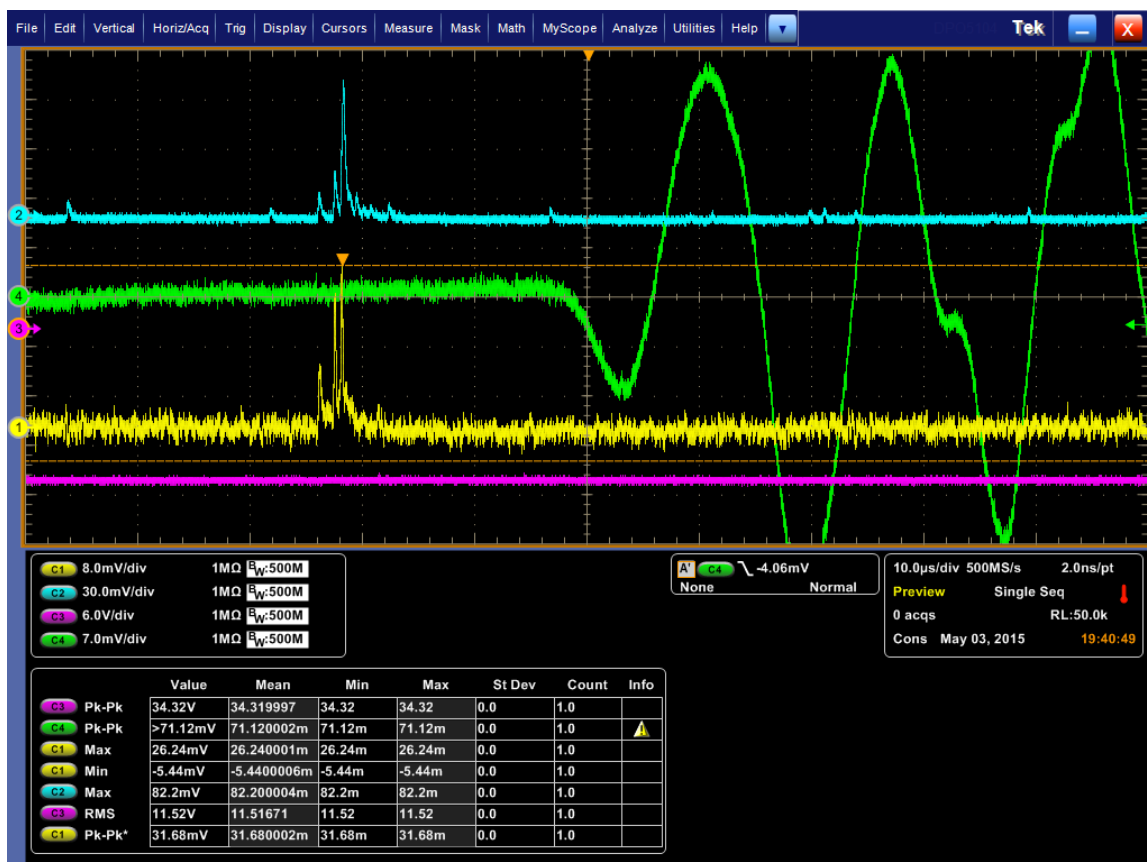
Figure 29 - Negative Partial discharge in Galden at sinusoidal voltage showing electrical (1) and light (2) correlation, as well as acoustic (4) signal with the characteristic time delay of approximately 20 µs.

The electrical PDs detected in Midel were small, typically 2-4 pC. Occasionally large PDs would occur, typically in the positive half cycle as shown in Figure 30.
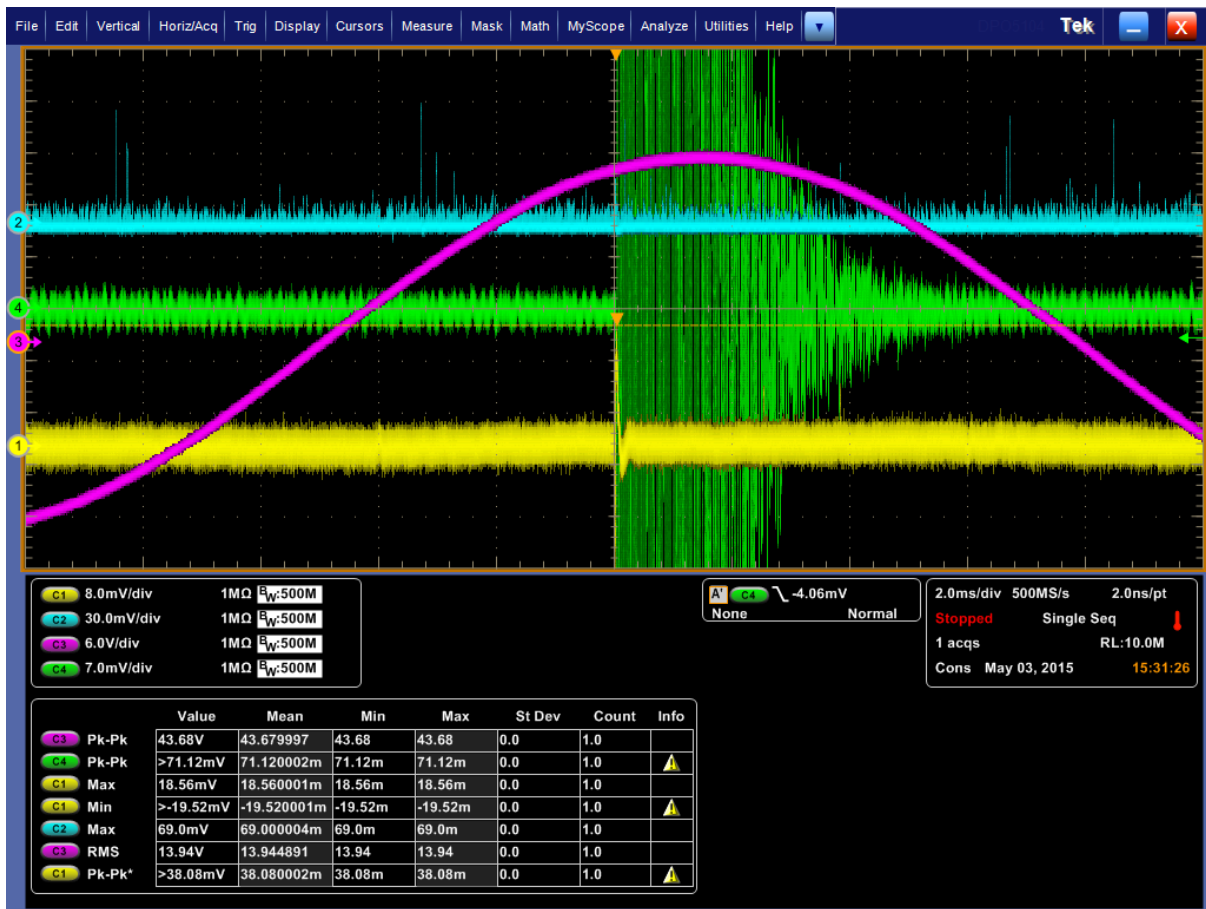
Figure 30 – A large positive PD in Midel with amplitudes exceeding the detection frame

4.3.2   Breakdown location

When breakdown occurred, an audible and distinct clicking sound was present inside the cabinet. At PCBs without Parylene, the breakdown propagated through the oil. Many boards were examined after breakdown in a VHX digital microscope with magnification ratio in the range of 100-1000. Figure 31 shows a PCB-trench tested in Nytro where numerous BD tests were conducted. Both electrodes have small burning marks. The streamer has initiated at the HV side and has grown into an arc after terminating at the groundside, bridging the electrodes. Remains of Nytro oil is still present on the right electrode (ground) in Figure 31.
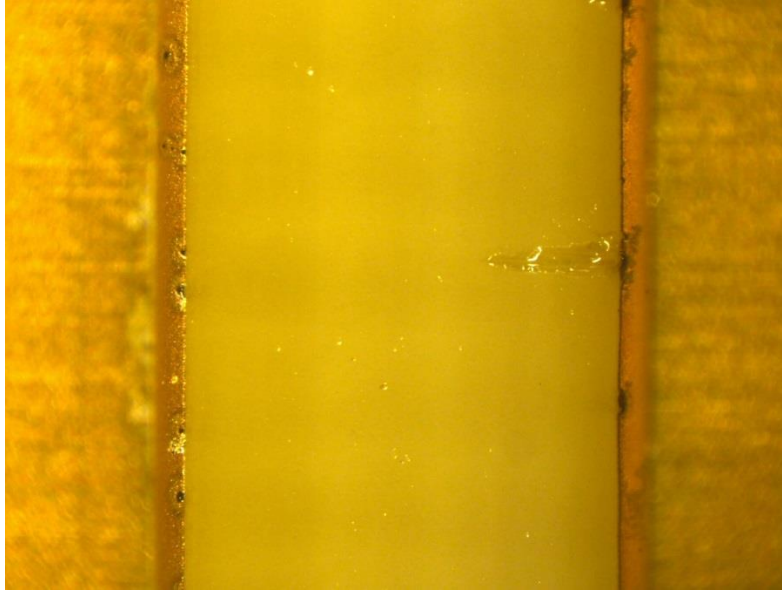
Figure 31: HV electrode (left), PCB trench (middle) and Ground Electrode (right). Showing burning marks along the edge where the breakdown has bridged the electrodes.

At surface covered boards, observations indicate that the breakdown followed the surface of the trench for most of the boards. This is shown in Figure 32.
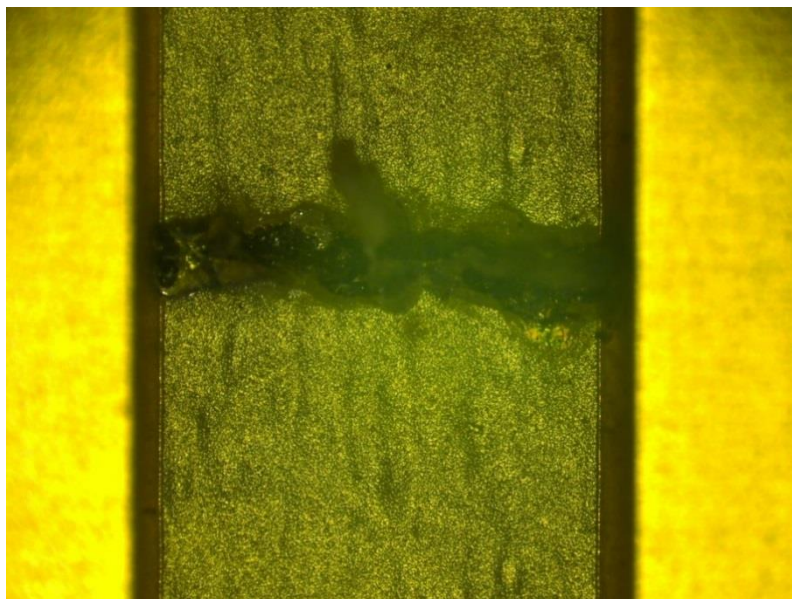
Figure 32 - Surface breakdown across the trench when the board had Parylene surface cover.

4.3.3   Effect of conducting several breakdown test per board

On each of the eight non-covered boards tested per liquid at sinusoidal voltage, five breakdown tests were conducted.   The average BDV, after each test per board, was calculated for all liquids. For all the eight boards tested the average BDV in Nytro increased for each test conducted. The average BDV in Midel increased slightly, but remained approximately constant. For Galden, on the other hand, the BDV was significantly reduced after the first test on each board. It was decided to exclude the four extra tests done per board in the breakdown analysis for all liquids, and only focus in the first test. All the BDVs are shown in Appendix 9.6. Further

43

breakdown testing with cover and at fast switching was only performed one time per board, to avoid the effect of change in the BDV.
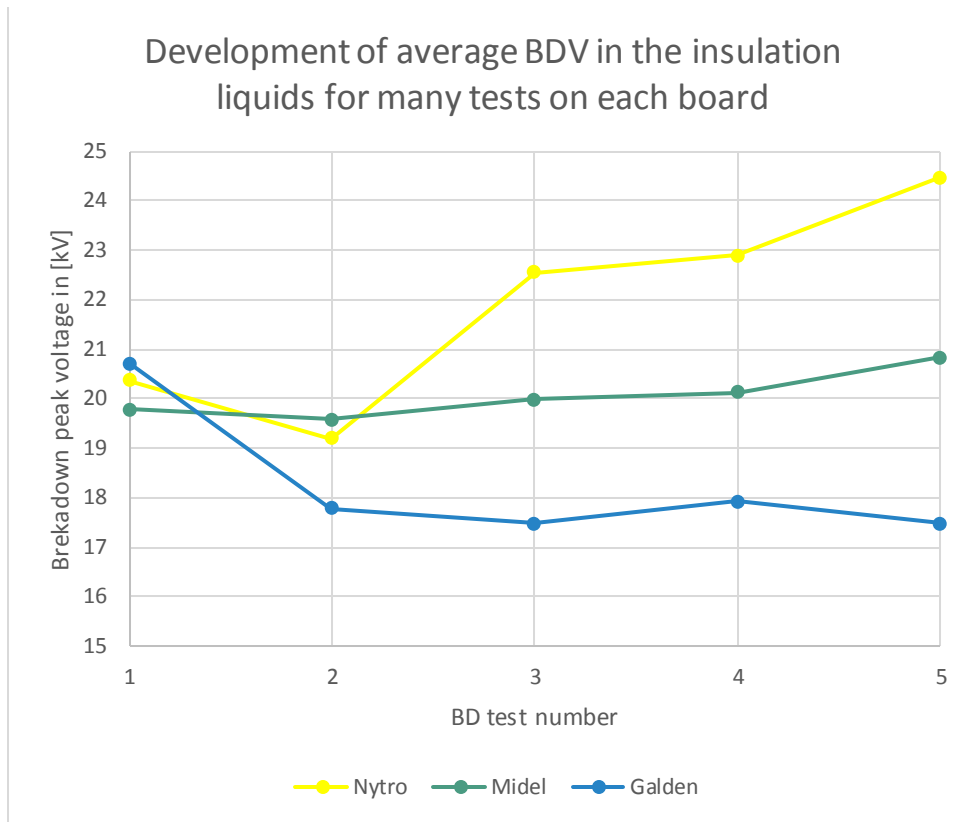
Figure 33 - Average BD voltage changing with each test on one test board

4.3.4   Statistical analysis of the breakdown data

In this chapter, the Weibull parameters of the breakdown data will be presented both in numbers and in Weibull plots with comparison of different cases. The calculated correlation coefficients in Appendix 9.5 show that Weibull analysis fits well for all the breakdown cases. The PDIV was also checked for correlation to the Weibull distribution, but the fit was not sufficiently good, so the PDIV is reported by the mean instead.

Table 6 - Weibull Breakdown parameters for sinusoidal testing

Test object	N	Characteristic value U_{63} [kV]	90% Confidence Bound for U_{63} [kV]	Shape parameter b	90 % Confidence Bound for b
Nytro	8	21.8	19.46 – 23.98	5.92	3.77 – 10.81
Nytro w/C	10	33.0	30.50 – 35.45	7.38	4.92 – 12.36
Midel	8	20.6	19.30 – 21.87	9.92	6.31 – 18.09
Midel w/C	10	33.9	31.80 – 35.77	9.45	6.31 – 15.83
Galden	10	21.7	20.39 – 23.00	9.20	6.14 – 15.42
Galden w/C	9	30.0	28.14 – 31.85	9.37	6.10 – 16.17

Table 7 - Weibull Breakdown parameters for fast switching testing

Test object	N	Characteristic value U_{63} [kV]	90% Confidence Bound for U_{63} [kV]	Shape parameter b	90 % Confidence Bound for b
Nytro	9	23.1	22.36 – 23.84	18.13	11.82 – 31.29
Nytro w/C	7	34.0	25.47 – 34.80	9.21	5.42 – 19.31
Midel	10	23.7	22.12 – 25.17	8.59	5.60 – 14.82
Galden	9	34.2	31.37 – 37.07	6.94	4.63 – 11.62
(Nytro Neg)	5	30.2	25.47 – 34.80	5.03	2.86 – 12.07

In Table 6 and Table 7, the characteristic Weibull parameters and their 90 % confidence interval are summarized. The confidence interval is more narrow the more tests performed (N) per case. The shape parameter, b, notes the slope of the linear trend line in the Weibull plot. A larger value of b imply an increase in the failure rate when increasing the voltage. The most important parameter to note is the U_{63}-value, which is the most likely expected breakdown value; the peak in the Weibull distribution density plot.

4.3.5 Effect of voltage shape

The average PDIV-value for sinusoidal voltage is summarized in Table 8. The PDIV was not recorded if no PDs were observed before breakdown occurred. For sinusoidal testing without cover, the PDIV was recorded at all the five tests per board. The average PDIV for the first test and the average for all five tests per board are included here.

Table 8 - Average PDIV for sinusoidal breakdown testing

Test object	N	Average PDIV (only first BD) [kV]	Difference between PDIV and U_{63}	Average PDIV (all 5 BDs) [kV]
Nytro	8	16.2	5.6	18.6
Nytro w/C	10	26.0	7.0	
Midel	8	17.4	3.2	18.0
Midel w/C	10	28.7	5.2	
Galden	10	17.7	4.0	15.1
Galden w/C	9	26.1	3.9	

Table 9 - PDIV at fast switching

Test object	N	Average PDIV [kV]	Difference between PDIV and U_{63}
Nytro	9	20.2	2.9
(Nytro Neg)	5	21.0	9.2

No discharges were reliably detected at fast switching voltage, except for in Nytro without surface cover.

As expected fast switching introduces transients in the system. The switching noise affects the electrical so much that it cannot be used for PD detection. The ability to detect PDs rely entirely upon acoustic or optical methods. Additionally, the switching will introduce some **constant noise** in these signals, shown in Figure 34. The shape of the noise in the optical and acoustic signal are constant, but rises in amplitude proportional to the test voltage.

Figure 34 - Circuit response with persistence from 25 kV fast switching (3) showing the constant noise for the acoustic (4) and light signals (2)

Ch1 in Figure 34 shows the square wave signal from the signal generator used to control the switch, which explains why the voltage signal at the test object at Ch3 switches at the same time. The switching time response is shown in Figure 35 with 10 ms per division. The turn-on is extremely fast with a measured slew rate of 43.3 kV/µs. The time constant $\tau_3 = 1.05ms$ can be recognized as the as the discharge time constant.

Figure 35 - Time response waveform of fast turn-on switching voltage across the test object

Figure 36 show a typical 1 minute persistence screen shot with extensive light emission. The screen shots presents the complete switching period with 2 ms per time division. The yellow voltage signal at Ch1 in Figure 36 is the voltage from the signal generator controlling the switch. The signal has been included at the oscilloscope screen in order to show the instant of the switching impulse, since the HV probe was not used.
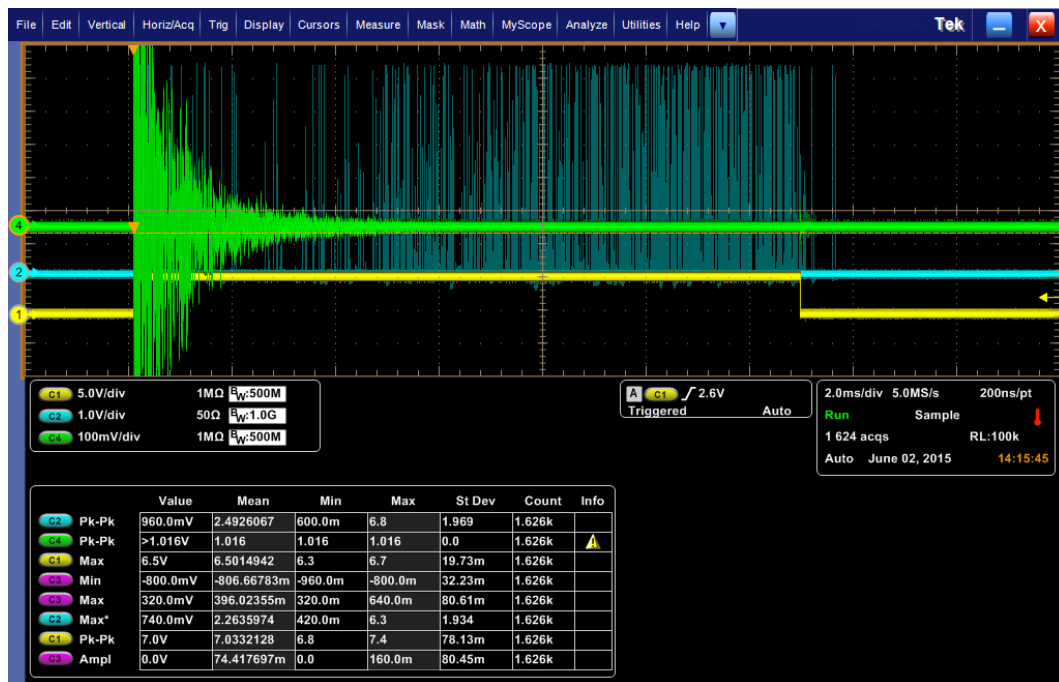
Figure 36 – Fast switching: Extensive light emission at Ch2 possibly originating from PDs elsewhere in the circuit at 36 kV test object voltage

A Weibull plot comparing two breakdown data to show the effect of voltage shape in Galden is presented in Figure 37. The effect in Nytro and Midel are shown in Appendix 9.3 in Figure

52 and Figure 53. They show very similar BDVs at fast switching as in sinusoidal. A slight increase in BDV, of 5 % and 15 %, is present for fast switching in Nytro and Midel respectively.
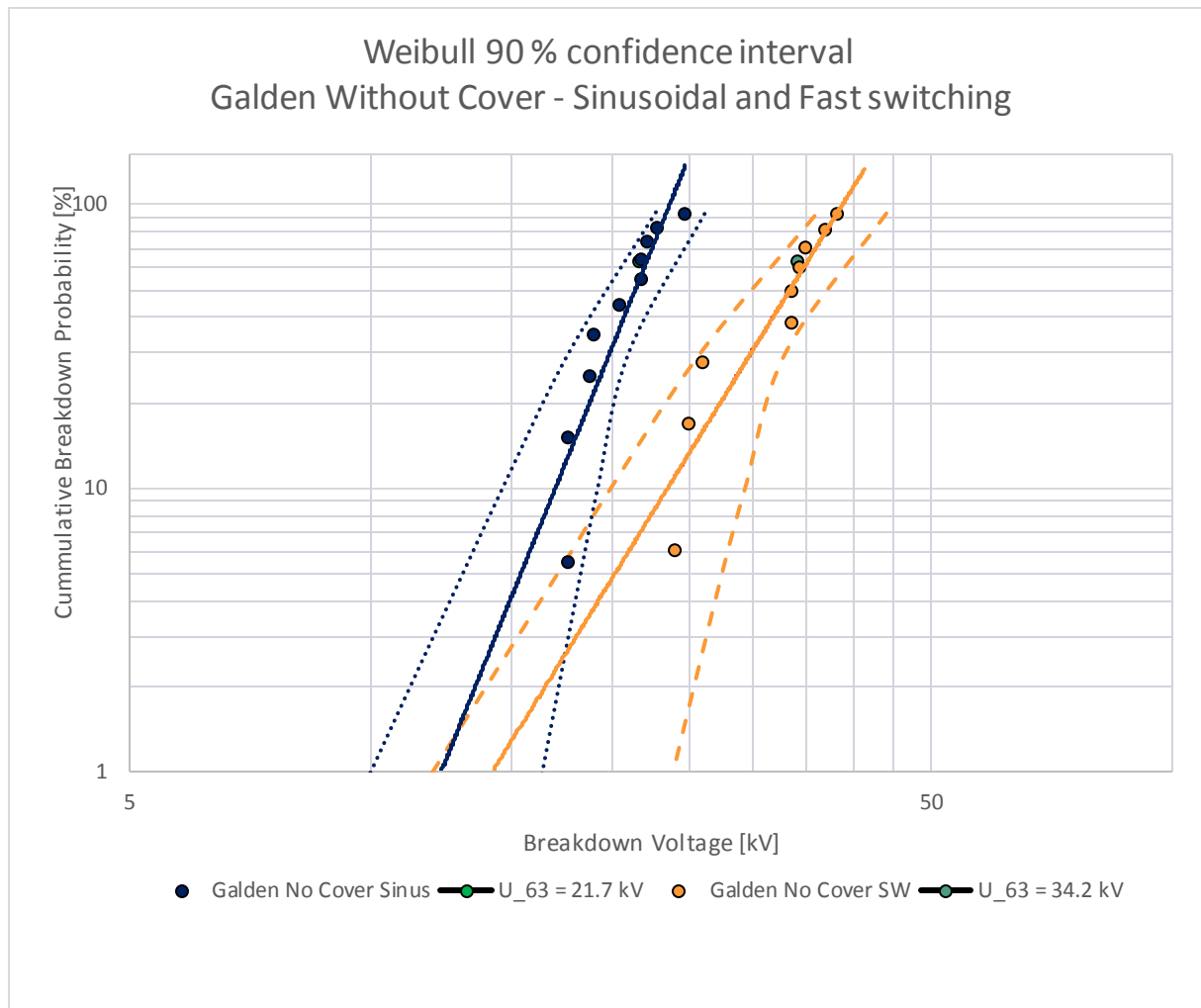
Figure 37 -Weibull confidence interval sinusoidal and. fast switching for PCB without cover in Galden

4.3.6   Effect of Parylene surface cover

Observations shown a larger PD magnitude of the Parylene covered boards compared to the ones without cover. The PDIV was quite clearly defined when a sudden increase in PD activity was observed. A hypothesis is that once the Parylene cover is broken through, there is a lot of PD activity, which appear on all detection channels shown in Figure 38. The PD activity sustained until breakdown occurred.
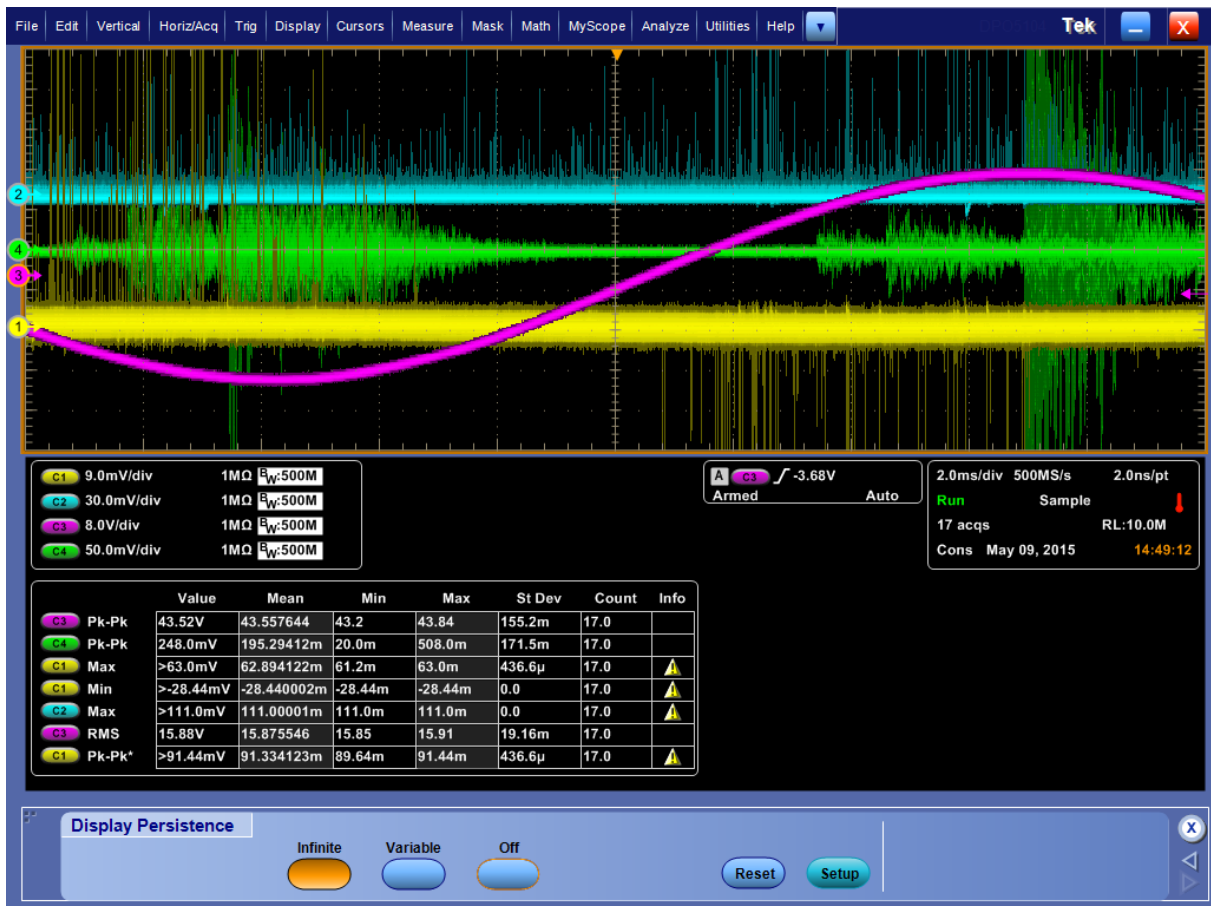
Figure 38 - A lot of PDs were captured with persistence control for 30sec at covered boards in Galden at 22 kV voltage. The acoustic PDs are large with a peak-to-peak range of 500 mV.

The Weibull breakdown data of Midel with and without surface cover is compared in Figure 39. The same comparison for Nytro and Galden at sinusoidal testing is shown in Appendix 9.3 in Figure 56 and Figure 57. They show similar behaviour as Midel.

At fast switching only Nytro was tested with and without surface cover, and the comparison is shown in Figure 40. The confidence interval for Nytro with cover at fast switching is included, even though the limits are invalid.
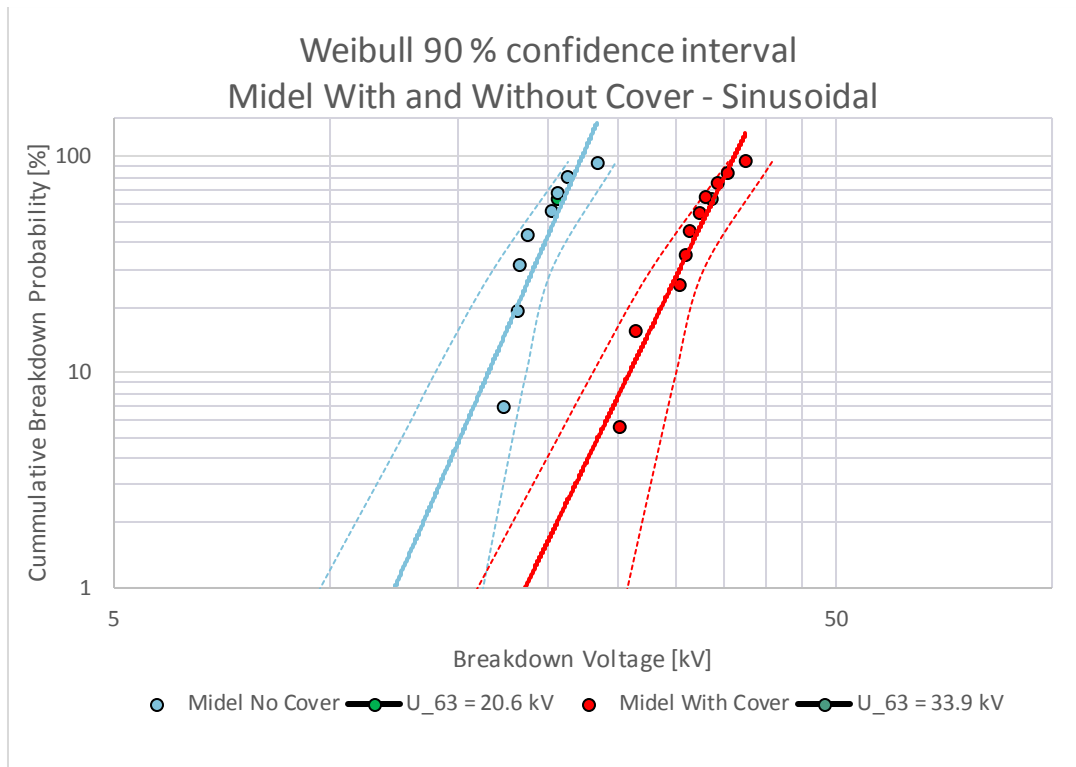
Figure 39 - Weibull Breakdown data plot for Midel comparison with and without Parylene cover
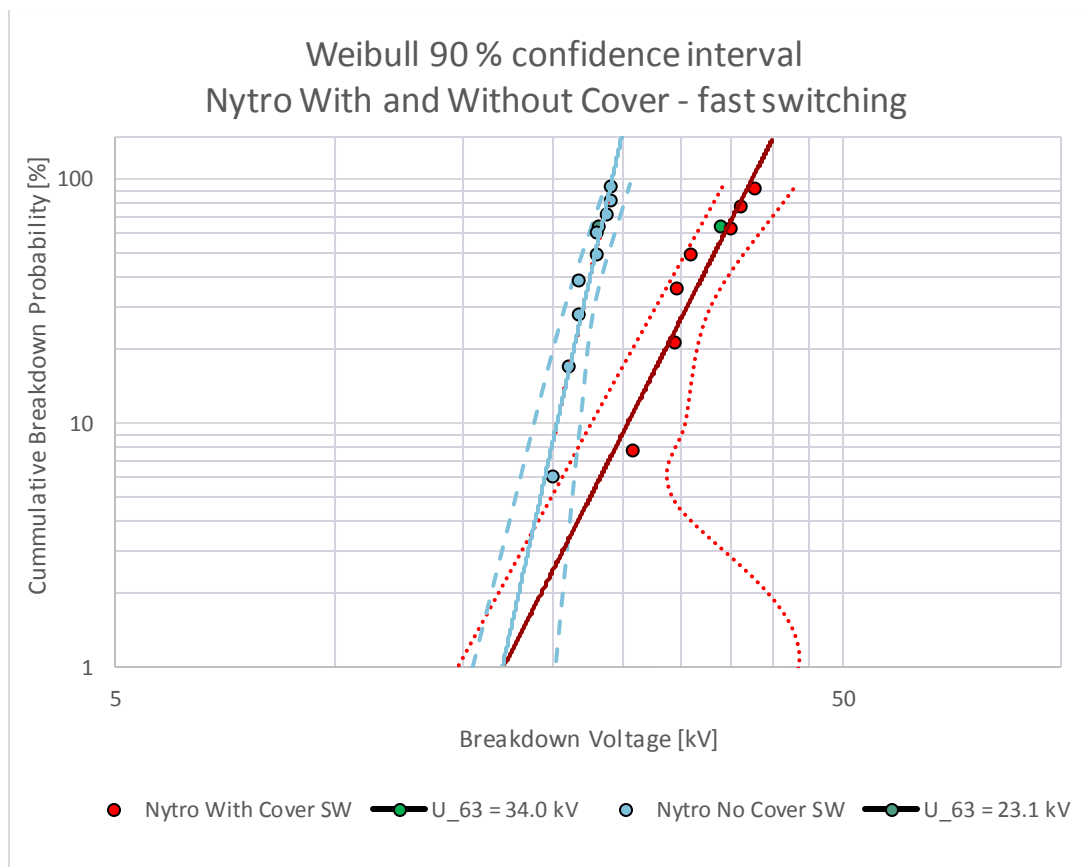
Figure 40 - Weibull Breakdown data plot for Nytro comparison with and without Parylene cover at fast switching

4.3.7   Effect of switching polarity

All fast switching tests were performed with positive switching polarity. Nytro without cover was however also tested at negative switching polarity. This was done by interchanging the terminals at the switch and change the DC source to negative polarity.
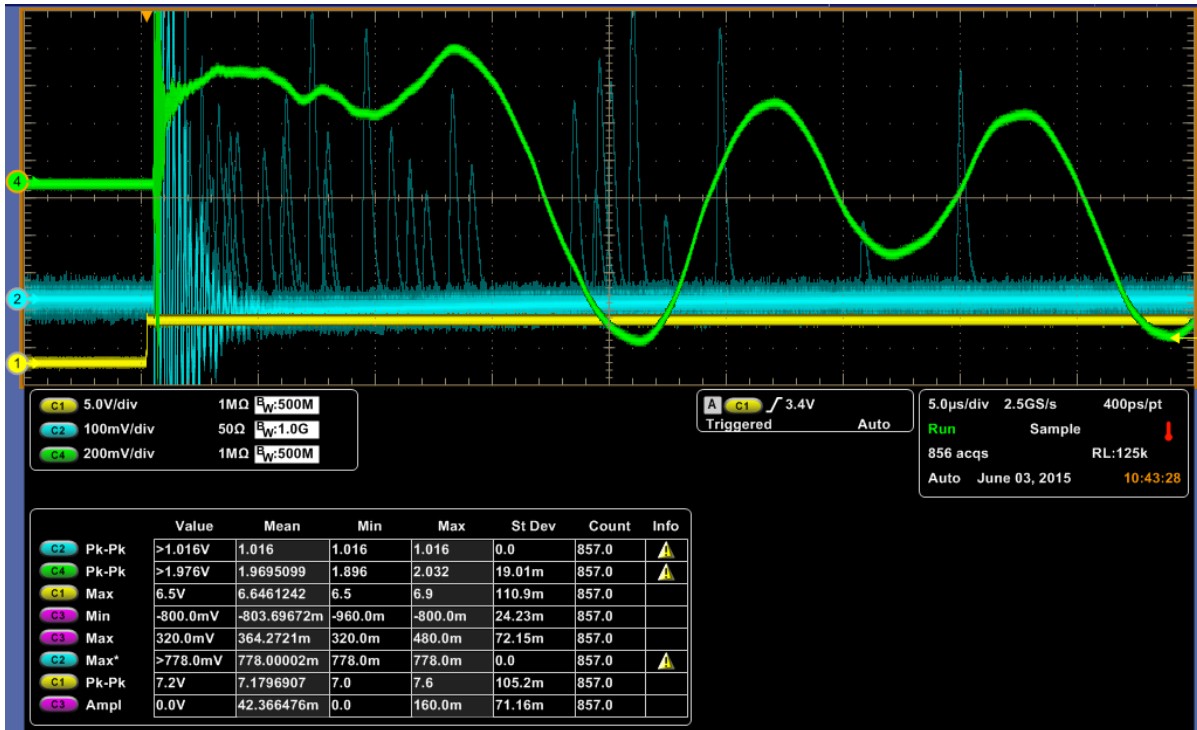
Figure 41 - Nytro without cover at 21kV positive fast switching: Persistence shot with PD light signals appearing close to the voltage switching impulse. The acoustic PD signal (4) is not visible above the noise.
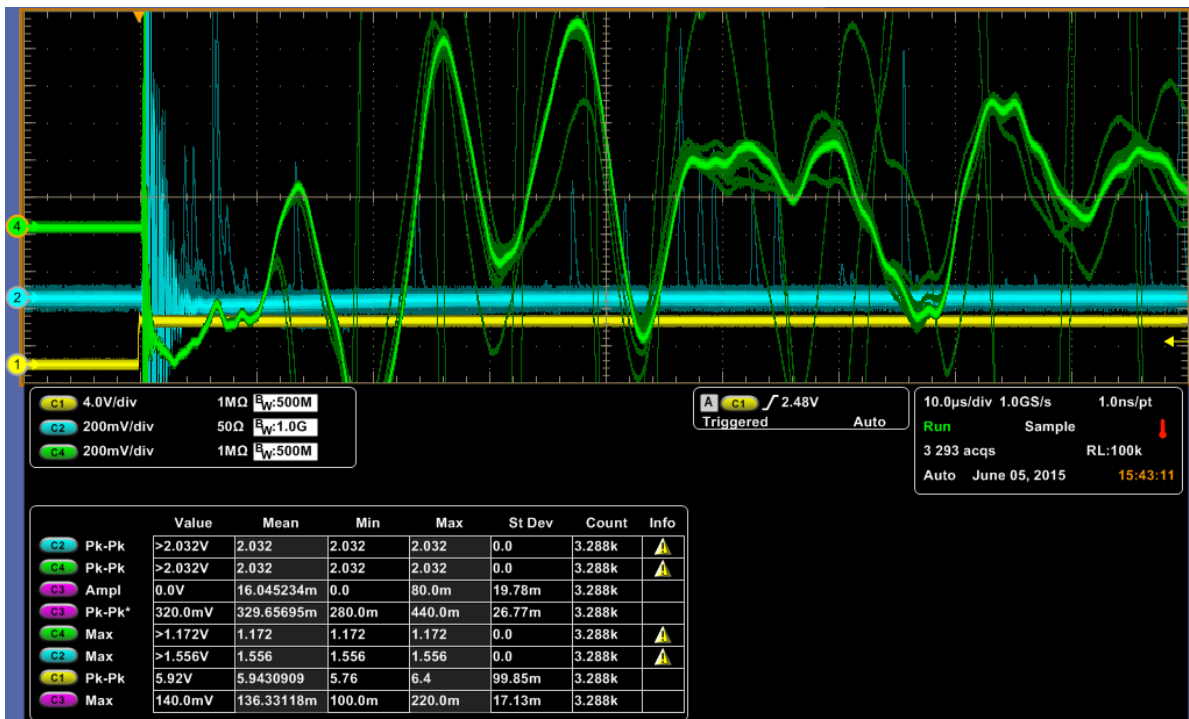
Figure 42- Nytro without cover at 27kV negative fast switching: Persistence shot with PD light signals appearing close to the voltage switching edge and extensive correlating acoustic signal after 20μs

52

PDs captured with persistence screen shot at negative polarity is shown in Figure 42. At positive polarity in Nytro, light was the main PD detection method possible, as no acoustic signal appeared. Figure 41 shows PD light signals above the constant PMT oscillating noise.
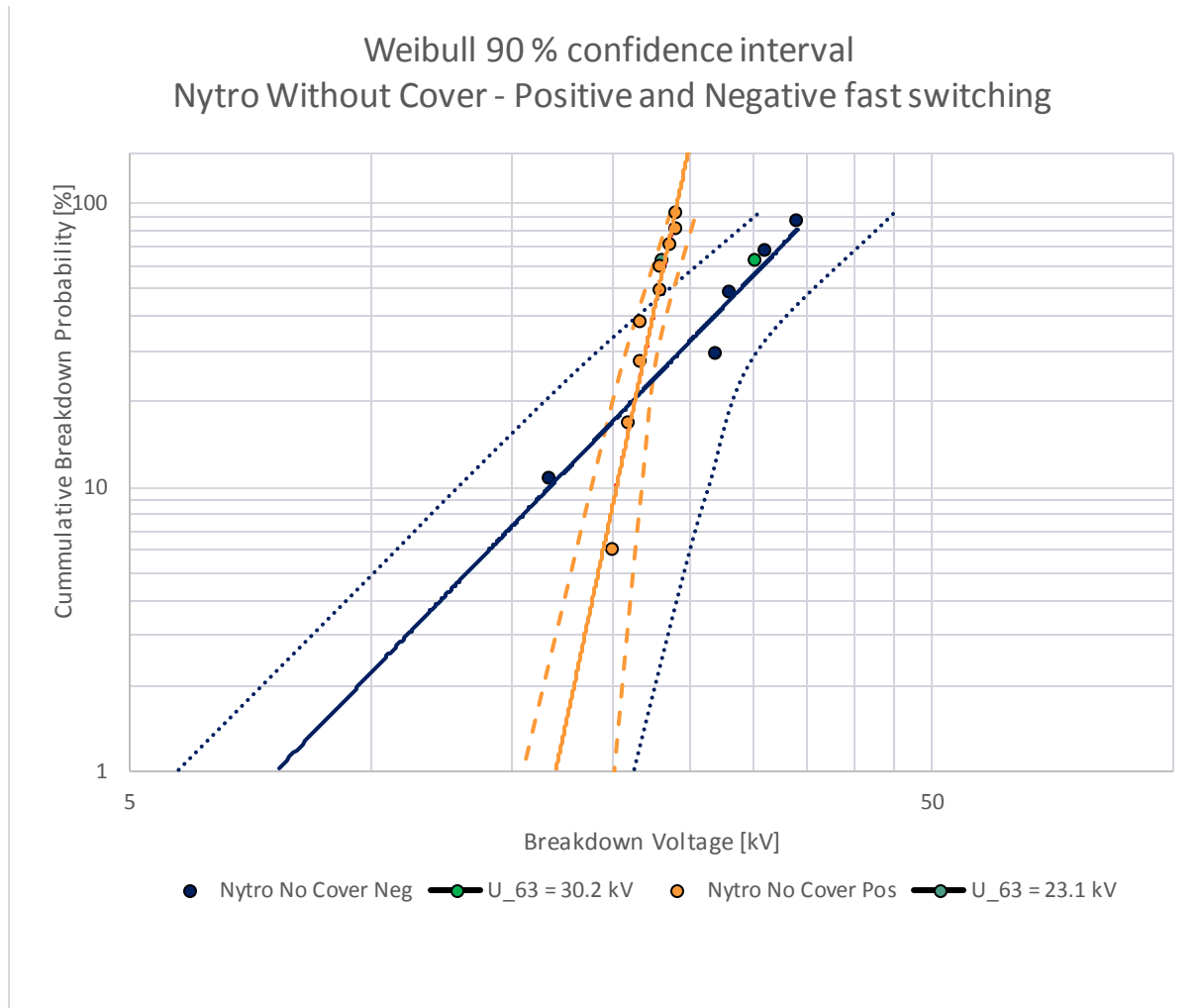
Figure 43 - Comparison of positive and negative switching voltage at Nytro board without cover

Figure 43 shows a Weibull diagram with the results of a larger BDV at negative switching polarity.

4.3.8   Comparison of different liquids
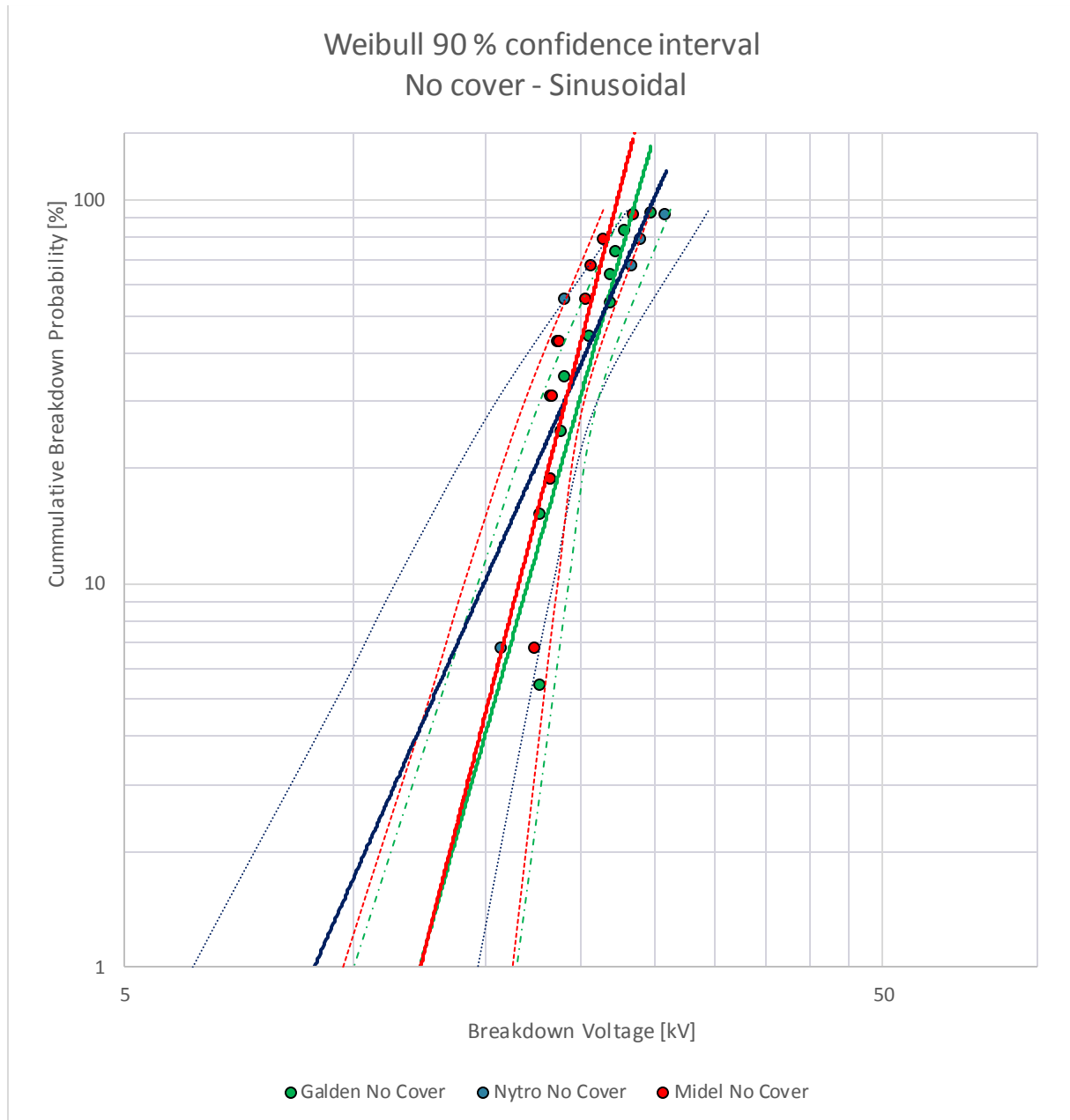
Figure 44 - Comparison of all liquids with non-covered boards at sinusoidal voltage

The breakdown data with confidence interval for all liquids at sinusoidal voltage is shown in Figure 44. The breakdown data appear quite similar for all liquids. The results for covered boards at sinusoidal voltage shown in Figure 55 in Appendix 9.3 are similar. Figure 45 shows the comparison of liquids in non-covered boards at fast switching voltage. Galden sticks out with a noticeably higher BDV.
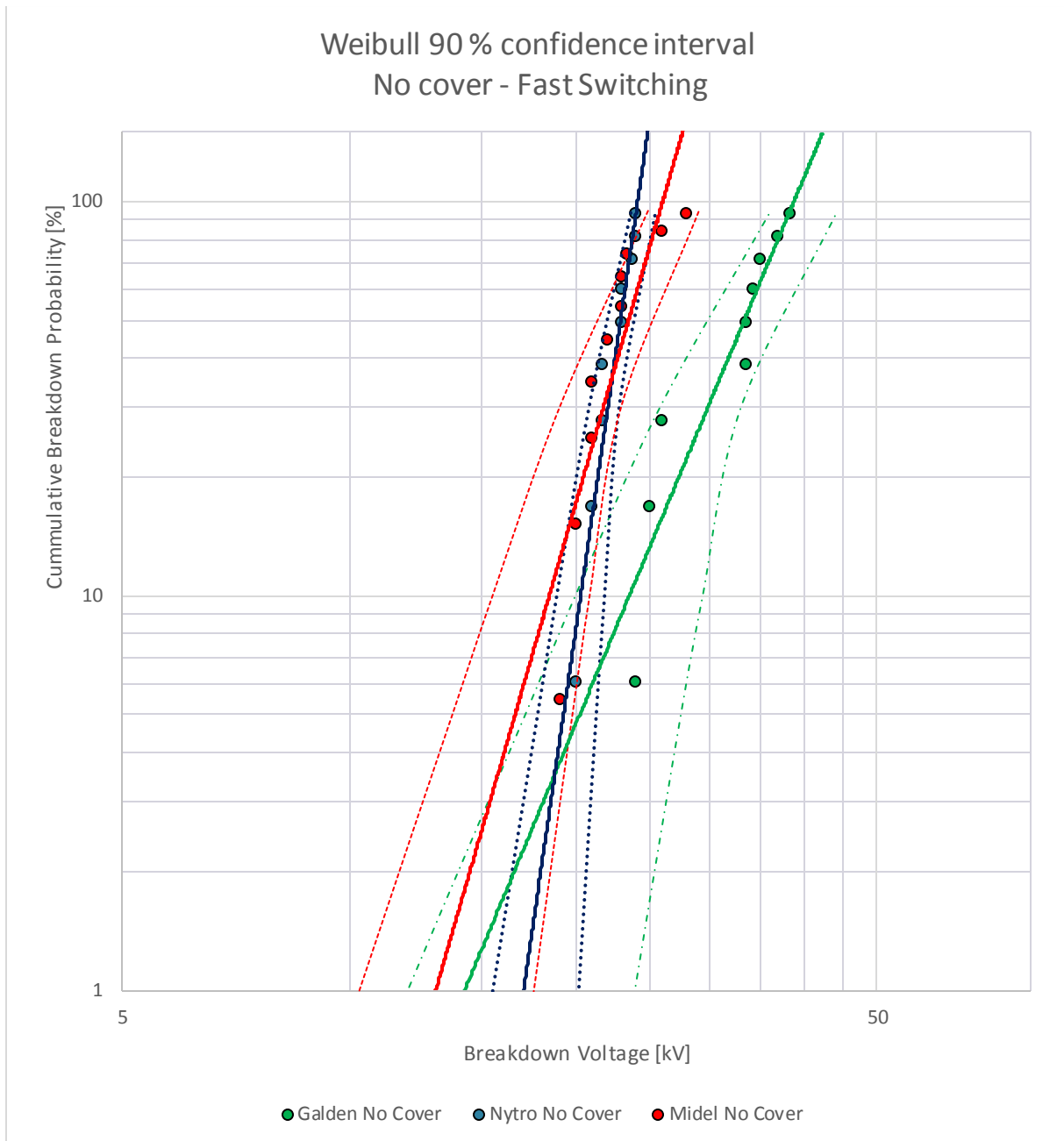
Figure 45 - Comparison of all liquids with non-covered boards at fast switching voltage

4.3.9   Switching circuit design limitations

The breakdown test matrix from Table 4 was not completed. For testing with surface cover, only Nytro was used, and only 7 out of 10 board broke down. Neither Midel nor Galden was tested with Parylene surface cover at fast switching. It was decided to terminate the testing due to the expectations that many boards would not break down because the voltage source could not deliver sufficient voltage. Means to increase the voltage across the test object are discussed in 5.8. Decreasing the frequency will give an increase test voltage. The symmetry function set so that the time the switch is turned off is extended. Both half and the quarter of the number of pulses during the same time-period has been tested. The results in Table 10 show the increase in U_{TO}.

Table 10 - Frequency dependent test voltage

U_{DC} [kV]	F [Hz]	U_{TO} [kV]
20	38.5	13.3
20	19.3	16.7
20	9.6	19.1

At voltages of approximately 32 kV across the test object, a sparking sound appeared inside the cabinet. The cabinet was run open under safe operation to check the location of the corona, which was both audible and visible. Preventive measures to reduce the field stress on the critical areas was to wrap semi-conductive tape tight around as illustrated in Figure 46 . The semi-conductive tape made the field distribution smoother. The voltage where corona occurred was enhanced to 36 kV after adding the tape.

Figure 46 - Fast switching setup showing a critical distance from the grounded cabinet to a HV connection wrapped with semiconductive tape to avoid corona

56

5 DISCUSSION

In this section, the results are discussed and explained. Some hypothesises are presented, which will require further testing.

5.1 EFFECT OF SEVERAL BD TESTS PER BOARD

The boards without a cover had breakdown going through the oil, so the boards where not particularly damaged after one breakdown test, due to the self-healing effect of liquid insulation. Conducting five progressive breakdown tests per board at sinusoidal voltage, showed both increase and decrease in mean average voltage, dependent on the liquid.

The increased withstand voltage at Nytro can be explained by the fact that the sharp edges and most critically high field areas are smoothed out and rounded when PDs and BD occur. The electric field at the electrodes are reduced due to the etching of the copper shown in Figure 31, resulting in a reduced electric field stress in the area.

The reduced BDV in Galden can be explained by investigating the boards tested in Galden. They showed that part of the breakdown had gone through the substrate. The arc from the first breakdown left a small burned and carbonised channel in the substrate at the ground electrode side. The burned marked will work as a leading channel, reducing the distance between the electrodes, lowering the voltage required for breakdown. The four subsequent tests per board in Galden gave a lower and more constant BDV. The BDV in Midel did not change significantly, as it did in Nytro and Galden.

5.2 EFFECT OF VOLTAGE SHAPE

It should be noted that the BDV at sinusoidal voltage refers to the sinusoidal amplitude, and the BDV for fast switching refers to the amplitude of the switching voltage.

There is a 90 % confidence that the breakdown at all sinusoidal cases are above 19 kV. For fast switching the BDV is above 22 kV with a 90 % confidence for all cases. However, the U_{63}-value does not differ more than a couple of kV between sinusoidal voltage and at fast switching for Nytro and Midel. Galden, on the other hand, shows a significantly better dielectric strength at fast turn-on. The U_{63}-value was 12 kV or 58 % higher with a fast switching source compared to sinusoidal.

Fast switching introduced a periodic, oscillating noise in the optical and acoustic signals. The constant acoustic noise signal looks a lot like a normal acoustic signal with a large starting amplitude followed by gradual attenuation. The acoustic noise may likely be due to electrostriction. The noise at the light is probably EMI or stray capacitance from the switching.

Only light signals that appear close to the rising edge, it can be assumed to be PDs. Some correlating response at the acoustic signal with a time delay of ≈20μs should be observed. This

is shown in Figure 42. In Nytro a lot of light was observed above a certain voltage, which is assumed to be the PDIV.

A lot of light was detected when testing at high voltage for fast switching. First, it was assumed to originate from PD. However, it did not appear close to the rising voltage edge, so it probably came from somewhere else. PD and corona had both been heard and observed elsewhere in the test cabinet at test voltage above 32 kV, so the light is assumed to originate from there.

Two identical progressive voltage tests were run without and without the test object in the cabinet see check the difference in light emission. The test showed light emission both with and without the test object. However, it appeared to be more light activity when the test object was connected. The PDIV for covered boards in Nytro at fast switching could not be defined due to the uncertainties of whether the light is originating from the test object or not.

In Nytro without cover, the shape parameter is 5.92 at sinusoidal voltage and 18.13 at fast switching. This means that the variance in voltage values is much less at fast switching. It may be that the mechanisms leading to breakdown at fast switching is more predictable at unipolar fast switching than at sinusoidal voltage stress. Also for covered boards, the shape factor is larger at fast switching than sinusoidal switching. Even though the difference is not that huge, it supports the hypothesis.

5.3 EFFECT OF PARYLENE SURFACE COVER

For covered boards PDs were sometimes detected many time steps before breakdown. The process of breaking through the Parylene cover probably required a lot of PD activity before it led to complete breakdown.

Parylene coating had a positive effect on both the PDIV and breakdown strength. The average PDIV was increased with approximately 10kV for all three liquids at surface covering, analogous to the increase in breakdown strength. The average PDIV for non-covered boards tested 5 times followed the trends shown for the breakdown strength in Figure 33; increasing strength for Nytro, decreasing strength for Galden and approximately the same strength for Midel.

The increase in breakdown strength for Nytro, Midel and Galden at sinusoidal voltage was 51 %, 65 %, and 35 % respectively. The breakdown strength will increase with surface cover as Parylene has a higher permittivity. In addition, the effect of contaminations lining up and enhancing the field will be avoided.

At fast switching in Nytro, the surface cover increased the BDV by 47 %. Three out of ten boards did not break down for this case. This was taken into account by progressively censoring the data. This ruins the ability to plot the confidence limits according to the IEEE Guide performed in this thesis [29]. The confidence limits for the boards with cover will look strange and be invalid as shown in Figure 40.

The correlation to the Weibull distribution was typically 0.99 for covered boards and 0.94 for the non-covered. The reason for the better correlation with cover can be that Weibull is a weakest-link failure distribution. Once the voltage required to break through the Parylene layer is obtained, the breakdown will happen fast. Most PCBs, with cover, followed the surface of the Parylene when breaking down. This crated a permanent failure with a short circuit from the HV side to ground. A few number of boards broke through the Parylene layer and then the rest of the breakdown propagated through the liquid. This might be if the layer had a particular weak point.

5.4 EFFECT OF SWITCHING POLARITY

The PD occurrence at negative polarity is easy to detect. Even above the constant noise, both acoustic and light signals are noticeable. The PD activity was much higher at negative polarity, which can be explained by the presence of space charges. At negative polarity, the electrical field becomes even more divergent due to electron injection from field emission causing good conditions for PD initiation. The fast travelling electrons will however decrease the mean electric field across the trench. This is why the breakdown strength was 7.1 kV or 31 % higher for negative polarity compared to positive polarity. At positive polarity, field ionization and slow positive ions will enhance the mean electric field. This causes breakdown to occur at lower applied field, making the positive polarity the most crucial.

5.5 COMPARISON OF THE DIFFERENT LIQUIDS

There is barely any light emission from Midel, which is also found in the specialization project. Therefore, the acoustic signal had to be trusted in order to evaluate the PDIV. In general, the breakdown tests in Midel showed that the PD activity starts very close up to when the breakdown occurs.

At sinusoidal voltage, the difference in breakdown strength between the liquids is not very prominent. The U_{63}-values are just a couple of kV in difference. Of all three liquids, Nytro shows best strength without cover at 21.8 kV. With cover, Midel has the highest BDV of 33.9 kV.

The 90 % confidence interval for all three liquids overlap even at the higher percentiles shown in Figure 44 and Figure 55 in 9.3. This suggests that the breakdown probability distribution and mechanisms behind breakdown is quite similar for all liquids at sinusoidal voltage.

At fast switching the BDV was almost equal for Nytro and Midel at 23.1 kV and 23.7 kV respectively. Galden showed an increased breakdown strength of 58 % with a withstand voltage value of 34.2 kV. This enhanced BDV is comparable to the BDV at surface covered boards. When comparing the three liquids in Figure 45, the large breakdown strength of Galden appears obvious.

All the test cases show a high dielectric strength with expected breakdown value above 20 kV. Hence, all insulation combinations could be appropriate for insulation systems for the subsea

converters operating at maximum 6.6 kV [3]. Galden showed very good dielectric performance for the fast switching source that was consistent on all the tests performed. To explain this, the material properties of Galden should be analysed. An explanation can be Galden's low viscosity, making it an excellent coolant. Another explanation can be Galden's high electron affinity caused by its fluorinated content. At positive switching polarity, only positive space charges can be generated. The high electron affinity of Galden my likely limit the rate of field ionization. Less generated space charges will give less field enhancement. Testing should be done with negative polarity as well to see if the electron affinity would cause extensive field emission and higher BDV.

To reduce the chance of failure, at least for unipolar switching, the best insulation choice would probably be Galden with surface cover. Although this case is not tested the other tests indicate that this combination would give the highest withstand voltage for a fast switching source.

5.6 OTHER REMARKS

- All the S/N ratios are quite bad so the PD detection must be done with care. The acoustic signal shows the best ratio, even with the peak-to-peak signal is divided by two. Another advantage of acoustic detection is that is shows no particular dependence upon the liquid tested.

- To increase acoustic detection sensitivity, a high pass filter should have been connected in series with the acoustic signal to get rid of the worst transient noise in the fast switching testing. The acoustic signal has a broad frequency band so it would still be detectable even though this filter is introduced [35].

- The optical detection has a bad S/N ratio because of the occurrence of dark currents. When light signals are particularly large, the signals might be a superposition of a dark current and a photon excited pulse. To be certain of PD occurrence a PD signal should detected in all three detection channels. Using two PMT's would help excluding the dark currents. The properties of the PD i.e. polarity, phase response and amplitude should appear as expected, explained in 3.7.

- A tendency shown during testing was that PDs were observed many time steps before breakdown occurred, followed by some time steps with no PDs. In the step before BD or right before breakdown, the PDs appeared again. The PDs detected early at non-covered boards may likely be due to particles or bubbles mechanisms. The PDs close to breakdown is probably due to electronic processes. The EHD motion is likely to move any contaminations away from the high field region.

- Not all board breakdowns could be included in the results because of circumstances that required them to be suspended. At sinusoidal testing of a board with Parylene cover in Galden, the board broke down during the voltage ramp up. The BDV was not recorded and the test object was singly censored from the data set. Causes of early

breakdown could have been weaknesses in the board and that the voltage ramp up was too fast.

- Most of the results in the Weibull diagram are linear, but in some cases, the data points tend to curve a bit to the right for higher breakdown values. The pattern looks similar to the 3-parameter Weibull plotted in a 2-parameter Weibull diagram shown in Figure 47 . This indicates that the three-parameter Weibull distribution might describe the breakdown probability more accurately. The three-parameter model includes a certain minimum value required for breakdown. This value is difficult to predict, but a suggestion can be to use the PDIV-value. This could have given a better statistical estimate and confidence interval.
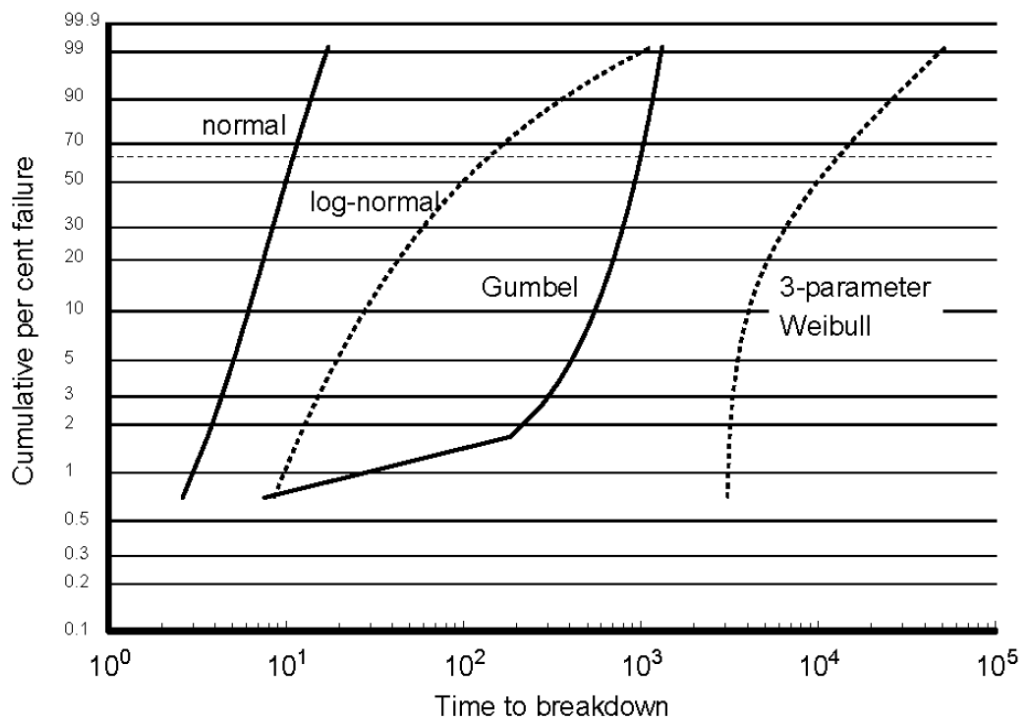
Figure 47 - Plots of other distributions on the two-parameter Weibull paper [29]

5.7 SOURCES OF ERROR

- The voltage of PD occurrence was noted when more than one PD, or a large PD was observed during the resting time between each voltage increase. The PDIV can be inaccurate, as not all PDs occurring were detected. PDs detected could also be random noise signals looking like PD signals. Even though the initial test voltage should have been below the PDIV, some tests showed PDs at the first voltage step. It must be emphasised that the PDIV-level determined in this thesis is very much a guiding value.

- It must be noted that the voltage step size during progressive testing is inaccurate as it is tuned up manually at the signal generator. The estimation is that the voltage steps of 1 kV will have an error of approximately $\pm$ 0.1 kV at each step. The same error estimate is considered for in the testing with the DC source at fast switching. Increasing the voltage too fast or too much could have affected the breakdown strength.

61

5.8 SWITCHING CIRCUIT DESIGN LIMITATIONS

- The switching circuit worked fine at low voltages, but was not designed for the high voltages required to break down all the PCBs.

- Rebuilding the circuit form sinusoidal to switching voltage introduced unwanted PDs at high voltages. The PDs and corona was observed in the lower section of the Faraday cage. An effort was made to block the light from getting to the upper section where the test object was placed, by the use of a blanket. It was not successful.

- The sensitivity of the circuit should have been improved in order to increase the reliability of the PD detection. Making more space between the high voltage connections and ground would help. The improvements were not done, due to time limitations.

- When testing the covered boards at fast switching, the BDV reached values above what the voltage source could deliver to the test object at progressive testing. The fast switching circuit was not designed to deliver such high voltages across the test object, U_{TO}. The maximum DC source output is 60kV, which corresponded to 40 kV across the test object.

- Several measures could have been done in order to increase the voltage across the test object using the same DC source. First of all, the circuit had to be made PD free, so that the high voltages would not cause PD noise or breakdown elsewhere in the circuit. By increasing the discharging resistor, $R_2 = 35M\Omega$, to a larger value of for instance $100M\Omega$, the voltage across the test object, $U_{TO,}$ would have been increased with 5.3 kV (at 30kV applied) shown in Appendix 9.1. Another efficient way to increase U_{TO} can be to decrease the frequency of the turn-on switching by changing the switching symmetry at the signal generator. Reducing the frequency to a quarter of its original frequency of 38.5 increases the voltage across the test object from 13.3 to 19.1 kV. Increasing the time where the switch is open, results in a longer time for the capacitor bank to recharge itself between each turn-on. The increased recharging results in an increased voltage

6 CONCLUSION

PDs are fast, small and broad-banded with a stochastic nature, making them difficult to detect. A low-noise test setup made it possible to determine the PDIV for different liquids at sinusoidal and fast switching voltages. The PD detection is obtained with both electrical, optical and acoustic detection. The sensitivity of acoustic detection is the best, with a S/N ratio of 4.4. Acoustic detection did not show any liquid dependence as light emission did. Galden and Nytro had sufficient light emission for optical detection, unlike Midel with less light emission.

At fast switching voltage, only acoustic and optical detection could be utilized due to the large electrical switching transients. The switching introduced noise in the acoustic and optical methods as well. It was possible to determine a PDIV only in Nytro, for fast switching. Preferably, the sensitivity should have been improved to increase the reliability of the PDs detected. The sensitivity could have been improved by the use of a high pass filter for acoustic detection or by using two PMTs for optical detection. Furthermore, a PD free circuit should be obtained by a larger spacing between high voltage connections and ground.

Breakdown tests were performed simultaneously with the evaluation of PD activity. The BDV obtained from all testing cases showed a good correlation to the Weibull distribution. A 90 % confidence interval was calculated resulting in good predictions for the breakdown value. Fast switching in general, had a higher withstand voltage than sinusoidal voltage, especially in Galden. The highest Weibull breakdown voltage was obtained in Galden at 34.2 kV switching peak voltage. This may be because Galden has a high electron affinity, limiting the rate of field ionization. As positive streamers has proved to be most critical, positive switching polarity was tested primarily. Negative switching polarity was tested only in Nytro. It showed a higher withstand voltage but more PD activity, due to the effect of space charges.

By using Parylene surface cover, the BDV was increased with up to 65 % in Midel compared to no cover. Correspondingly, the PDIV increased with 65 % for covered boards in Midel. For all liquids in general, the increase in PDIV and BDV was approximately 10-12 kV with surface cover, which is a significant increase in dielectric strength.

All three dielectrics tested have a high dielectric strength that would give sufficient insulation for subsea power converters. To increase the reliability and reduce the effect of contaminations, surface cover should be used. With the event of a breakdown in surface covered boards, results show that the breakdown will probably follow the board surface causing permanent failure. Boards without cover have a lower breakdown strength, but they are self-healing as the breakdown has shown to propagate through the oil.

7 FURTHER WORK

Some improvements that can made to the existing methods and test circuit summarised here. Time limitations also limited the scope of the thesis. A lot of time went to troubleshooting in order to obtain a circuit that worked. Suggestions for further work is to:

- Make the fast switching circuit PD free by providing more space between HV and ground.
- Increase test object voltage by:
    - Increasing the discharging resistor.
    - Reducing the switching frequency, by adjusting the switching symmetry.
    - Or: Change the DC source.
- Build a fast turn-off switching circuit, and analyse the effect on PD activity and BDV, compared to the fast turn-on circuit.
- Test more specimen to obtain a narrower confidence interval.
- Test more candidate liquids.
- Test with different surface cover, e.g. Polyamide.
- Connect a high pass acoustic filter to reduce the noise and obtain higher sensitivity.
- Check if the three-parameter Weibull and Gumbel distribution could give an even better distribution correlation.
- Conduct more tests with the AlN-board to compare the breakdown behaviour to that of PCBs.

8 BIBLIOGRAPHY

[1]   "OG21," [Online]. Available: http://www.og21.no/prognett-og21/Nyheter/Ny_OG21rapport_viser_hvordan_teknologi_kan_halvere_subseakostnader/1254009276973.

[2]   "Aker Solutions Feature Stories Subsea," [Online]. Available: https://www.akersolutions.com/en/Global-menu/Media/Feature-stories/Subsea-technologies-and-services/Solving-subseas-biggest-challenge/. [Accessed 8 June 2015].

[3]   "Presspack," SINTEF Energy Research, [Online]. Available: http://www.sintef.no/home/projects/sintef-energy-research/presspack/. [Accessed 8 June 2015].

[4]   M. D. Borge, "Subsea Insulation for Power Electronic Converters, Specialisation Project," NTNU, Trondheim, 2015.

[5]   E. Ildstad, High Voltage Insulation Materials, Trondheim: NTNU, Department of Electrical Power Engineering, 2012.

[6]   P. Ceccato, "PhD report: Filamentary plasma discharge inside water : initation and propagation of plasma in a dense medium," Ecole Polytechnique Palaiseau, LPP laboratory , Paris, 2009.

[7]   J. Skaar, "TFE4120 - Elektromagnetisme," pp. 26-33, 2012.

[8]   T. Grav, "Mechanisms Governing the occurence of Partial Discharges in Insulation Liquids," Master thesis, NTNU, Trondheim, 2013.

[9]   J. Eikeset, "Photon Activity from Partial Discharges in Liquid Dielectrics," NTNU, Trondheim, 2014.

[10]   IEC, "IEC 60156 - Insulating liquids - Determination of the breakdown voltage at power frequency - Test method," 1995, ed2.0.

[11]   E. K. W. S. Z. John Kuffel, High Voltage Engineering Fundamentals, 2nd ed., Newnes, 2000.

[12]   J. G. Hwang, M. Zahn, L. A. A. Pettersson, O. Hjortstam and L. Rongsheng, "Modeling Streamers in Transformer Oil: The Transitional Fast 3rd Mode Streamer," Massachusetts Institute of Technology, Massachusetts, USA, 2009.

[13] D. Andrë, "Conduction and breakdown initiation in dielectric liquids," *IEEE Internation Conference ofn Dielectric Liquids (Trondheim, Norway),* pp. 1-11, June 2011.

[14] P. D. -I. A. Küchler, Hochspannungstechnik, Springer, 2009.

[15] M. Z. L. A. A. P. J. George Hwang, "Mechanisms Behind Positive Streamers and Their Distinct Propagation Modes in Transformer Oil," IEEE, Cambridge, 2012.

[16] A. N. L. L. A.A. Abdelmalik, "Partial Discharges in Narrow Gaps on Power Electronic Converter," Annual Report Conference on Electrical Insulation and Dielectric Phenomena, Trondheim, 2014.

[17] P. O. Å. S. I. M. U. N. Davari, "Excitation energies and ionization potentials at high electric fields for molecules relevant for electrically insulating liquids," Journal of Applied Physics, Trondheim, 2013.

[18] P. D. I. A. Schnettler, "Lecture Notes - High Voltage Engineering - Insulation systems - Summer Term," Aachen, RWTH Aachen University, IFHT, 2014, p. 253.

[19] E. O. Forster, "Partial Discharges and Streamers in Liquid Dielectrics," IEEE Transactions on Electrical Insulation, Newark, 1993.

[20] W. F. Schmidt, Liquid State Electronics of Insulating Liquids, Berlin, 1997.

[21] L. L. G. B. D. Linhjell, "Streamer Propagation under Impulse Voltage in Long Point-Plane OIls Gaps," IEEE Transactions on Dielectrics and Electrical Insulation, Trondheim, 1994.

[22] G. M. O. Lesaint, "Positive Streamer Propagation in Large Oil Gaps," IEEE, Genoble, 1998.

[23] L. E. Lundgaard, "Partial Discharge - Part XIII: Acoustic Partial Discharge Detection - Fundamental considerations," IEEE Electrical Insulation Magazine, 1992.

[24] S. T. K. F. Sacha M. Markalous, "Detection and Location of Partidal Discharges in Power Transformers using Acoustic and Electromagnetic Signals," IEEE, Stuttgart and Kesselsdorf, 2008.

[25] V. S. R. E. Newnham, "Electrostriction and polarization," in *Ferroelectrics*, 1992, pp. 431-446 .

[26] V. F. K. S. K. V. Ya. Ushakov, "Nature of the electrostriction pressure," in *Impulse Breakdown of Liquids*, 2007, p. 3.

[27] U. Kogelschatz, "Dielectric-barrier Discharges: Their History, Discharge Physics and Industrial Applications," May 2002.

[28] F.-C. C. Yi-Che Su, "Synthesis and characterization of fluorinated polybenzoxazine material with low dielectric constant," Science Direct, 2003.

[29] I. D. a. E. I. Society, "IEEE Guide for the Statistical Analysis of Electrical Insulation Breakdown Data," IEEE, New York , USA, 2005.

[30] O. L. A. V. T. J.-L. Augé, "Partial Discharges in Ceramic Substrates Embedded in Liquid and Gels," IEEE Transactions on Dielectrics and Electrical Insulation , 2013.

[31] B. E. GmbH, *Data Sheet: Fast High Voltage Transistor Switches - HTS 651-03-LC.*

[32] N. E. KOMITE, "High-voltage test techniques - Partial discharge measurements," NEK & IEC, 2000.

[33] S. Hvidtsten, "ELK-30 "Condition assessment of high voltage apparatus - Power cables - partial discharge measurements","￼ SINTEF Energi Research, Trondheim.

[34] Hamamatsu Corporation, *Product Bulletin PB-103-01 R1635,* 1982.

[35] L. E. Lundgaard, "Partial Discharge - Part XIV: Acoustic Partial Discharge Detection - Practical Applications," IEEE Electrical Insulation Magazine, 1992.

[36] "Nytro 10XN Products and Safety datasheets," Nynas, [Online]. Available: https://nyport.nynas.com/Apps/1112.nsf/wnpds/Nytro_10XN_IEC/$File/PDS_Nytro_1 0XN_EN.pdf. [Accessed June 2015].

[37] M. M. Ltd, "Dielectric Insulating Fluid Overview," September 2014. [Online]. Available: http://static.mimaterials.com/midel/documents/technical/MIDEL_7131_Dielectric_In sulating_Fluid_Overview.pdf. [Accessed January 2015].

[38] C. G. A. A. C. U. Piovan, "A Comparison of the Voltage Withstand Properties of Ester and Mineral Oils," *IEEE Electrical Insulation Magazine,* 2014.

[39] C. P. A. B. Jean-Luc Bessede, "High performance dielectric oil and the use thereof in high voltage electrical equipment," [Online]. Available: https://www.google.com/patents/US7833440. [Accessed 8 June 2015].

[40] S. S. Polymers, "Galden® HT PFPE - Heat Transfer Fluids," Solvay Specialty Polymers, 2014.

[41] ChemicalBook, "ChemicalBook," [Online]. Available: http://www.chemicalbook.com/ChemicalProductProperty_EN_CB2101484.htm. [Accessed 31 May 2015].

[42] J. R. Morris, "Electrosurgical instrument having a parylene coating". Patent US5380320 A, 10 January 1995.

[43] S. K. D. M. Mandeep Kaur, "ELECTROMAGNETIC INTERFERENCE," IEEE, 2011.

[44] N. -. N. E. Komite, "NEK EN 60270 - High-voltage test techniques - Partial discharge measurements," IEC, 2001.

[45] P. D. I. R. K. Nilsen, Electromagnetics in Power Engineering - TET4140, Trondheim: NTNU, Autumn 2012.

[46] A. International, "Standard Test Method for Dielectric Breakdown Voltage of Insulating Liquids Using Disk Electrodes," 2013.

[47] A. International, "Standard Test Method for Dielectric Breakdown Voltage and Dielectric Strength of Solid Electrical Insulating Materials at Commercial Power Frequencies," 2013.

[48] A. International, "Standard Test Method for Dielectric Breakdown Voltage and Dielectric Strength of Solid Electrical Insulating Materials at Commersial Power Frequencies," ASTM International, West Conshohocken, 2013.

[49] A. International, "Standard Test Method for Dielectric Breakdown Voltage of Insulating Liquids Using VDE Electrodes," ASTM International, West Conshohocken.

[50] T. E. Toolbox. [Online]. Available: http://www.engineeringtoolbox.com/relative-permittivity-d_1660.html. [Accessed May 2015].

[51] IEEE. [Online]. Available: http://www.ieee802.org/3/10G_study/public/jan00/sayre_1_0100.pdf. [Accessed June 2015].

[52] K. Gibbs, "School Physics," 2013. [Online]. Available: http://www.schoolphysics.co.uk/age16-19/Medical%20physics/text/Piezoelectric_transducer/index.html. [Accessed 29 March 2015].

[53] P. D. S. GmbH. [Online]. Available: http://www.pdix.com/products/pd-accessories/quadrupoles.html. [Accessed 9 January 2015].

9 APPENDIX

9.1 SIMULINK

The Simulink model in Figure 48 was used to evaluate the voltage time response of the circuit before building it. Changing some of the parameters can give an overall improved circuit response. The objectives of this circuit is to get a fast turn-on and a high voltage at the test object.
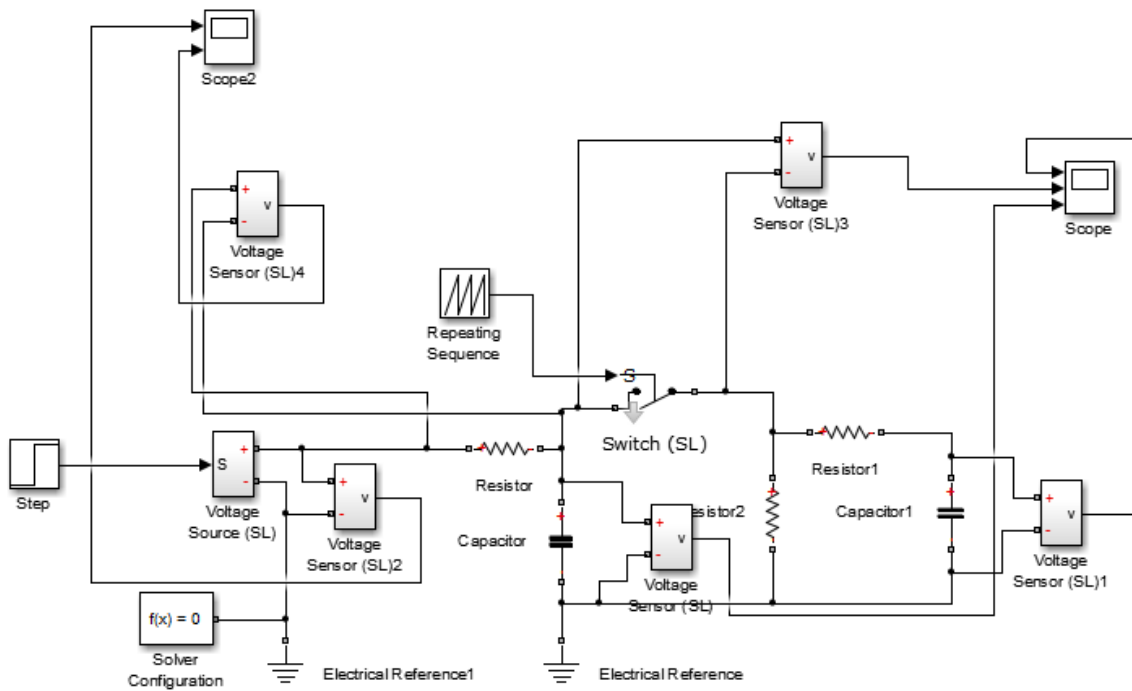
Figure 48 - Fast turn on circuit model in MATLAB
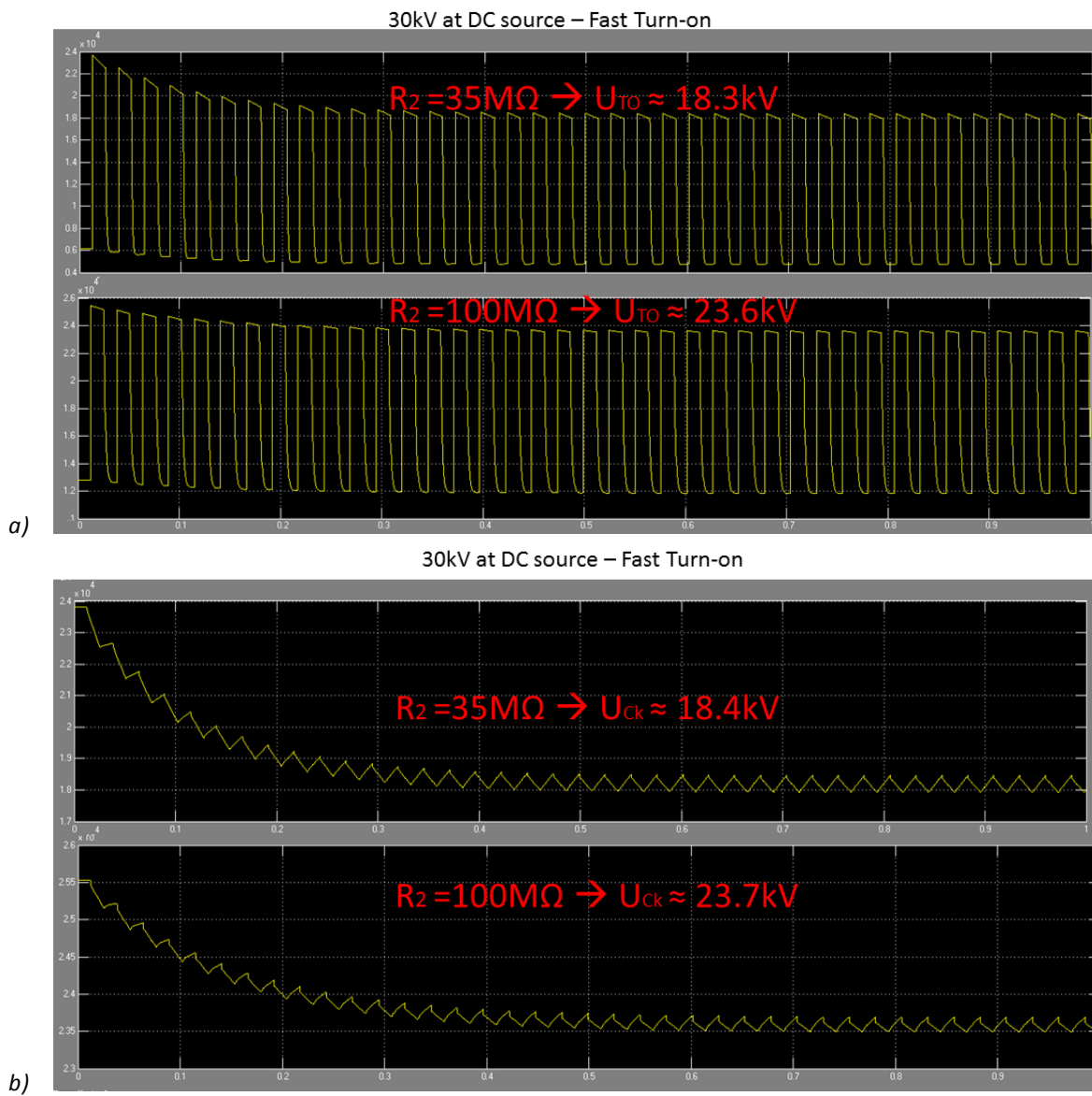
Figure 49 – Time response of voltage in 10^4 Volts for U_{TO} and U_{Ck}. Two different values of the discharging resistor R_2 is simulated showing that increasing R_2 increases both voltage U_{Ck} and U_{TO}.

9.2 COMSOL

This appendix shows more of the COMSOL simulation. Figure 51 shows how high voltage has been applied to the left electrode, while the right and bottom electrode has ground potential. The dielectric relative permittivity of the oil is set to 2.2, which corresponds to transformer oil [50].The permittivity of the board of FR-4 is set to 4.5 [51]
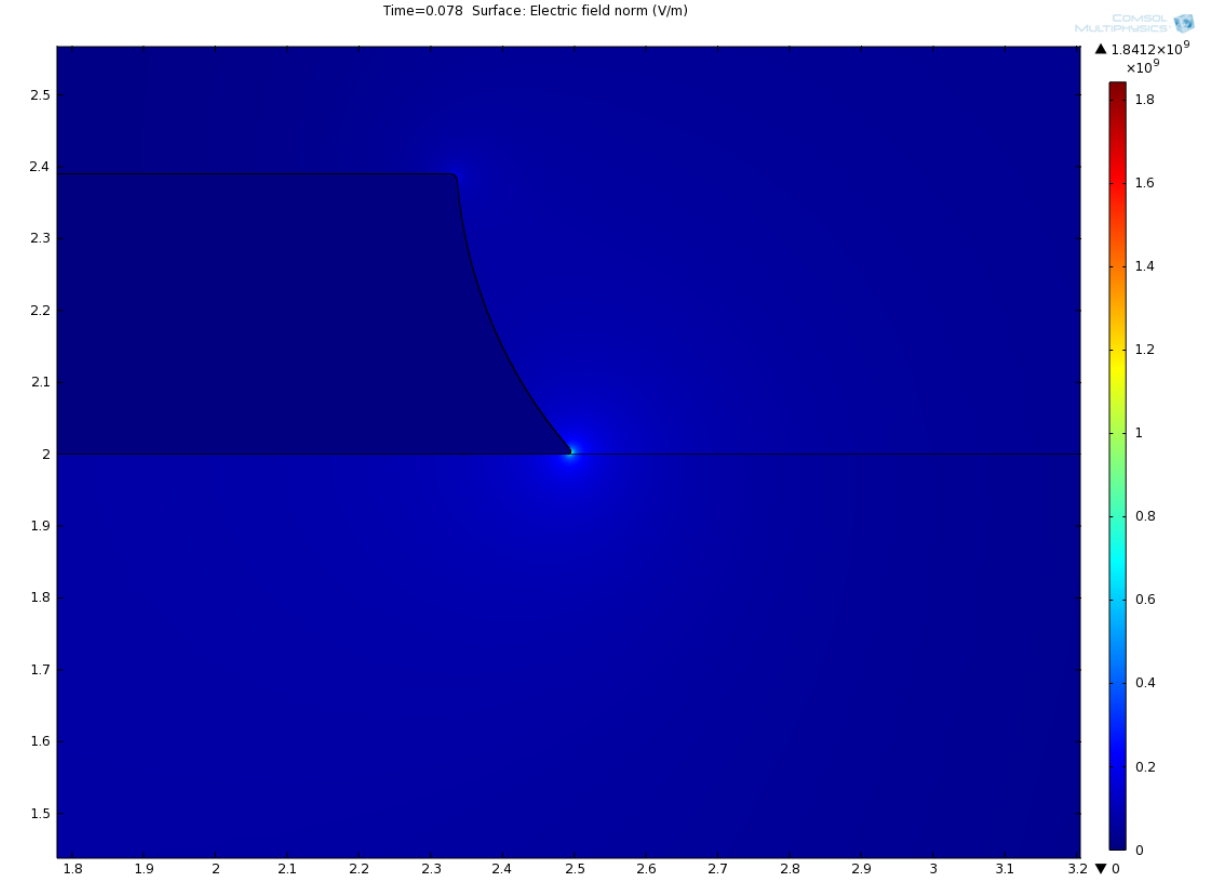
Figure 50 - COMSOL layout of high voltage electrode with the local high field stress from electrostatic differential equations. Maximum field stress in the case of 25 kV AC voltage applied is $1.84 \cdot 10^9 \ V/m$.
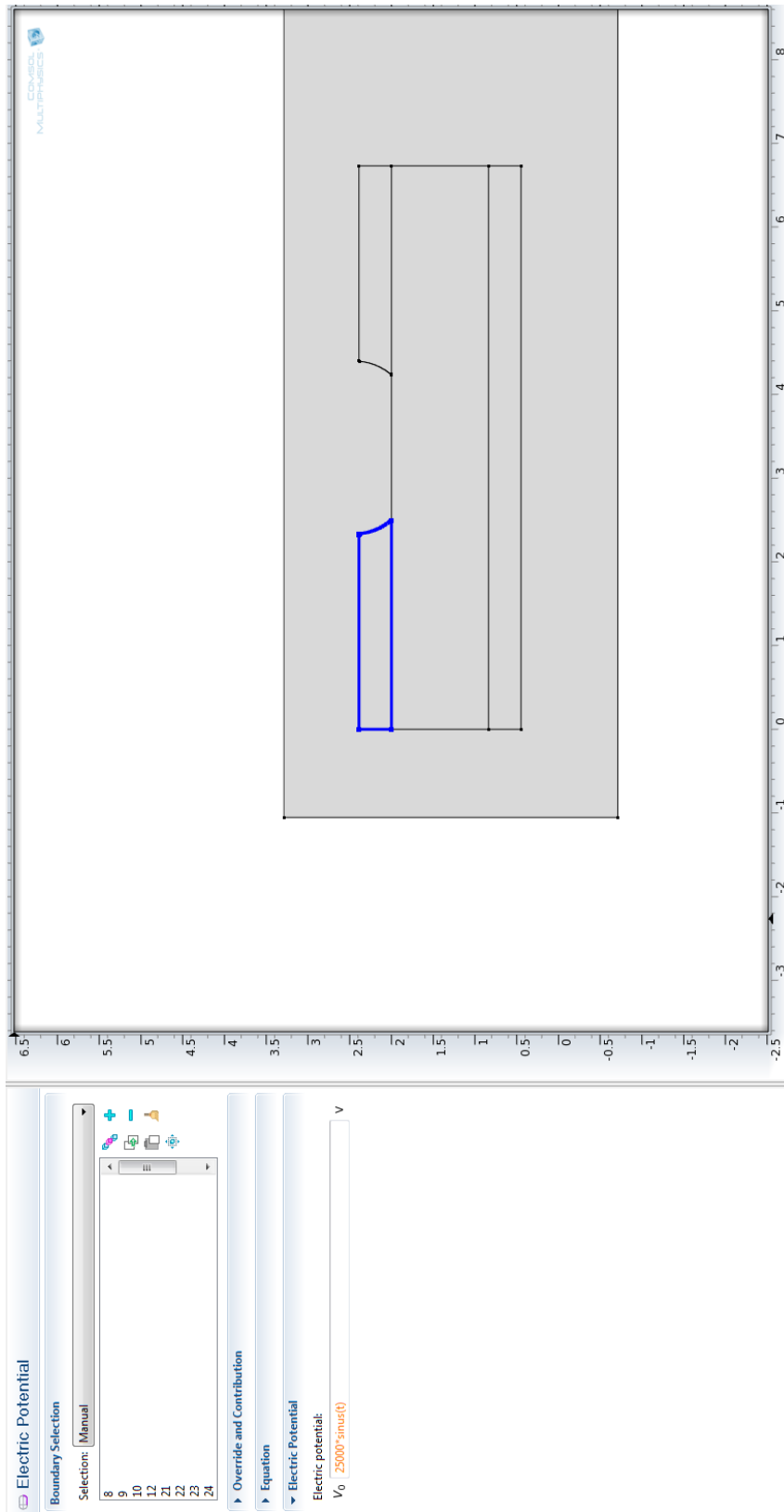
Figure 51 - Drawn COMSOL-model with 25kV applied sinusoidal voltage to the HV electrode

9.3 Weibull plots
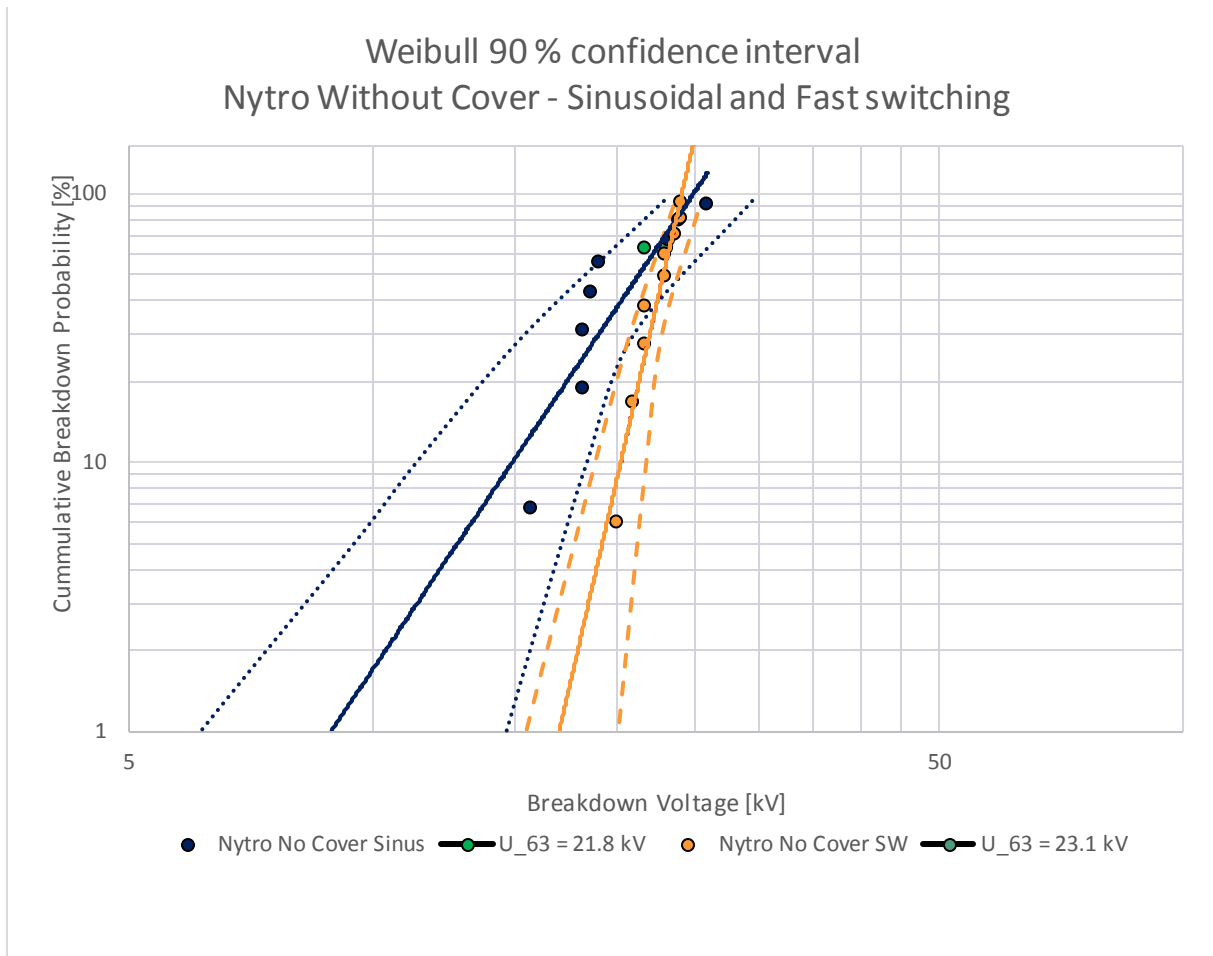
Figure 52 - Weibull Breakdown data plot for Nytro comparing sinusoidal and fast switching voltage
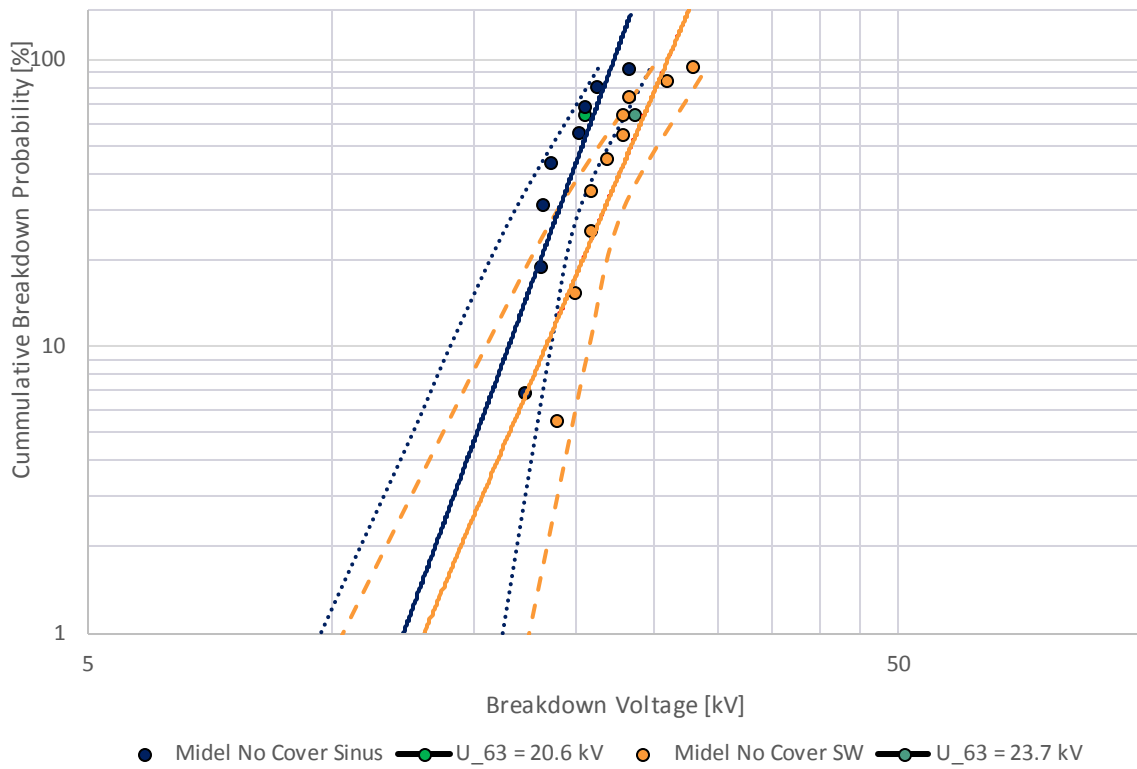
Figure 53 - Weibull Breakdown data plot for Midel comparing sinusoidal and fast switching voltage
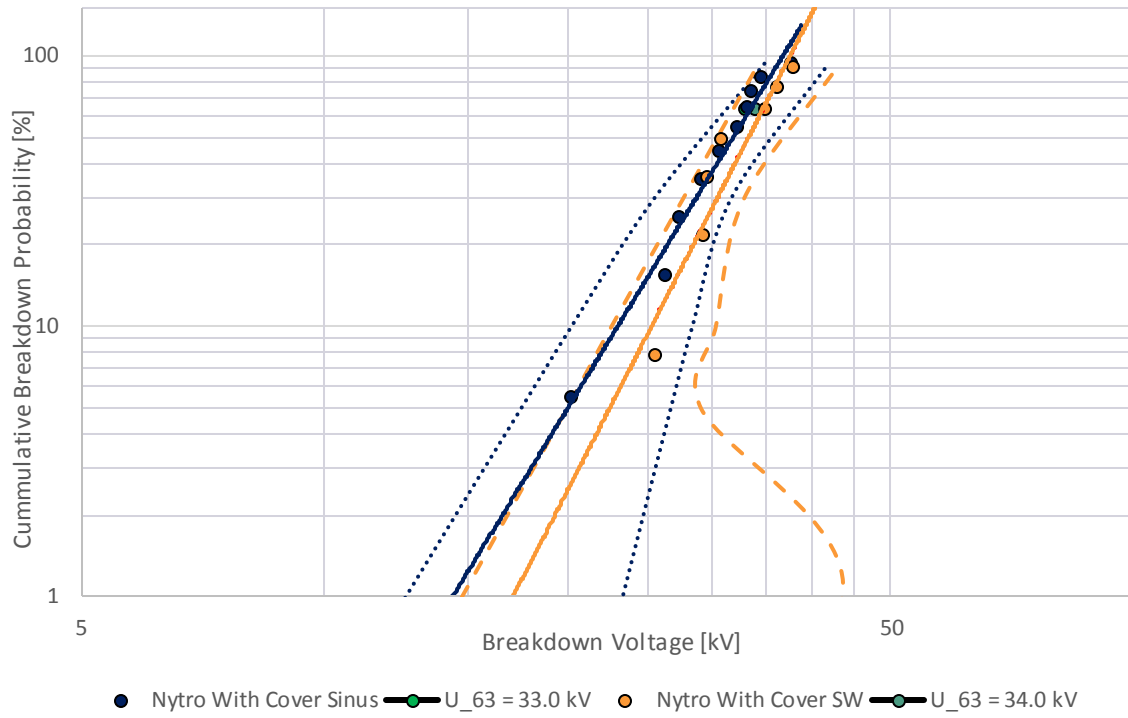
Figure 54 - Weibull Breakdown data plot for Nytro with cover, comparing sinusoidal and fast switching voltage

Figure 55 - Comparison of all liquids with covered boards at sinusoidal voltage
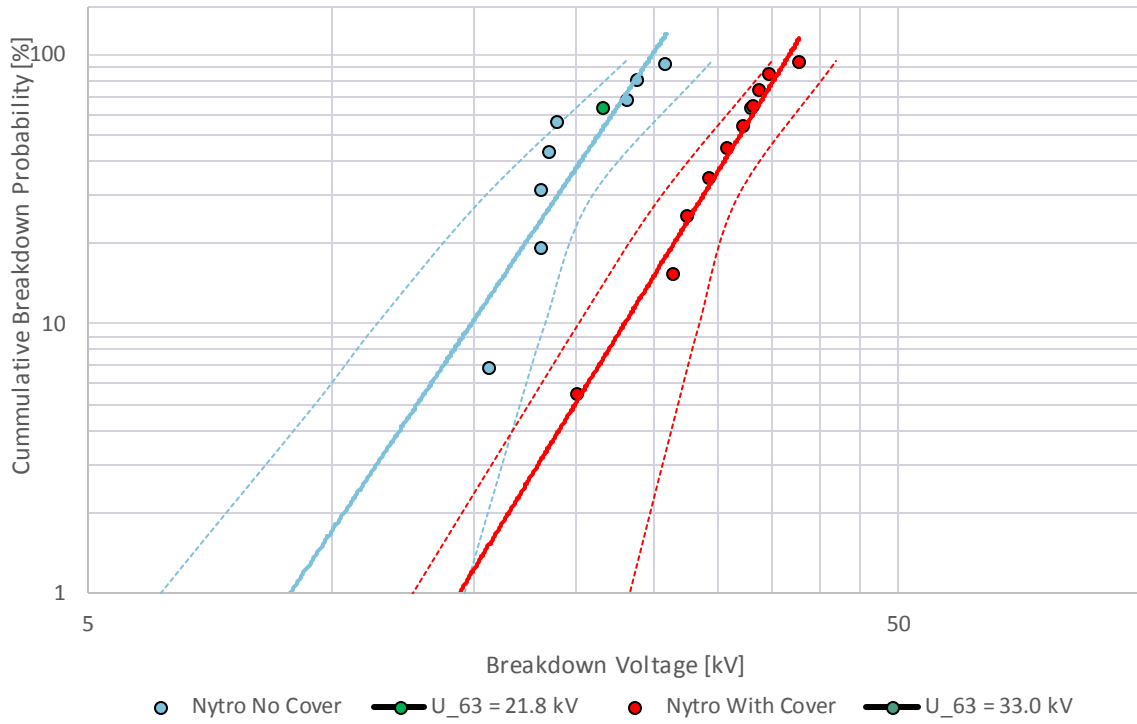
Figure 56 - Weibull Breakdown data plot for Nytro comparison with and without Parylene cover
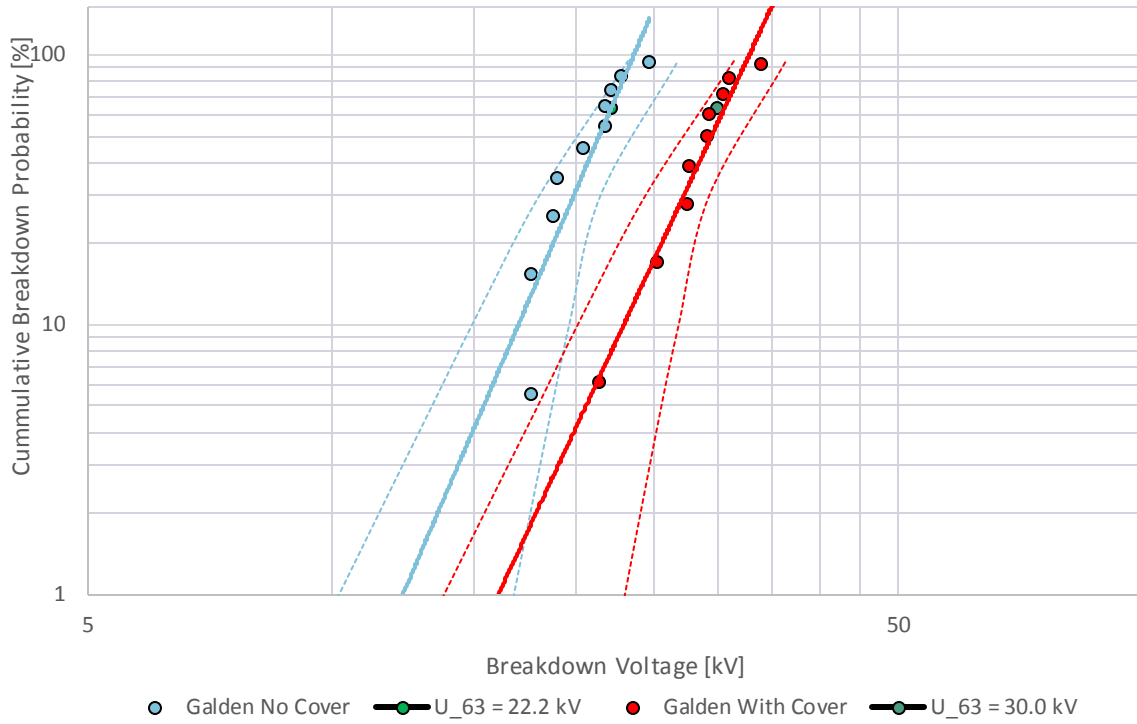
Figure 57 - Weibull Breakdown data plot for Galden comparison with and without Parylene cover

9.4 METHOD OF WEIBULL DISTRIBUTION ANALYSIS

To test if the Weibull distribution can describe the experimental data in a satisfactory way a simple test can be performed by plotting the points in a Weibull diagram that has logarithmic scaling at both axis. If the points give an approximate linear curve the distribution is a good fit. The fit can also be checked mathematically by the use of least square regression or with the White method.

If the data set is complete, meaning no data have been censored the validity is easily checked by plotting the voltage and approximate probability given by for *i* test specimen broken down

$$F(i,n) \approx \frac{i - 0.44}{n + 0.25} \cdot 100\%$$ *Eq. 15*

When testing, not all test turn out to be valid and should hence not be included in the results. The results will be incomplete, but the correct censoring makes it valid. The censoring of data is done either in a singly or progressive way. **Singly censoring** can be performed by removing a sample that did not break down. **Progressively censoring** is removing an object from the analysis, that did break down, but due to the circumstances of the test it should not be included. For instance, if the specimen broke down during the voltage ramp up prior to the initial voltage it should be excluded. To test the adequacy of the Weibull distribution for censored data in plotting positions the rank *i* in Eq. 16, is a modified function:

$$I\,(i) = I(i - 1) + \frac{n + 1 - I(i - 1)}{n + 2 + C_i}$$ *Eq. 17*

,where I(0) = 0 and C_i is the sum of the number of specimen broken down and censored when the ith breakdown occurs.

To check the correlation mathematically one can compare the X and Y values in the Weibull diagram and use a built-in function found in Excel called **CORREL**. The function returns a number in the range of 0-1, explaining how good the linear curve fits the data points, hence how well the data set is explained by the two-parameter Weibull distribution. Xi and Yi are calculated from:

$$Y_i = \ln(U_i)$$ *Eq. 18*

$$X_i = \ln(-\ln(1 - \left(\frac{F(i,n)}{100}\right))$$ *Eq. 19*

9.4.1 Calculating U$_{63}$ and b:

For small data sets with less than 15-20 breakdowns the White method should be used as it can allocate different weights, w$_i$, to different data points,. The weightings can be found in a in the IEEE Guide.

U_{63} and b are obtained from:

$$b = \frac{\sum_{i=1}^{r}[w_i (X_i - \bar{X})^2]}{\sum_{i=1}^{r}[w_i (X_i - \bar{X})(Y_i - \bar{Y})]},$$

Eq. 20

$$U_{63} = exp\left\{\bar{Y} - \frac{\bar{X}}{b}\right\},$$

Eq. 21

Where the weighted averages are calculated from:

$$\bar{X} = \frac{\sum_{i=1}^{r}[w_i X_i]}{\sum_{i=1}^{r}[w_i]},$$

Eq. 22

$$\bar{Y} = \frac{\sum_{i=1}^{r}[w_i Y_i]}{\sum_{i=1}^{r}[w_i]},$$

Eq. 23

9.4.2 Calculating confidence interval

In the Weibull distribution, it is common to calculate a confidence interval with a percentage probability of breakdown with upper and lower limits of the U_{63}-value. When testing few specimen the interval will become quite broad. With many tests performed, the confidence interval will be narrow.

The Guide proposed by IEEE provide a simplified procedure for estimating a 90% confidence interval for samples sizes from n=4 to n=100. However, the technique can not be used on progressively censored data.

The confidence interval for the parameters will in the range between U_{63_U} and U_{63_L} for the scale factor, and b_U and b_L for the shape factor, where the subscript U and L stands for upper and lower.

$$U_{63\_U} = U_{63} \cdot \exp\left\{\frac{Z_U}{b}\right\}$$

$$U_{63\_L} = U_{63} \cdot \exp\left\{\frac{Z_L}{b}\right\}$$

Eq. 24

$$b_U = W_U \cdot b$$

$$b_L = W_L \cdot b$$

Eq. 25

Z_U, Z_L, W_U, W_L are factor obtained from the guide. To plot the confidence interval of 90%, six percentiles have been used. The percentiles have p= 0.1 %, 1 %, 5 %, 10 %, 30 % and 95 % . They give the upper and lower bound for the 90% confidence interval U_U and U_L, where $Z_U(p)$ and $Z_L(p)$ are percentile dependent.

$$U_U = U_{63} \cdot \exp\left\{\frac{Z_U(p)}{b}\right\}$$

Eq. 26

$$U_L = U_{63} \cdot \exp\{\frac{Z_L\,(p)}{b}\}$$

Plotting the limits can be done by simply drawing a line through the six points obtained for the upper and the lower bound

A good way to compare different Weibull distributions for different insulation media types and conditions, is to compare the percentiles. One can do a quick comparison by checking if the percentiles overlap. Especially the 10th percentile is of interest as it normally overlaps for similar testing, while the higher percentiles do not. It can also be useful to plot the two graphs in the same Weibull diagram and include the confidence limits.

9.5   CORRELATION TO WEIBULL (RESULTS)

Table 11 - Adequacy for all test cases using Weibull Breakdown analysis

	Data points for PCB	r	Correlation (Y_i and X_i)	Good/ Bad fit
Sinusoidal	Nytro	8	0.929	Good
	Nytro w/C	10	0.985	Good
	Midel	8	0.936	Good
	Midel w/C	10	0.984	Good
	Galden	10	0.951	Good
	Galden w/C	9	0.986	Good
Fast Switching	Nytro	9	0.979	Good
	Midel	10	0.940	Good
	Galden	9	0.941	Good
	Nytro w/C	7	0.973	Good
	Nytro Neg	5	0.955	Good

Figure 58 - Plot to check the goodness-of-fit of a two-parameter Weibull distribution

9.6 MEASURED BREAKDOWN DATA

Note: Blank spaces means that no PDIV was recorded.

SINUS: Nytro without cover (each board tested five times)								
Board nr:	B1	B2	B3	B4	B5	B6	B7	B8
V_{init} 1	14,08	12,04	12,6	12,3	15,68	12,6	15,24	13,72
2	12,5	13,02	12	12,7	15,82	16,08	14,76	18,2
3	12,64	13,58	11,76	13,1	15,12	10,6	15,6	16,8
4	13	13,58	12,24	12,7	15,82	16,08	16,2	19,04
5	12,6	14,14	11,52	13,2	16,1	15,6	18,06	19,32
PDIV 1	17	16	15,72	16,4	15,68	17,64	15,24	15,68
2	13,5	17,22	15,24	17,8	15,82	19,32	14,76	21
3	17,8	22,68	16,68	20,2	18,06	22,56	19,8	23,24
4	17	19	14,16	19,8	17,5		27,16	20,3
5	17,5	20,02	21,15	18,4	17,08	20,64	30,1	
BDV 1	19	18,2	15,72	18,2	18,62	23,94	23,28	25,9
2	17,6	20,16	15,24	18,6	19,74	21,24	18,72	22,26
3	20,8	23,66	18,6	21,1	22,12	22,56	24,36	27,16
4	18,1	22,54	17,6	21,6	23,52	19,2	32,34	28,28
5	21,84	21,56	22,9	24,45	25,06	22,68	34,16	23,1

SINUS: Midel without cover (each board tested five times)								
	B1	B2	B3	B4	B5	B6	B7	B8
Vinit 1	15,12	14,56	14	13,16	13,02	13,2	13,2	16,68
2	14,7	13,58	13,72	13,58	13,72	13,56	15,24	16,08
3	14,56	14,14	12,74	13,16	13,06	13,32	19,08	16,56
4	14	13,58	12,88	13,58	12,84	14,28	17,64	17,16
5	14	14,56	12,88	13,58	12,84	15	17,16	16,8
PDIV 1	17,08		15,26		14,14	20,28	20,16	17,64
2	17,64		15,68	14,56		20,76	22,44	18,24
3				14	19,08	19,32		18,82
4	19,1	19,88	13,86	13,58	15,84	20,4		20,4
5	18,06	18,62	18,76	16,52	17,04	20,4	21,24	18,84
BDV 1	20,3	18,76	18,2	17,36	18,34	21,36	23,4	20,58
2	18,62	19,6	16,66	18,76	17,78	21,72	24,24	19,2
3	18,62	18,2	15,68	21	20,28	21,24	21,24	23,64
4	19,1	20,72	19,6	18,9	17,64	22	21,72	21,24
5	20,3	20,86	21,84	20,72	17,04	21,6	22,44	21,84

SINUS: Galden without cover (each board tested five times, except the last two)										
	B1	B2	B3	B4	B5	B6	B7	B8	B9	B10
Vinit 1	14,04	12,84	13,8	15,72	13,8	13,56	14,76	16,4	15,66	15,66
2	15,12	14,52	13,44	14,04	12,72	12,84	14,16	12,79		
3	14,16	13,56	14,04	13,8	13,2	14,04	13,8	12,6		
4	14,04	12,6	13,56	15,36	13,8	12,84	13,56	13,32		
5	12,96	12,84	12,96	15	14,04	13,56	13,8	12,36		
PDIV 1		15,96		17,88	19,8	16,56	19,68	16,4		
2	19,08	14,52	14,4	15,24	12,72	12,84		12,84		
3	14,16	14,54	14,04	14,64	15,24	16,08	16,56			
4	14,04	14,52	13,56	15,36	14,76	14,76	15,96	13,32		
5	13,92	12,84	16,2	15	16,2	13,56	14,76	13,44		
BDV 1	22,2	24,72	21,84	18,84	21,84	20,5	22,8	19	17,64	17,64
2	19,08	17,46	17,88	17,16	17,88	17,88	18	16,92		
3	17,16	17,64	16,32	17,76	19,32	17,28	17,4	16,92		
4	17,4	17,52	16,68	18,12	18,84	18	18,6	18,24		
5	18,2	16,68	16,2	17,16	18,48	17,64	17,88	17,64		

PARYLENE COATED at sinusoidal test voltage									
	Nytro			**Midel**			**Galden**		
Board nr	V_init	PDIV	BD	V_init	PDIV	BD	V_init	PDIV	BD
1	26,4	26,22	33,76	23,28	28,32	31,36			
2	25,28	26,42	32,32	22,72	28,32	33,12	25,76	30,08	31,1
3	14,4	16,32	26,4	21,92	27,36	37,6	17,44	17,44	21,44
4	26,24	27,52	27,52	25,2	25,2	25,2	25,6	29,6	30,56
5	18,72	20,16	20,16	25,4	35,4	35,4	24	26,24	29,23
6	25,92	32,16	37,8	25,4	31,4	32,4	25,76	26,72	27,52
7	25,92	29,7	34,74	25	26	31	21,12	24,96	34,08
8	25,74	27,72	30,78	25,4	29,4	30,4	24,8	25,92	27,68
9	23,04	22,54	29,28	25,4	25,4	26,4	24,32	25,28	25,28
10	25,38	31,32	33,3	25,4	30,2	34,4	24,96	28,48	29,28

Fast switching: No cover									
	Midel			Galden			Nytro		
Try nr	Vinit	PDIV	BD	Vinit	PDIV	BD	Vinit	PDIV	BD
1	10		28				20		20
2	16		26	16		33,7	16	20	23
3	20		20	16		26,0	18	19	21
4	18		21	19		24,0	17	18	20
5	18		19	18		35,0	17	23	24
6	17		21	26		33,7	18	21	23
7	17		23,3	24		25,1	18		24
8	16		23	22		37,0	18,7		21,7
9	17		23	25,3		34,3	18,7	19,7	21,7
10	18	20	22	28,3		38,3	16,7	20,7	23,7

Fast SW: NYTRO WITH COVER		
Vinit	PDIV	BD
22,0		31,0
24,7		29,7
24,3		*
24,7		25,7
25,3		29,3
24,7		*
25,3		36,3
26,0		*
30,0		38,0
28,0		35,0
		*Did not break down

Fast SW: NO COVER NEGATIVE POLARITY		
Nytro		
Vinit	PDIV	BD
11,7		16,7
12	23	28
15	19	34
20	<20	31
22	<22	27